VILNIUS UNIVERSITY

Mindaugas
JUSIS

Method of data synchronization of autonomous port handling processes

DOCTORAL DISSERTATION

Technological Sciences
Informatics Engineering (T 007)

VILNIUS 2021

The dissertation was prepared in 2016 – 2020 at Vilnius University.

Scientific supervisor:
Prof. Dr. Saulius Gudas (Vilnius University, Technological Sciences, Informatics Engineering – T 007)

Scientific consultant:
Prof. Dr. Arūnas Andziulis (Klaipėda University, Technological Sciences, Informatics Engineering – T 007)

https://orcid.org/0000-0001-8035-3938

VILNIAUS UNIVERSITETAS

Mindaugas
JUSIS

Uosto autonominių krovos procesų duomenų sinchronizavimo metodas

DAKTARO DISERTACIJA

Technologijos mokslai,
Informatikos inžinerija (T 007)

VILNIUS 2021

Disertacija parengta 2016 – 2020 metais Vilniaus universitete.

Mokslinis vadovas:
prof. dr. Saulius Gudas (Vilniaus universitetas, technologijos mokslai, Informatikos inžinerija – T 007)

Mokslinis konsultantas:
prof. dr. Arūnas Andziulis (Klaipėdos universitetas, technologijos mokslai, Informatikos inžinerija – T 007)

LIST OF TERMS AND ABBREVIATIONS

AGV – Automated Guided Vehicles.

ABP – Activation by Personalization.

AS – Application Server.

BPMN – Business Process Model and Notation is a graphical representation for specifying business processes in a business process model.

ED – End Device.

BLE – Bluetooth Low Energy.

4G – 4th generation cellular network technologies such as LTE.

FIS – Fuzzy Interference System.

GPS – Global Positioning System.

GW – Gateway.

ICT – Information and Communication Technology.

IEEE – Institute of Electrical and Electronics Engineers.

IoT – Internet of Things.

IP – Internet Protocol.

IR sensor – an electronic device, that emits light to sense some object of the surroundings.

LoRa – is a low-power wide-area network modulation technique.

LoRaWAN – Low Power, Wide Area (LPWA) networking protocol designed to wirelessly connect battery-operated things to the internet in regional, national, or global networks, and targets key Internet of Things (IoT) requirements such as bi-directional communication, end-to-end security, etc.

LPWAN – Low Power Wide Area Networks.

LTE – Long-Term Evolution. A mobile communication standard. In the cellular network, mobile data can be transferred over the air in larger amounts and at higher speeds than was possible under previous wireless communication standards.

MAC – Media Access Control.

MCP – Monte Carlo particle.

NB-IoT – Narrow Band IoT.

NS – Network Server.

OCR – Optical character recognition.

OTAA – Over-The-Air-Activation.

PI – proportional-integral controller.

PID – proportional-integral-derivative controller.

QC – quay cranes.

PWM – Pulse Width Modulation.

RFID – Radio Frequency Identification.

RTLS – Real-Time Location System.

SIM – Subscriber Identification Module.

STS – Ship-To-Shore gantry crane.

UHF – Ultra High Frequency.

UKF – Unscented Kalman filter.

Wi-Fi – (shortened form of Wireless Fidelity). A family of wireless network protocols, based on the IEEE 802.11 family of standards, which are commonly used for local area networking of devices and Internet access.

WSN – Wireless Sensor Network.

LIST OF FIGURES

LIST OF TABLES

CONTENTS

INTRODUCTION

The problem and its relevance

To reduce greenhouse gas emissions in ports (EU Directive 2018/410), it is important to propose new real-time data collection and processing technologies that will reduce the energy consumption of quay cranes and the fuel consumption of container trucks (AGVs) with future intent to make ports fully autonomous and "green". Existing energy consumption analysis methods, usually used for operations scheduling in terminals, take into consideration fuel or electric energy consumption criteria for yard, quay cranes operations, trucks and AGVs operations. On the other hand, little is done to study the entire process of cargo transportation from ship-to-shore optimizing the data synchronization process from trucks and cranes in a real operational environment. Lack of proper data synchronization methods increases the downtimes of various technological processes, thus increasing the fuel consumption and level of emissions in the port environment.

Existing planning technologies, such as trucks and cranes operations planning and process scheduling software tools and methodologies, since they do not cover the entire system (ship-container stack) in real-time, so the main task is to develop intelligent control algorithms using data collection and synchronization methodologies, including the control of handling procedures, planning the operations, and integration of external information assessing tools into a single port control system.

To increase the efficiency of the container handling process, one of the most promising solutions is to develop efficient data synchronization methodologies using real-time data of the quay crane and container trucks, using the support of various ICT tools/technologies, and developing combined container handling solutions from the planning perspective.

Existing planning systems do not evaluate real-time data synchronization received from all sensory units scattered across the container terminal, which leads to downtimes for every machinery in use, which harms the duration of the handling process and increases the energy costs required to transport the cargo across the terminal to the stack.

There is a lack of practical knowledge on how to solve this type of planning problem from a technological point of view. Scientific concepts for the synchronization of individual technological and cargo handling processes were discussed by many authors, and in recent years, with the introduction of new fast wireless communication systems, data manipulation methods for Big Data analytics, new research opportunities arose in relevant areas of Informatics engineering (ICT), according to Industry 4.0 and European

Commission (2020; COM (200) 65 final) regulations. So, it is important to propose new real-time data collection and processing ICT technologies using combined technology control and planning solutions. The synchronization of existing planning technologies is not enough, so the development of intelligent control algorithms using new data collection and synchronization methodologies, including the control of handling procedures, planning of the processes, and integration of external information sources for knowledge extraction, becomes a key challenge for this Thesis.

Klaipėda Sea Port has distinguished itself in the Baltic region due to its rapid increase in cargo flows and adoption of Blue Economy regulations and strategies that require a decrease of CO_2 and other harmful gasses in the industry surrounding the sea port and related to the port activities (including shipbuilding, bulk cargo transit, fossil fuel trans-ship, fishing and production).

Many practitioners and action methodology developers in the transport chain carried out research in this area, ranging from communication and control systems application with deep insights and relevant reviews, economical calculations, and practical use cases [1]–[3]. Overall, the possibility to adopt new technologies in such closed environments is a rare opportunity. In practice, the implementation of complex control solutions is limited by the cost-efficiency in comparison to standardized and commonly used solutions.

Adoption of new ideas is difficult even to "modern minds". In a real situation, it is difficult to come close to working equipment and to acquire an agreement for their monitoring on-site. The initial visual analysis suggested developing new ideas on how to lower fluctuations of the container's gripper. Its movements are random, due to external impacts, such as wind or physical contact with other objects. It is difficult to predict such random deviations in a real environment [2].

In comparison, European ports such as Rotterdam or Hanover apply new systems for vibration decrease in the cables during lowering procedures. Dampening control systems decrease unnecessary strains arising during the accelerated movement of containers by synchronizing operators' actions with the total lowering process of engines and control units. Artificial Intelligence (AI) systems with stochastic algorithms for efficient learning and fast adoption to unlikely events are used in high risks scenarios [1]. Control and coordination of operator movement is a task for unconventional systems, mainly used to solve competence shortage problems in engineering, medicine, and explorations environments.

Today, most Baltic Sea region ports handled automated systems, but only on the surface. Context procedures and IT operations are automated in the

most "brutal" fashion. Equipment is bought, but not relied upon to solve critical tasks. That is why the implementation of the quay crane even in modern ports is still a rather innovative and theoretical step. In reality, the crane operator has to wait for the automated guided vehicles (AGV) or the AGV has to wait for the operator to finish his unloading routine, even when the most modern control systems are used.

Research object
Intermodal container terminal quay crane and container truck interaction processes, synchronization of their communication data.

Work objective
To develop a method and algorithm for synchronizing the data for the autonomous handling processes in the port's harsh environment using wireless long-range communication technologies LoRaWAN and software agent system in order to speed up the procedures, reduce downtimes, and vehicle energy consumption for the entire operation.

Work tasks
1. To analyze and compare the applied data and technical means and synchronization solutions for individual cargo-handling processes, modern data extraction and transmission technologies in harsh environments and their efficiency in the cargo handling cycle.

2. To develop a new method, including assignment, positioning and data exchange algorithms for process data synchronization between quay cranes and container trucks for the autonomous containers handling processes in the harsh environment.

3. To test experimentally the capabilities of LoRaWAN networking technology in the container terminal and verify its adoptability for the proposed synchronization method and algorithms.

Research methods
The following methods were used in the study of the research object:
1. Classification, which allows us to define and understand the object of research, summarizing the analyzed features, advantages and disadvantages of the data presented in the literature.
2. Theoretical (analysis and synthesis), allowing us to choose the strategy of searching for the solution of the set tasks.
3. An exploratory study to find a solution to a problem.
4. An experimental study, allowing us to test the hypotheses.
5. Applied statistics to assess the statistical significance of the findings.

6. Data modeling notation like UML, ERD, and functional modeling method IDEF.

The novelty of the study

1. A new mathematical model and algorithm of synchronizing the autonomous handling processes in the harsh port environment have been developed, including container lowering time estimation for transportation by a quay crane according to a trajectory template.

2. A new method of wireless data collection and transmission based on LoRaWAN technology, enhanced with data security add-ins, has been developed for synchronizing data exchange between quay cranes and container trucks.

3. A new mathematical model and algorithm for reducing the time of operation and fuel consumption of a container truck from real movement data have been developed and implemented.

Results

1. A mathematical model of the autonomous container loading process synchronization has been designed and verified using real data collected in the container terminal, which describes the "quay crane – electric carrier" interactions in the intermodal terminal.

2. A virtual prototype and a model simulating the autonomous container loading terminal processes "ship – quay crane – AGV – stack" has been developed, which allows studying of the process data synchronization between the autonomous electric carrier and the autonomous crane in dynamic mode.

3. A new method of synchronization of autonomous loading processes in the port's harsh environment has been developed, combining LoRaWAN

technology and software engineering capabilities with proposed software engineering solutions.

The practical value of the research

1. Based on enhanced LoRaWAN technology a new prototype of the system for wireless data collection and transmission was developed, which synchronizes data exchange between quay cranes and container trucks.

2. The developed mathematical model for calculating the fuel consumption of container tugs from real movement data will allow more efficient use of fuel resources in ports in compliance with the EU Directive 2018/410.

3. Research results can be used for the design or modernization of various types of loading process control systems (not only in the port).

4. The results of the performance characteristics of the LoRaWAN prototype obtained during the study are useful in the development of data synchronization systems for long-distance and harsh environments.

Defensive statements

1. To maintain the connection without interruptions for data synchronization in the harsh environment, the developed LoRaWAN network signal strength will not exceed a -120 dBm threshold, considering the whole container terminal area.

2. Applying the method of data synchronization of two nodes (autonomous moving objects, increases the efficiency of the analyzed processes by decreasing total process duration and energy consumptions.

3. Development and application of enhanced LoRaWAN technology in the port area provides large-scale secure network capabilities to control container handling processes in near real-time by minimizing downtimes for collaborating nodes.

Dissertation structure

The dissertation consists of three main sections, each having several sub-sections detailing the research work.

Section 1 reviews related work in the same research area including wireless and control technologies application in autonomous ports.

Section 2 details the development of a context data synchronization method and algorithm for cargo handling processes in the container terminal.

Section 3 details the experimental investigation of developed fuel consumption calculation and the proposed LoRaWAN communication system enhanced with a double encryption protocol.

The dissertation consists of 119 pages, 57 figures and 6 tables. 108 bibliographic references are listed at the end of the thesis.

Approval and publication of research

The main results of this dissertation have been published in the scientific publications:

CA WoS publications with IF:

1. T. Eglynas, S. Jakovlev., V. Jankunas, R. Diziokas, J. Janutėnienė, D. Drungilas, **M. Jusis**, E. Pocevicius, M. Bogdevičius, A.Andziulis. 2021. Evaluation of the energy consumption of container diesel trucks in a container terminal: A case study at Klaipeda port. Science Progress. Vol. 104(3), 1-25.
2. T. Eglynas, A. Andziulis, M. Bogdevičius, J. Janutėnienė, S. Jakovlev, V. Jankūnas, A. Senulis, **M. Jusis**, M. Bogdevičius, S. Gudas. 2019. Modeling and experimental research of quay crane cargo lowering processes. Advances in Mechanical Engineering. Vol. 11(12) 1–9.
3. T. Eglynas, **M. Jusis**, S. Jakovlev, A. Senulis, A. Andziulis, S. Gudas. 2019. Analysis of the efficiency of shipping containers handling/loading control methods and procedures. Advances in Mechanical Engineering. Vol. 11(1) 1–12.
4. Andziulis, T. Eglynas, M. Bogdevičius, M. Jusis, A. Senulis. 2016. Multibody dynamic simulation and transients analysis of quay crane spreader and lifting mechanism. Advances in Mechanical Engineering. Vol. 8(9) 1–11.

In presentations at international scientific conferences:

1. S. Jakovlev, T. Eglynas, **M. Jusis**, S. Gudas, V. Jankunas. Use Case of Quay Crane Container Handling Operations Monitoring Using ICT to Detect Abnormalities in Operator Actions. 6th International Conference on Vehicle Technology and Intelligent Transport Systems (2020), Čekija.
2. S. Jakovlev, T. Eglynas, **M. Jusis**, S. Gudas, E. Pocevicius, V. Jankunas. Analysis of the Efficiency of Quay Crane Control. The 7th IEEE Workshop on Advances in Information, Electronic, and Electrical Engineering, Liepaja, Latvija 2019.
3. T. Eglynas, **M. Jusis**, S. Jakovlev, A. Senulis, P. Partila, S. Gudas. Research of Quay Crane Control Algorithm with Embedded Sway Control Sub-routine. 27th Telecommunications Forum TELFOR 2019, Serbija.
4. **M. Jusis**, T. Eglynas, A. Senulis, S. Gudas, S. Jakovlev, M. Bogdevičius. Pietryčių Baltijos konteinerių terminalų apžvalga ir krovos tendencijos. Jūros ir krantų tyrimai 2017. p. 86-90.

1. LITERATURE REVIEW OF WIRELESS AND CONTROL TECHNOLOGIES IN AUTONOMOUS PORTS FOR CRANES AND AUTOMOTIVE GUIDED VEHICLES

1.1. Autonomous container terminals – new challenges and problems

Ports play a major role in the globalization of the world economy, as they provide the backbone for international trade. The increasing globalization of the leading European economies calls for higher efficiency from all transport sector participants. Lately, the seaports of the European Union have increasingly been under pressure to improve the efficiency of the operations by ensuring that transport and on-site cargo handling services are provided on an internationally competitive basis and following the EU regulations on the decrease of emissions. The efficiency of each port is linked not only to separate countries' economic development but also with the entire Region and thus monitoring the operational efficiency of each cargo handling process and comparing one technological solution with others in terms of their efficiency is an essential part of each country aim for improvement [4]. In recent times, the Baltic Sea region has shown great growth potential, even despite the global geopolitical challenges raised. The Lithuanian shipping containers' transportation sector has increased in volumes thanks to the timely modernization of the port operations and management systems.

In the section below, we will look at the main challenges and the latest technologies applied in ports to control not only individual processes but also the whole supply chain by using novel ICT solutions, context data acquisition, and knowledge extraction methods and algorithms for decision support.

1.1.1. The role of quay cranes to improve the performance of container terminals

Today, the Klaipėda city container terminal (LKAB Smeltė) located in Klaipėda Port is among the fastest-growing seaports in the entire region. The volume of the container traffic has increased, yet the operational efficiency has halted due to new regulations and standards. The most effective means to enhance the container handling operations is to improve the existing systems by synchronizing the operations on a technological level, by improving the level of services provided, which can be realized by fully utilizing invested resources such as quays, cranes, yards, and handling equipment.

Quay cranes play an important role in seaports for loading and unloading processes. They are used to move cargo from ship to store in a minimum time so that the load reaches its destination without swinging [5], [6]. The main

control objective is to move the trolley to a required position as fast as possible with low payload oscillation [7], [8]. This would decrease the time for cargo stabilization above the trucks, and thus, promote the adoption of newer operational mechanisms. Based on other research [9], we developed a concept for container terminal operation visualization in the perspective of operation synchronization (Figure 1).

Figure 1. Visualization of a container terminal in the case of operation synchronization area.

In the container transportation industry, loading velocity is an important issue as it translates into seaport productivity and efficiency. However, external disturbances such as wind can easily initiate an oscillation. Uncontrolled oscillations may cause cargo stability and safety problems, especially during the deployment and retrieval phases of the container. Usually, a skillful operator is responsible for quay crane loading and unloading operations. In precise container positioning by a human, who relies solely on his visual feedback, the operation can prove to be extremely challenging and time-consuming [10], [11]. During the handling operations, the load is free to swing. If the swing exceeds a safe limit, it must be dampened or the operation must be suspended until the oscillations decrease. It is practically impossible to completely remove payload oscillations in all possible situations. External disturbances such as wind, weather, or operator actions can easily initiate an oscillation [7]. This unavoidable cargo swing frequently causes loading and unloading processes efficiency to drop, damages the containers, or even causes accidents [12]. Nevertheless, the cargo handling operations are required to move the container to a required position as fast as possible, however, at higher transportation velocity, cargo oscillations become larger and complicate the unloading process [13], [14].

Also, this will cause the positioning inaccurate. To attain better positional accuracy of the quay crane spreader, a control system that accounts for the acceleration of the trolley and oscillation of the cargo is required. One of the most efficient and easiest ways given practical implementation is to use motion-profiling methods; however, fast motion commonly conflicts with the smoothness of motion due to the residual oscillation [15]. Reaching a compromise between the velocity of motion and the oscillation reduction is one of the challenging tasks in the motion profiling area for automated control systems [16]. To increase the motion velocity, it is necessary to control rapid increments or decrements of acceleration, which would cause high jerks. These jerks can be controlled. The jerk-limited profile is a common trajectory pattern used by modern motion systems and it is a time-optimal solution of jerk limited body control. The jerk limitation is used for the limitation of deformations and vibrations induced by the reference trajectory, which can be generated to cancel or reduce the oscillations [17]. The jerk-limited integration into the trapezoidal velocity profile gives us the symmetric or asymmetric s-shaped velocity profile. The smoothness of motion in these profiles depends on jerk duration. Longer duration increases smoothness but decreases the time efficiency.

Information regarding the control of the processes (decreasing the inaccuracies of cargo fluctuations during handling operations) could theoretically be synchronized with the central planning system, which appropriately includes these factors in the Time Scales plan. In this way, evaluating the crane operators and other technical characteristics of the system can enable the synchronization of individual processes to achieve optimal planning results.

1. 1. 2. The role of automated guided vehicles to improve the performance of container terminals

The AGV system is widely used in the manufacturing industry, port, and dock as a material conveying robot in the logistics system. AGV is flexible and intellectualized. But many factors make an error during AGV implementing a given route. With the development of port construction and automated terminals, AGV positioning technology of current ports is single and the perception and understanding of the external environment are insufficient, which directly affects the operational efficiency of ports.

To achieve greater efficiency of container terminals the researchers apply a variety of efficient modeling approaches. Lal Kumawat et al. applied a stochastic modeling approach to parallel process flows using two-phase

servers to estimate the throughput gap between parallel and sequential process flow models [18]. Similarly, stochastic modeling is used for analyzing the performance of overlapping loading and unloading operations that recorded the complex stochastic interactions among quayside, vehicle, and stack side processes. In this way scientists, by creating a fairly accurate model, can analyze terminal design decisions such as analyzing the effect of guide-path topology (dimensions and number of shortcuts), varying proportions of loading/unloading on system performance [19]. Other modeling techniques are also developed for multidimensional performance evaluation of container terminals according to logistics and operational, corporate social, financial, and environmental dimensions [20] or looking for ways to design new terminals with maximum efficiency [21].

With the growing popularity of AGV in container terminals, some previous studies have focused on integrated scheduling for handling equipment coordination and AGV routing [22], multi-AGV scheduling for conflict-free path planning [23], or optimal strategies for the yard truck scheduling in container terminal [24] to minimize the traveling distance and finding the shortest time to finish the loading and unloading of containers. Other studies of crane scheduling in automated container terminals are also conducted applying mathematical models, metaheuristics, numerical experiments, or random topology particle swarm optimization algorithms [25], [26].

In the research literature, some relevant information is still missing concerning the place of AGV in the supply chain, by synchronizing various contextual information (e.g., instant fuel consumption, battery reserve, and energy consumption, etc.), the position in the terminal, the status of the operation and other information related to planning activities. All this information synchronized with the planning tools will allow us to plan the cargo handling operations more accurately, but will also make changes to the plan in near real-time, depending on the real situation in the container terminal area.

1. 1. 3. The analysis of container lowering processes

Intermodal shipping containers are widely used in the global transport chain to deliver various goods to end-users. Despite the obvious advantages, there is still plenty of room for improvements, when it comes to increasing time efficiency and quality. The global transport market is a network of companies and end-users, who rely on well-managed standards and systems. Recent trends and numbers suggest that about 90% of non-bulk global trade is being managed by shipping containers worldwide [27], [28]. In 2016

Europe alone managed 0.8 billion tons of cargo [29]. Statistics show that between 2007 and 2017, shipping volume increased by 66% (up to 148 million TEUs), taking into account the global merchandise trade by marine traffic [30]. Many engineers and managers worldwide foresaw such a rapid increase. Yet, they could not manage it optimally. Thus, efficiency is a criterion, which needs to be increased to adopt new challenges of the future. Cargo loading operations rely on loading and unloading speeds, the safety of operation [31], and energy consumption in the vicinity of the port [28]. These factors tend to make final decisions when adopting new and untested technologies in practice.

The modernization of container terminals through modern ICT (Information and Communication Technology) solutions partly solves the problems concerning the "green" terminal initiative [32]. The autonomy of operations is adopted in many areas to control the stability of container handling, transportation using terminal trucks, AGV [33], etc. Even now, newly built cranes are using operators on-site to manage the loading procedures [34]. Each new operator sees the loading standards as guidelines but not strict rules. Therefore, crane autonomy [35] is necessary to increase the efficiency of adopted standards and regulations, mechanical systems, and associated port investments. An autonomous quay crane is not an innovation on its own [25]. These complex systems already exist [36]. They are applied in many areas of the industry including port operations [37]. On the other hand, the modernization of existing infrastructure is a priority for most companies, working with container handling. A more practical and real solution is to modernize existing systems, rather than purchase all new expensive infrastructure. Overall, there are crane stabilization systems that are already in use [38], but they mostly lack quality feedback and operator experience, which makes a huge impact on the efficiency of these expensive systems [39].

In practice, the realization of complex control solutions is limited by the fluctuations of the spreader with the load. Its movements are random, due to external impacts, such as wind or physical contact with other objects [40]. It is difficult to predict such random deviations in practice. In the most advanced European ports, such as Rotterdam or Hanover, the handling procedures and IT operations are mostly automated. However, the inclusion of the modern automated quay cranes is still an innovation for smaller ports throughout the world. In the light of the research and progress made in this area [1], [3], [12], [41], [42], many ports in the world lack the application of these innovations.

Increasing the time efficiency of the cargo process is a topical issue addressed in the scientific work, for which various solutions are proposed,

from management algorithms to cargo planning solutions [28], [33], [43]. The quay cranes are analyzed in the way of increasing loading time [28], [44], damping the load swinging during the loading-unloading process [44] using additional feedbacks in control system with the PID or PI controllers or using artificial intelligence analysis [13], [45]. One of the commonly used controller models is presented in Figure 2.

Figure 2. Crane control model using PID regulator (MATLAB Simulink) [13].

The application of these modern control tools alone results in the increase of efficiency in all cargo handling situations so that it can be applied in practice. However, the research results of recent years show that input profiling together with the PID controller yields promising results [13], [14], [45]–[47]. The PID controller is most widely used in industry due to its simple structure and stable operation under various conditions [48]. Liu [49] has developed a control system that used fuzzy logic and a PID controller to manage the transport of bridge crane loads. The scientist presented a complete system and the results of the research that show that the combination of these modern control technologies yields effective results and could be realized in real systems. However, most scientists are confronted with the correct setting of the PID controller in the crane operation [50]. Traditional parameter matching techniques, such as the test and error method, are one of the easiest ways to reconcile the PID controller, but the results obtained by this method do not guarantee significant and effective results. Depending on the results obtained due to the aggressiveness and excessive fluctuations in the variations, researchers have used other methods to reconcile the parameters of the PID controller.

The port crane and the truck data synchronization is the main problem addressed here. The crane operator has to wait for the terminal truck or the terminal truck has to wait for the operator to finish his unloading routine. Due to constant operators' faults delaying the end-of-shipment procedures many operations require changes and delays occur. Many solutions propose to use real terminal truck and crane spreader sensory data to make their synchronization. Depending on the actual position of the terminal truck or the

crane, decisions are made systematically to slow down the speed of movement so that the target point is reached at the same time by all involved bodies. This saves both energy resources and technical resources, and increases crane and consequently, the entire port efficiency [51].

To sum up, if these handling processes were monitored using sensory data recorded and transmitted to the information management centers in a near real-time manner, it would optimize the cargo handling operations for the entire supply chain. Each operation plays an important role in managing transportation costs, synchronizing the tasks for subsequent processes in the terminal.

To achieve greater efficiency of container terminals the researchers apply a variety of efficient modeling approaches. Lal Kumawat et al. applied a stochastic modeling approach for parallel process flows using two-phase servers to estimate the throughput gap between parallel and sequential process flow models [18]. Similarly, stochastic modeling was used for analyzing the performance of overlapping loading and unloading operations that recorded the complex stochastic interactions among quayside, vehicle, and stack side processes. In this way by creating a fairly accurate model, scientists can analyze terminal design decisions such as examining the effect of guide-path topology (dimensions and number of shortcuts), varying proportions of loading/unloading on system performance [52].

However, if the terminal were upgraded for higher load capacity and minimal energy consumption, the tasks of scheduling, optimization, and synchronization of the loading processes would be solved more efficiently. Sha et al. [3] propose a novel integer programming model to solve the optimal problem of yard crane scheduling with minimal energy consumption at container terminals from the low carbon perspective. The yard crane scheduling problem considering risk caused by uncertainty was also analyzed by [53].

With the growing popularity of AGV in the container terminals, some previous studies have focused on integrated handling equipment scheduling, coordination and routing [22]. Other research included multi-AGV scheduling for conflict-free path planning [23], or optimal strategies for the yard truck scheduling in container terminals [54] to minimize traveling distance and find the shortest time to finish the loading and unloading of containers. Other studies of crane scheduling in automated container terminals are also conducted applying mathematical models, metaheuristics, numerical experiments, or a topology particle swarm optimization algorithm [26], [55].

Many researchers have focused on optimizing container stacking and unstacking in the container terminal. Zweers, Bhulai, and van der Mei

proposed a new optimization model in the stochastic container relocation problem in which the containers can be moved in two different phases: a pre-processing and a relocation phase [56]. Xie and Song proposed optimal planning for container pre-staging by applying a stochastic dynamic programming model to minimize the total logistics cost [57]. Some previous studies proposed an integrated optimization approach to determine optimal crane and truck schedules and optimal pickup sequence of containers [25], [58]–[60] leading to lower time and energy costs in the logistics process.

The optimal scheduling problem was also analyzed by Lu [61]. The author examined the multi-automated stacking cranes and their scheduling methods for automated container terminals based on graph theory. Other critical factors, like energy consumption of quay cranes (QCs) were analyzed by Tang et al. [32]. The author dealt with the performance of peak shaving policies for quay cranes at container terminals with double cycling where some evaluation indicators were selected for assessment including the observed peak power demand, the productivity, and utilization of QCs and the average waiting time of yard trucks (YTs).

The modeling of processes in container terminals is also not limited to the application of classical methods. Advanced methods are used in recent studies. Zhang et al. applied machine learning-driven algorithms for the container relocation problem [62]. A combined data mining – optimization approach to manage trucks operations in container terminals with the use of a truck appointment system that reduce empty-truck trips was proposed by [63]. Some previous studies have also shown that a multi-agent optimization approach can be used for container terminals for the reactive and decentralized control of container stacking in an uncertain and disturbed environment [64] or a system dynamics simulation model to achieve the stable state of the main parameters of intermodal terminals [60] [23].

The scheduling and optimization of technological processes is a key problem while developing autonomous container terminals considering energy consumptions and container loading process synchronization that has not been fully investigated in the literature.

1. 2. Methods for autonomous vehicles movement control and navigation in port area

Taking into account the need for data exchange and process synchronization, assessed in section 1.1, it is necessary not only to make a correct choice choosing the right data exchange technology and synchronization method, ensuring the integrity and sustainability of the port

operations. In this section, widely known truck and AGV navigation technologies are presented that are currently used by many ports all around the globe. The following technologies are used in modern AGV navigation systems in port areas:

- Electromagnetic lines method.
- Electromagnetic reference point method.
- Laser navigation method.
- Optical navigation methods.
- GPS navigation method.

These technologies are briefly summarized and their key parameters are discussed below in this section. This analysis was conducted to show the main disadvantages of these systems and their low adaptability in the autonomous terminal. However, most of these technologies can be combined and with new emerging methods and systems, to increase response time, the accuracy of navigation and agility for autonomy. Despite the technology being used for tracking AGV in the port environment, cranes still miss the vital information to adjust their handling processes efficiently. The crane operators and control system lack in-time information to assess the container handling capacity in the long term.

All these technologies allow us to identify the location of the AGV or other transport vehicles in the port, increasing the level of autonomy for all container handling processes, it is possible to achieve the higher objectives that the European Union is pursuing today to achieve the Green Port initiative [4].

1. 2. 1. **Electromagnetic lines method**

AGV navigation by electromagnetic lines (Figure 3) is an old and reliable control method with an accuracy of ± 2 mm that is applicable to the control of both open and closed AGV [65]. The main components of this method are: guidewire, very a low-frequency generator, antenna, and autonomous vehicle. The metal strip is laid out according to the required, pre-planned route on the concrete pavement or in an incision of approximately 2.5 cm of concrete. An electric current of appropriate frequency flows through this band, which generates an electromagnetic field. The frequency required for the line is generated by a very low-frequency generator e.g., HG G-57400 with standard generated frequencies ranging from 5 kHz to 10 kHz.

Figure 3. Metal strip with a very low-frequency generator [66].

The antennas that are attached to the carriage are very close to the ground and sense the electromagnetic field. The antenna itself consists of two coils. Each coil generates a different electrical voltage, which increases as it deviates from the route. It is the difference between these voltages that determines where the electromagnetic line is and a control signal is generated to tilt the AGV towards the route [67] (Figure 4).

Figure 4. Antenna interaction with magnetic field [67].

In order for the AGV to know its position, a cross-antenna is used that looks for other electromagnetic lines perpendicular to the route. The system will know the position of the relevant AGVs on this basis. Electromagnetic reference points are installed at the intersection of routes, which have their unique codes [67]. With the help of these points, the control system decides where to rotate the routes at the intersection.

The analysis of this management system distinguishes the following advantages [65], [67]: reliable system, low error probability; the system is suitable for working in a dirty environment; such systems will have an integrated emergency stop function; developed technology used for more than 60 years.

The main disadvantages mentioned in [52], [65], [67]–[69] are as follows: the metal next to the line affects the magnetic field and distorts it; this reduces the accuracy of route tracking; the electromagnetic line will be placed only on a hard surface such as concrete; laying a line on ordinary land would be a

challenge if the line is broken, without the assistance of additional systems, the AGV will not move further and the whole system may become stuck; it takes time to troubleshoot such system failures, as it is necessary to change the line or part of it; lines are installed for the realization of a specific route. It is necessary to change the whole line in order to change it, which is costly. It is essential to choose the right route layout and to carry out detailed planning to obtain maximum efficiency.

1. 2. 2. **Electromagnetic reference point method**

When discussing the electromagnetic line system (Figure 5), it is necessary to mention another system of a similar type, the electromagnetic reference point system. The electromagnetic reference point system replaces continuous metal bands into transponders. It is used to control the AGV in the port of Rotterdam and is also used in conveyor and automatic assembly platforms and container cranes. It has an accuracy between ± 3 and 30 mm [65].

Figure 5. BPMN diagram of electromagnetic reference point navigation method.

The main components of the electromagnetic point system are transponder, antenna, scanner, an autonomous vehicle with an inertial navigation system. In this system, unlike in the electromagnetic line system, AGV does not follow the route according to metal lines but uses electromagnetic reference points – transponders. The transponder itself is a passive component that has a recorded code within it that transmits to the system when a variable electromagnetic field is activated by an inductive transponder when a floating electromagnetic field is created by an AGV antenna [65]. When the scanner receives the sent code, it is interpreted and then the system decides in what position the AGV is in and where to go further (Figure 6). In order not to deviate from the route, as in the method in Section 1.1, the antennas will

measure the deviation from the electromagnetic field and, as appropriate, the deviation-generated control signal for the route diversion of the AGV [69].

Figure 6. Working principle of the transponder [65].

Transponders are positioned at appropriate distances from each other and distances are selected as needed. It should be noted that the greater the distance between transponders the lower the accuracy of the system, since then it all depends on the inertia system that controls the movement of the AGV from point to point by following the movement trajectory of the machine and the antenna may not be deducted the transponders if the AGVs appear in the center of the transponder group and these are located further than the antenna visibility field [70]. Deviations from the route in this system occur because the inertia systems increase their error over time. Various filters are used for this purpose, one of which is the Kalman filter [71]. Deviations in the system are also caused by the reflection of the antenna signal from various objects, thus reaching a single transponder several times (multi-path phenomenon) per signal. For this purpose, the distance from the antenna to the transponder will be as small as possible and the Dolfo-Chebyszew antenna array method may be used, which allows the suppression of signal reflections and the achievement of more transponders [72].

The analysis of this navigation system distinguishes the following advantages [65]: high accuracy; there is no need to physically build long lines compared to the electromagnetic line method, but it is sufficient to install transponders over appropriate distances. Also, changing the route is cheaper; it can operate in all weather conditions and the system is resistant to snow, dust, ice; transponders require little care because they are passive.

Disadvantages [25], [67], [71] are metal structures near the route affect accuracy; signal reflections mislead the system and reduce accuracy; the AGV inertia system increases its bias over time, so additional methods and techniques need to be used to solve this; failure of any transponder causes problems in the system that may damage traffic.

1. 2. 3. **Laser navigation method**

After a discussion of electromagnetic systems, it is possible to access other types of systems that are based on optical navigation methods. The first is a laser system. The laser operation of the AGV navigation system is based on the principle of laser scanner interaction with reflected reference points. It can achieve an accuracy of up to ±2 cm and is used in enclosed spaces with good visibility [65]. The main components of the laser control system are a laser scanner, reflective reference points, and autonomous vehicles. The laser scanner acts as a transmitter and a pager. It rotates at an angle of 360° around the vertical axis and emits laser beams in one direction at a speed of 8 revolutions per second. These rays return to the laser scanner at different points of time and count the distances to the reference points and the angle at which they are from the scanner [67]. Below is an example of interaction between the laser scanner and the reference points (Figure 7).

Figure 7. BPMN diagram representing AGV laser navigation method.

When the angles and distances to the reference points are determined and these data are sent to the control system, the target will calculate the location of the AGV following the principle of triangulation and compare it with the known map (location) of the reference points recorded in memory [67]. When comparing existing data with the default system, the AGV movements are made to allow it to return to the route and move it through regular verification of its location. Also, the laser system has the ability not only to search for reference points but also to respond to obstacles, thus further expanding and

exploiting the laser scanner. It can scan the outlines of obstacles, draw a two-dimensional contour map [71] and decide how to overcome the obstacle with the help of the control system. A two-level map with a module can be used to increase the adaptability and flexibility of the navigation system. The first level is a map showing the objects closest to the AGV, and the second level is a map showing the location of the environmental zones. Such a system allows for more complex autonomous transport, loading and unloading operations [73]. The laser control system can be adjusted using the unscented Kalman filter (UKF) and the fuzzy interference system (FIS). UKF is used for system error measurement and processing, for guessing sensor values based on available data, and FIS for dynamic noise reduction. With the help of these improvements, AGVs can move at higher speeds [74].

The laser localization system can be extended using the IEEE 802.15.4a wireless sensor network (WSN), which is used as a localization and communication module. The Kalman filter is replaced by the Monte Carlo particle (MCP) and anchor box methods to find passive reference points. In such a system laser localization takes a secondary role and is used to adjust the system. The most important advantage of such a system is the determination of the AGV position without any preconception [75].

The analysis of this navigation system distinguishes the following advantages [65], [71]: high precision system (± 2 cm); no need to make any changes to the running surfaces, which makes this system flexible and the cost of changing routes is not high. The laser scanner can detect obstacles and their dimensions.

Disadvantages include [65], [69]: extraneous reflective surfaces can cause inaccuracies and errors in the system; snow, dirt, light may also have a negative impact on the system's activity. Reference points will be freely visible and will not be obstructed by other objects so that the return beam reaches the scanner. For this reason, considerable time is spent adjusting the positions of the reference points.

1. 2. 4. Optical navigation method

In addition to the laser system, there are also several methods based on optics: navigation by tracking colored bands, navigation by following environmental features. The color tape method, presented in Figure 8, is characterized by accuracy of ± 2 mm and an object identification system with accuracy of less than ± 5 cm. The optical methods in question are used in enclosed, clean rooms with good visibility [65]. Main components of the AGV

navigation method based on color tape tracking: colored tape, IR sensor array or other optical sensor arrays, autonomous vehicle.

This method is very similar to the electromagnetic line method considered in Section 1.1, only here it is a passive band that does not generate electromagnetic fields.

Figure 8. BPMN diagram of AGV control method using a color line.

Accordingly, sensor arrays are selected based on the color or black and white of the bands. If a black band is used on a light drive surface, an infrared matrix may be used; if the tape is colored, an optical matrix must be used which is capable of distinguishing bands of different colors. The matrix is attached to the front of the AGV to observe the strap underneath. The separation of the color tape from the background in the optical system takes place in a relative contrast, in the case of black-and-white bands – a dark strip on a light background or a light tape on a dark background. This contrast difference allows you to find the edges of the tape and thus separate it from the background. During movement, the tape is tracked if the AGV deviate from the route (the tape moves away from the middle of the sensor), then control signals are generated to rotate towards the route [67].

Transponders (as in Section 1.2.2) may be used to mark important locations on the route. These places may include intersections, stopping points, loading points, etc. An optical navigation system based on the memorization of environmental features (objects) no longer uses colored bands for routing, and the camera tracks objects in the environment and their features. As the AGV moves, the distinctive features in one frame are shifted in the other frame, and by comparing a few frames and creating an optical flow vector, the system can decide where these features have moved [67], [71].

The analysis of the object tracking navigation system can distinguish the following advantages [67], [69]: no environmental change is required; can see obstacles; metals or metal structures adjacent to the route are not affected;

Disadvantages [67], [69]: blurred, distorted image misleads the system; the system does not function properly without recording the features and their change in the frames; poor operation in unlit, low visibility rooms. Some calculations are required for frame processing, which means that a significant amount of computer resources is needed, i.e. memory to do so.

1. 2. 5. GPS navigation method

GPS is used for the management of AGV. A BPMN diagram of such a system is presented in Figure 9. This system is used in open areas because the satellite signal does not pass in closed areas. The system can reach an accuracy of up to ±2-10 cm [65]. The main components of the satellite AGV navigation system are a GPS module with an antenna, satellites, base station, and an autonomous vehicle.

Satellites send information about their location and time at appropriate time intervals, while the GPS module with an antenna captures the signals of these satellites and calculates the time of arrival of the signals. The estimated times are proportional to the distance from the satellite to the GPS module and the GPS module learns its coordinates using the triangulation method [76].

Figure 9. BPMN diagram representing a GPS-based AGV control system.

To obtain greater positioning accuracy (up to some centimeters), a base station (Figure 9) is used, which is located in a fixed location and also captures satellite signals. When the GPS module is connected by radio to the station, the position is adjusted to increase accuracy. It is also necessary to assess where to attach the GPS antenna, as this position may alter the change in positioning efficiency to 600%, thus creating additional errors [77].

The analysis of the satellite navigation system distinguishes the following advantages [65]: a flexible system because routes can be programmed and reprogrammed through management programs. The only additional environmental change required is the mother station.

Disadvantages are: [65], [71], [76] adverse weather conditions or satellite signals can render the GPS almost incapacitated; the system operates only in

open areas; to calculate the exact position of the AGVs, the GPS module must contact at least 4 satellites. The accuracy of GPS is directly linked to the number of satellites and the signal strength. The construction of the base station on-site is a costly initiative.

1. 2. 6. Short sub-section discussions

The technologies mentioned in Section 1.2 could be used to track the movement of AGV or other heavy port vehicles. They are used more frequently nowadays to optimize the planning and scheduling of tasks. New technologies are widely adopted by the industry to fill the technological gaps and provide the port operators with all necessary information for decision support. Technology combination provides more opportunities to implement green port ideas and brings them closer to solving the challenge of synching individual processes. Wireless technologies analyzed in the next section (RFID, LoRaWAN, Wi-Fi, 4G, 5G, etc.) could improve the existing infrastructure both at the technical and software levels. It is no secret that the performance of the container terminal depends not only on the technical equipment and other resources but also on the planning methods and systems. A well-planned container handling process ensures optimized operations for other technical means of the port.

However, in many cases, the systems in question do not evaluete the near real-time triggers. Navigational and other systems for tracking the movement of the vehicles on-site do not ensure operational handling. Therefore, researchers analyze not only factual information received from the planning systems but also the contextual information received from sensory technologies. This allows making the right decisions during the container handling process.

In Section 1.3, other technologies are presented which provide the necessary additional information for knowledge extraction to make an optimized decision for container handling.

1. 3. Alternative wireless communication technologies and LoRaWAN application for port operations

In many ports around the world, various IT technology infrastructures for data transfer and reception at the terminal are increasingly being expanded. Modern network technologies and positioning equipment are some of the most necessary infrastructures in modern port operations to efficiently automate the port loading process. Real-Time Locating System (RTLS) allows determining the location of process operators on-site or heavy moving objects in near real-

time. This system uses tags that are attached to the objects needed to be tracked. Base main stations can scan these tags remotely to determine their location and get primary information about the object. Various technologies are applied to increase the accuracy of the measurements, including GPS, Wi-Fi, RFID, mobile communication (4G, 5G, etc.), LoRaWAN, and more. These technologies have their advantages, but also restrict their technological adaptability.

1. 3. 1. Analysis of RFID data transmission

RFID means the use of radio frequency waves for wireless data transmission. RFID systems consist of three main parts – RFID scanner, RFID antenna and RFID tags. RFID systems can be divided into active RFID and passive RFID (Figure 10). The main difference between active and passive RFID systems is the use of tags. RFID tags are divided into two categories: active and passive tags. Active tags have a separate power source and operate in a larger range. Passive tags do not require an additional power source but operate in a smaller range. Passive RFID tags have two main components: an antenna and an information storage chip connected to it. Meanwhile, active RFID tags have three components: an antenna, an information storage chip connected to it, and its own separate power source.

Communication between the RFID scanner and the tag is conducted in several different ways, depending on the frequency band used for the tag. The markings operating in low LF and high HF frequency bands are very close to the scanner antenna in relation to the radio wavelength. In this nearest field region, the tag is closely connected to the scanner transmitter. The tag can change the electromagnetic field created by the scanner by changing the electrical load in the mark. When switching between lower and higher relative loads, the tag creates a change that the scanner can detect.

At UHF and higher frequencies, the tag is more than one radio wavelength from the reader, so a different approach is needed. To retrieve information that is stored in the passive RFID tag, the tag must be within the range of the electromagnetic field emitted by the RFID scanner. The electromagnetic field created by the scanner causes the movement of electrons through the tag antenna, thereby acting as a microchip for storing tag information. The chip in the bookmark then responds by sending stored information to the scanner in the form of another radio signal. This is called retrospective dissemination. The scanner detects and interprets electromagnetic radio wave feedback, which then sends data to a computer or microcontroller [78].

Figure 10. BPMN diagram of passive RFID tag read principle.

When sending a signal to the antenna, a certain amount of energy is radiated. The antenna cannot generate more energy but can concentrate the transmitted energy to make it more concentrated. This concentration or focus effect performed by the antenna is called antenna stripper, measured in dBi. The antenna concentrates energy, so we get more signals, range or distance.

RFID systems are of different frequencies. Different radio frequencies behave differently in certain situations. It is therefore necessary to choose the appropriate frequency for the development of the radio transmission system. Low-frequency RFID systems operate at long wavelengths. This helps the signal to overcome even thin metal surfaces. In addition, low-frequency RFID systems are ideal for reading water-rich items such as fruits or beverages, but the range of operation of such systems is small, limited to centimeters. High-frequency RFID systems can operate without interference when installing RFID marks on metal surfaces. Also, such systems can work with objects that contain water. Typically, HF RFID systems operate in a range of 5-15mm, but their maximum reading range is approximately 3 meters. Ultra-high frequency RFID systems typically have a higher operating range (up to 15 meters depending on the RFID system setup), as well as faster data transmission than low- and high-frequency RFID systems. However, since UHF radio waves have a shorter wavelength, their signal is more watered down. This reduces the efficiency of such a system when working with metals or water.

In the laboratory scaled prototype of AGV, the RFID tag was mounted on the aluminum container model, which was raised by an aluminum design crane. In the light of the literature examined, it was decided to choose an RFID data transmission system with an operating frequency of 13.56 MHz. Higher frequency RFID systems can operate at high speeds and transmit information faster compared to lower frequency RFID systems. However, the transmission of low-frequency information is a better solution to the

development of the described container security system laboratory model, due to the reduced response of communication signals to metal objects located nearby.

1. 3. 2. GPS technologies in ports

The GPS positioning system is a Global Navigation Satellite System (GNSS) via US satellites. There are also more existing GNSS systems: Russian-owned GLONASS, China's Beidou and Galileo in Europe. This system works by receiving signals from the satellites flying around the planet. The device on Earth's surface receives signals from at least 4 satellites. A triangulation method is used to determine the position of the device at a certain point in time [79]–[81].

There are many seaports around the world using GPS positioning technology to determine the location of cranes or AGV. One example is that the GPS positioning system was adapted to Busan Port terminal [82]–[86]. The system used low-cost GPS positioning devices that were connected to AGV and ECH. This made it possible to monitor the location of the technique in real-time.

The use of GPS is widespread in the freight transport market due to reasonable price, system stability and sufficient accuracy. However, such a system often results in poor GPS connectivity or the complete absence of GPS signals in container terminals. For example, in a container terminal, under an STS crane, where containers are placed in rows to heights. Interference occurs when the GPS positioning device captures signals that are reflected from nearby surfaces. This problem is even greater when signal interference is caused by metal surfaces. In places where the satellite signal is poor, the accuracy of the positioning system may decrease drastically [87], [88].

1. 3. 3. Advantages of the combination of RFID and GPS technologies

The alternative that scientists around the world point out is a positioning method that combines two or more technologies and thus compensates for each other's shortcomings. In other words, although the overall positioning is performed by GPS, RFID technology activates and starts positioning operations when the satellite signal is unstable, its quality is poor and there are not enough visible satellites. In places such as tunnels where the satellite signal is completely switched off, the satellite navigation system cannot calculate positions. RFID technology could be used here to combine GPS and RFID. Until the satellite signal is received, the RFID antennas are positioned

in that field to scan the RFID tags on moving objects, thus complementing the accuracy of the positioning system [52].

1. 3. 4. **Wi-Fi technologies in port**

Ports are changing. The level of integration of different wireless devices, software agents and activities, together with increasing connectivity between different logistics chain actors has created a new ecosystem in which new risks have appeared. Cybersecurity is one of the challenges of the industry and policymakers, and an engineers and cybersecurity specialists should work alongside to ensure that these critical infrastructures [89] are adequately protected while facilitating the full development of new remote communication technologies in a sector that has relatively lagged behind others in transitioning to the new "4.0 world" [90].

Wi-Fi, called Wireless Fidelity technology, is a wireless network communication industrial standard, proposed by IEEE and called the IEEE802.11 standard. It is short-distance wireless communication technology. In port operations, Wi-Fi and wireless subsequent communication play an important role in data transmission between local network points [91] to increase the data flow security and speed [89]. These communication links work as a key technological solution for inner data flows within the organization, supplying the transport chain with decision support functionality, allowing operators to make predictions and control operations, plan shipments, trucks and supporting logistics services.

Global location services are being developed by many companies all over the world. Major players of the smart logistics domain, namely HERE Technologies with Sigfox company, proposed new opportunities to apply Internet of Things (IoT) solutions for containerization, particularly in supply chain and logistics [92]. By integrating global coverage of Wi-Fi hotspots and utilizing the worldwide network and geolocation engines, the industry is presented with unique assets localization tools, for both indoors (including inside factories warehouses and other buildings) and outdoors, without any additional infrastructure, regardless of the size and quantity of assets [93].

On a global scale, the use of IoT asset tracking solutions for the supply chain and logistics sectors could theoretically create huge economic value for all participants, according to Cisco and DHL. Taking into consideration that current RTLS technological and software solutions are not always viable due to high costs and short battery life constraints, the adaptation of low-power and high range technologies is a vital key for success in the coming years, namely the adoption of LoRaWAN with local decision support.

By referencing thousands of Wi-Fi hotspots in the container terminals around the globe companies will be able to pinpoint the location of millions of connected containers, trucks, cranes, technological solutions and control devices all around the world in the coming years.

1. 3. 5. Honeycomb network technologies in port (4G, 5G)

Recently ports started to use worldwide technologies like 4G or new generation 5G. These new technologies and communication standards will transform the cargo handling operations by developing intelligent infrastructures that will allow the container to communicate directly with both the target destination as well as all machines and humans along the supply chain in the port and to synchronize its movement with little downtime. With the many different departments and organizations operating at seaports, including coastguards, customs, transport authorities, operators, managers share data using a single platform, decreasing the delays and promoting a smarter, safer and more efficient working environment [94].

These new collaborative research opportunities, promoted by a number of research organizations worldwide, along with the key technology innovators, show that the autonomous and fully digitized inter-connected seaports are becoming a reality, and a key ingredient to making it happen is 5G technology [95]. It provides fast and high bandwidth and is an ideal platform for standardized and seamless communications [96].

1. 4. LoRaWAN Technology in port

It is necessary to use new generation wireless technologies in ports. LoRaWAN [97] in the case of wide range data transmission combined with modern nowadays technologies could be the best choice to increase data transition accuracy and decrease installation costs.

1. 4. 1. Analysis of LoRaWAN technology

Recently, LoRaWAN has been proposed (Figure 11) to enable IoT low data-rate applications that require transmitting and receiving a small amount of data with a range of a few kilometers. The data rate in LoRaWAN can vary between 0.3 and 50 kbps. The maximum achievable data rate depends on the receiver range and the environment interference level. LoRaWAN technology is designed to be power efficient to cope with the power constraints of IoT devices [97]. Also, LoRaWAN operates within unlicensed frequency bands, ranging between 868 MHZ and 900 MHZ, which compensates for the licensing cost and makes this technology affordable. However, transmitting at

low frequencies and long range is restricted in some regions. Consequently, the LoRa Alliance has defined different frequency plans that vary on a regional basis. Furthermore, in the same region, there might be a difference in the permitted transmission frequency bands based on countries' regulations.

Figure 11. Rich picture of the LoRaWAN network for IoT applications in ports.

Generally, LoRaWAN uses a wide bandwidth which helps to resist both interference and noise. On the other hand, LoRaWAN uses the star topology as shown in Figure 11. IoT devices are connected to LoRa End-devices (EDs): AGV, stacking crane, quay crane, which are connected directly to one or many gateways (GWs). Each GW is connected to the network server (NS), which can be connected to one or many application servers (ASs). The connection between LoRaWAN EDs and GWs is a LoRaWAN wireless communication, while the connection between the GW and the NS and AS is an IP connection [98]. Additionally, an ED can be connected to a LoRa GW by using one of the following activation techniques: Over-The-Air-Activation (OTAA), or Activation by Personalization (ABP). After the activation phase, the EDs start communicating their messages to the GW. However, these messages should be authenticated and encrypted by using a network key and an application key AppKey. The NS knows all NwKeys of all EDs, while the application server knows all AppKeys of all EDs. However, the difference between the ABP and the OTAA activation modes is that in the ABP activation mode, all the secret keys and addresses are static and they are stored at the ED, and the EDs are

directly connected to the NS without any request. While in the OTAA activation mode, the secret keys are dynamically generated.

1. 4. 2. Short comparison of data transmission methods for synchronization

According to the information presented in sub-sections 1.3 and 1.4.1, the following technologies more relevant to port operations improvement are compared. Figure 12 demonstrates the 3 main categories of wireless communication, taking into account the Range of communication and Bandwidth.

Figure 12. Comparison of wireless communication technologies [99].

Despite the fact, that communication methods like Wi-Fi or Cellular networks prove to be efficient in transferring a large amount of data, their adoptability in harsh environments is limited by many factors (shielding of the signals, added noises, weather conditions, etc.). The comparison of these technologies is presented in Table 1.

Table 1. Comparison of wireless communication technologies.

	LoRa	Wi-Fi, BLE	Cellular (4G)
Range	Long	Short	Long
Bandwidth	Low	Low	High
Power usage	Low	Low	High
Usage examples	Sensors, actuators and tags	Video/Voice, consumer IoT	Remote outdoor use case
Cons for application in port	Lower bandwidth	Low coverage, a lot of equipment needed	Dependency from a service provider

Port operations require stable communication with enough bandwidth to send basic sensory data to the planning systems. LoRaWAN technology provides the best technical characteristics to be used in various scenarios for improving port operations, including long-range communication in container terminals, between base stations and moving objects, eliminating signal shielding by metal obstacles. Many other advantages of this method were described previously.

1. 5. Section conclusions

1. Many researchers have focused on optimizing container stacking in the container terminal. Zweers, Bhulai, and van der Mei proposed a new optimization model in the stochastic container relocation problem in which the containers can be moved in two different phases: a pre-processing and a relocation phase [56]. Xie and Song proposed optimal planning for container pre-staging by applying a stochastic dynamic programming model to minimize the total logistics cost [57]. Some previous studies proposed an integrated optimization approach to determine optimal crane and truck schedules and optimal pickup sequence of containers [58], [59], [100], [101] leading to lower time and energy costs in the logistics process. These studies are relevant in dealing with processes synchronization and improving the efficiency of current systems.

2. Modeling of processes in container terminals is also not limited to the application of classical methods, advanced methods must be applied to ensure the efficiency of long-term operations for the entire transport chain. Some previous studies have shown that a multi-agent optimization approach can be used for container terminals for the reactive and decentralized control of container stacking in an uncertain and disturbed environment [64] or a system dynamics simulation model to achieve the stable state of the main parameters of intermodal terminals [60].

3. The port transport tracking systems reviewed in the section show that their individual use often does not produce the desired result, and their application in planning systems has so far not been sufficiently discussed in scientific work. However, it is often mentioned that the adjustment of these tracking systems, by combining additional technologies, allows for more precise positioning in the area of the terminal, as well as the possibility of collecting not only movement data but also contextual information. Applying the latter data to synchronization and real-time planning of loading work can have a significant impact on optimized

performance. To synchronize the movement data between trucks and quay cranes, LoRa technology was chosen due to its unique properties dealing with long-range communication tasks in harsh environments, optimal for port operations. LoRaWAN networks provide higher interference immunity compared to other wireless communication technologies (SIGFOX, LTE-Cat 1, LTE-M, NB-LTE) while maintaining optimal battery usage using sleep mode and high link threshold values. Therefore, it was concluded that in order to solve these problems it is necessary to use LoRa technology for secure and reliable connections for handling processes synchronization.

4. This whole overview allows evaluating individual operations and in the context of synchronization to optimize the loading process and maximize port autonomy. Also, it enables the selection of the correct technologies for each handling operation. In the following section, we will discuss the methodology developed for port process synchronization and the method proposed for sensory data transfer.

2. DEVELOPMENT OF METHODOLOGY FOR PORT OPERATION SYNCHRONIZATION – METHOD AND ALGORITHM

2.1. Application of LoRaWAN technology for data synchronization in the port area

2.1.1. LoRaWAN technology and its adoption for data synchronization

Among the various wireless technologies used to bridge the gap between sensors and gateways to the Internet, there are solutions inspired by the cellular communication approach. In these cases, the wireless end-devices are linked with the base station, which defines a one-hop cell; the base stations are connected with a backbone network (wired or wireless). However, despite the current cellular network infrastructure, 4G technology could potentially address many IoT scenarios. The complex architecture and the demanding protocol stack result in the high computational capability of the end-nodes, which in turn implies high-cost and high-power consumption, something not compatible with most of the actual applications. Only the next generation technology (5G) promises a mass deployment in the future. Therefore, other technologies are used in this field today: Low Power Wide Area Networks (LPWANs). Their main advantages are the wide-area coverage and the reduced number of base stations, thanks to the innovative radios that trade off the sensitivity with the throughput; the simplified communication protocol stack that, in turn, reduces the infrastructure complexity. Consequently, both the power consumption and the cost are diminished. Currently, the consumer market, the industry, and the academic world are proposing/using several LPWANs; the 3rd generation partnership project (3GPP) itself standardized the so-called Narrowband-IoT or NB-IoT in LTE release 13, focusing on machine-to-machine, delays tolerant communications. Nevertheless, the use of licensed bands affects costs as well and makes device management cumbersome (e.g., due to SIM cards). At this time, most of the adopter consensus is achieved by LoRaWAN, which has been turned into a de-facto standard. It is an open standard defined by the LoRa Alliance that now is implemented in many commercially available devices from multiple manufacturers. The LoRaWAN wide success is demonstrated [102] by both the constantly increasing applications in various scenarios, and the huge available scientific literature.

Figure 13. Rich picture of the proposed LoRa application concept.

Uplink is of main concern for typical LoRaWAN networks and the focus of the test methodology is about uplink data flow characterization. In this case, end-user traffic is injected in the LoRaWAN network under test employing a probing node and it is collected out of the AS in accordance with the actual AS implementation. A simplified diagram is shown in Figure 13, where for sake of simplicity a single NS implementing all the network level functionalities is depicted. In particular, in agreement with the LoRaWAN specifications, the uplink user data flow can be further split into the following sub-flows (it has to be noted that a similar approach can be used for evaluating the joining procedure as well): F0: from the end-user data source to the mote (data injection); it is out of the backend scope; F1: from the mote to the gateway; it is the only wireless portion of the overall data flow; F2: from the gateway to the NS; F3: from NS to the AS; F4: from the AS to the end-user data destination (data extraction).

2. 1. 2. Application of LoRaWAN: security and application possibilities

NB-IoT (Narrow Band IoT) is LPWAN technology mainly used by 3GPP cellular systems. NB-IoT is characterized by a small degree of complexity and high throughput. This technology has been also integrated into the LTE system with some enhancements such as extending the battery lifetime and reducing the device cost. This optimization was also intended to ensure better performance by introducing new measurements related to channel quality. However, NB-IoT uses the same frequency as LTE and uses the QPSK modulation [103]–[106]. As a result, a comparison has been made and summarized in Table 2 between the new leading technologies such as SIGFOX, LTE-Cat1, LTE-M, NB-LTE.

Table 2. LoRaWAN and other wireless technologies comparison.

Features	LoRaWAN	SIGFOX	LTE-Cat 1	LTE-M	NB-LTE
Specification	Open	Private	3GPP	3GPP	3GPP
Spectrum	Unlicensed	Unlicensed	Licensed	Licensed	Licensed
Modulation	SS chip	UNB/ GFSK/ BPSK	OFDMA	OFDMA	OFDMA
Rx bandwidth	500 Hz – 125 kHz	100 Hz	20 MHz	20-1,4 MHz	200 kHz
Data rate	290 bps – 50 Kbps	100 bps	10 Mbps	200 Kbps – 1 Mbps	20 Kbps
Max. #Msg/day	Unlimited	UL: 140 msgs/day	Unlimited	Unlimited	Unlimited
Max output power	20 dBm	20 dBm	23-46 dBm	23-30 dBm	20 dBm
Link threshold	154 dB	151 dB	130 dB+	146 dB	150 dB
Power efficiency	Very high	Very high	Low	Medium	Medium to high
Interference immunity	Very high	Low	Medium	Medium	Low
Security	Yes	No	Yes	Yes	Yes
Mobility/ localization	Yes	Limited mobility, no localization	Mobility	Mobility	Limited mobility, no localization

It can be concluded that adding the haystack into LoRaWAN technology can solve certain limitations [102, 106] towards making LoRaWAN more efficient and secure. Also, open specification and usage of unlicensed spectrum simplify initial system development. High power efficiency and high interference immunity are promising features for communication system development in the harsh port environment.

Secure data transmission is the main aspect in LoRaWAN at port applications. Data encryption in a protocol is one of the ways to ensure secure data transfer between two nodes. Based on the LoRaWAN security survey issues, threats and possible mitigation techniques [98], the integrated security mechanisms for LoRaWAN were developed and presented in Figure 14.

Figure 14. Security mechanisms developed and integrated into LoRaWAN.

To join a LoRaWAN network, each device must provide credentials that satisfy a network server that it is a legitimate user. Conversely, the device needs to be able to tell whether it is connected to the systems for which it is designed. This ensures that only genuine and authorized devices will be connected to genuine and authentic networks. To support these requirements, at manufacture each LoRaWAN device is personalized with a unique 128bit AES key, known in the protocol as the AppKey. The device is also provided with a globally unique identifier, DevEUI that is based on the IEEE EUI64 address space. Each network has its identifier based on a 24bit address range and managed by the LoRa Alliance.

AppKey is central to the over-the-air activation or join procedure in LoRaWAN. It ensures that both the end-device and the network infrastructure can agree that they are talking to legitimate systems and so continue to bring the device onboard.

2. 1. 3. Algorithms of adoption of developed LoRaWAN technology

According to the conclusions of Section 1, LoRaWAN technology was chosen to develop a process synchronization method. LoRaWAN nodes (installed at the quay cranes and AGVs) execute a generalized algorithm for data extraction, processing and data transfer to a software agent (Figure 15).

Each network node periodically (at intervals 0.01 to 0.20 sec) reads the data from the sensory unit and performs data packet preprocessing for further transfer: groups into larger intervals, counts average values. This preprocessing is necessary to reduce the amount of data transmitted.

Figure 15. The data acquisition and transfer algorithm for each LoRaWAN node.

The data extraction interval could be pre-selected for a longer period, but recent studies have shown that it decreases the resolution of the data, which is relevant for the evaluation of the initial data. After the period and after processing, the data is encrypted applying the AES-128 algorithm using AppKey. The encrypted data is then added to the LoRaWAN data packet, which uses Network Session Key to additionally count the MIC (Message Integrity Code). MIC is similar to a checksum, except that it prevents intentional tampering with a message. Network Session Key is used to validate the integrity of each message by its MIC. Finally, the generated package is sent to the server.

Figure 16. Data flow diagram for the total AGV assignment process.

The data flow diagram in Figure 16 shows the AGV task assignment algorithm in the container terminal. This algorithm is initiated in the main control station and decisions are based on the data from the LoRaWAN nodes, presented in Figure 15.

The main station (decision support module) receives data from the quay crane and AGVs on-site, saving them in a database. Then, prediction methods are applied to estimate the exact container arrival time – time stamps. According to these time stamps, the system distributes the control tasks for the AGVs. This algorithm evaluates AGV motion characteristics in near-real time and decides which AGV must be assigned to take the container. This method is performed periodically (tested up to 1 second).

The next sequence diagram (Figure 17) shows an example of the synchronization of two processes.

Figure 17. Handling processes synchronization sequence diagram.

The sequence diagram shows that the STS crane node periodically transmits spreader movement parameters to the server. At the same time, the AGV node transfers its movement data to the same server, where the decision support module is located. It calculates the actual fuel consumption at each moment and makes predictions. The decision support module checks which nodes are communicating and are assigned for container pick-up tasks from these STS nodes (Figure 17). Decision support systems are often developed using various data-driven methods, including learning-driven solutions based on AI. As an example, Zhang et al. applied machine learning-driven algorithms for the container relocation problem [62], by developing a data mining optimization approach to manage trucks operations in the container terminals. Similar data-driven solutions considered multi-agent optimization approaches [64]. These complex solutions require detailed analysis of the operations, processes and technologies. By using AI to improve the process of decision support, industry representatives could increase the efficiency of not

only individual operations on-site, but also increase the turnarounds of the containers on a global scale.

The concept of LoRaWAN network for container terminal presented in Figure 18 was proposed by the author.

Figure 18. Concept of LoRaWAN network in a container terminal.

The equipment layout was based on the Google Maps picture of Klaipėda city container terminal presented in Figure 19.

Figure 19. The satellite view of the container terminal in Klaipėda.

The LoRaWAN network consists of LoRa nodes (7 stacking cranes, AGV, 3 quay cranes) that periodically send movement data to the network gateways. There are several gateways in the terminal area to ensure full coverage and effective communication when the moving nodes are between obstacles. The

gateways are connected via a fiber-optic network to a local Cloud server with the running software agent. If these nodes are interacting, then the preferred velocity is calculated for that specific AGV to arrive under the quay crane at the exact moment of container placement. This information is sent back to the AGV and thus this process of communication is performed constantly between all nodes in the network. The layout presented in Figure 18 is an ideal place to implement the proposed communication method. Other communication technologies described in the previous sections are limited by the environment. LoRaWAN can bridge sensors and decision support modules within this territory with fewer lost data packets than conventional systems.

2. 2. Methods developed for the synchronization of container handling processes

2. 2. 1. Developed concept for the data synchronization method

The concept of the developed container handling processes synchronization is shown in Figure 20. The white rectangles describe the inner processes of the quay crane, container trucks and newly designed modules; the green rectangles demonstrate the processes needed for data collection, transmission, and processing, thus, the synchronization of the overall processes presented.

Figure 20. Concept model of the synchronization of container handling processes (swim lane diagram proposed by the author).

53

During the container handling process, performed by the quay crane, data is continuously collected from the sensory units on the spreader, in the cabin and from other technical means. This data is periodically transmitted through the LoRaWAN communication module to the central server where the total container handling time is forecasted by the smart agent software modules. In parallel, the AGV data collection modules collect information about the movement of the AGV, preprocesses the collected data and periodically sends this information via LoRaWAN to the server. The sever then performs a forecast of the actual fuel consumption from the real data and calculates the best container pick-up scenario (speed and accelerations of the AGV or choose of another AGV already in place).

Finally, the decision-making module checks which AGVs are interoperable to reach the quay crane during the final stage of the container's lowering on the ground. The calculated needed speed is sent to a specific truck through the LoRaWAN communication network. The AGV control unit then gives a command to the speed control system to increase or decrease the actual movement speed. This operation is done permanently and without any stops.

2. 2. 2. AGV positioning algorithm

The existing AGV positioning systems combine inertia and ultrasonic navigation systems, global positioning systems via satellites and complement these systems with additional technological components (Figure 21). These combined positioning systems allow achieving greater accuracy when navigating is made between containers in a stack.

Figure 21. Developed algorithm for AGV positioning (flow chart diagram).

The described algorithm has an incorporated ultrasonic positioning system which is calibrated. The deviations of the axles are zeroed. If the coordinate system has recently been calibrated, the previously used settings are loaded.

The inertia navigation system is activated and the position tracking is started. Stationary position beacons used in this inertial navigation system are located throughout the terminal area, their position is constant. Mobile beacons are mounted on the trucks and AGVs. Stationary beacons generate a data package and broadcast it. Mobile beacons calculate their position using the triangulation method via computational modules. Information packages are then prepared and sent to the AGV to the data processing subsystem.

The following subsystems are enabled in the AGV controller: data processing, route control, chassis control, and interruptions detection modules. Interruption's modules are used for monitoring engine revolutions used for PID control. Then the saved route is loaded from the local server, updating the information and making comparative analysis. Upon acquiring the updated information, the exact points of the route are checked and the desired route points are calculated. Based on the calculated route, the control of the engines is performed, increasing or decreasing the speed of the truck. The constant speed of the AGV is ensured by controlling the breaks. The system of the brakes uses control subsystems, measuring interruptions affecting the actual rotation of each of the wheels, thus measuring the speed. This is done using the proposed PID control mechanism. The entire AGV control algorithm, starting from data acquisition and ending with the braking of the trucks (AGV) is executed cyclically.

The synchronization of load processes is aggravated by some factors (Figure 22). They can be arranged into 4 groups: human errors, environmental impact, technical equipment failures and software. The most important one is the human factor. Quay crane operators, although experienced or less experienced, still perform additional unnecessary actions, delay the start of operations, fail to help the ground personnel with the container handling at the initial stage. Also, often problems for the operators of the cranes begin with man-made errors during the planning stage. Although the planning is carried out by the specific software, it is unable to assess contingencies, constantly changing terminal infrastructure, so the final inspections and changes are carried out by a specialist who knows the specifics and operations of the terminal. This is a problem because due to his absence or illness, the accuracy of the planning decreases drastically. Since different companies work with different software, their interoperability is limited, many data transfer inconsistencies occur, making the data transfer process unreliable and too long for the optimized solution to be made. Data must be converted from one format to many others, which requires additional technical and human resources. The global supply chain also is limited by these factors, making global-scale decisions outdated from the start.

Figure 22. Port cargo handling process cause and effect (fishbone) diagram.

When customers provide documentation about the onboard containers, their placement is already mixed inside the stack of the ship and their position is not optimized for fast handling at the endpoint. This is due to unforeseen changes during the loading process which is forgotten and the planners are not notified. These errors are detected only during the container handling process by the cranes and must be repaired immediately, which immediately affects the time planned to complete process.

Another group of factors is the technical equipment. In it, each damage of the cargo requires a separate procedure for document forming. If the equipment fails, then additional equipment is required that can quickly replace the damaged ones, and if the cargo is unstable, this leads to greater fluctuations during its handling by the crane. All these factors prolong the process of container handling, both by the crane and the trucks (AGVs).

The handling process is also influenced by the environment. In the case of strong winds (more than 20 m/s), the container handling process is stopped due to strict safety regulations. Strong wind gusts increase the fluctuations of the container when it is moved by the gripper, which complicates the lowering process, and thus, the trucks have to wait additionally for the container to stabilize naturally, with little help from the operator, who can only stabilize

the container by increasing the tension of separate cables holding the spreader. This leads to downtimes for both, cranes and AGVs.

2. 3. Mathematical modeling and prototyping of the small-scale port environment

In this sub-section, a mathematical model is presented for the calculation of the fuel and energy consumption for each AGV. The calculated parameters show the momentum of fuel consumption at each point on the route of the AGV. This model is unique, allowing the near real-time data to be updated instantly in the server, calculating the needed parameters for process synchronization. To determine the best crane spreader sway oscillation control parameters for optimal container handling, a laboratory prototype was developed.

2. 3. 1. Method of fuel consumption calculation from GPS and acceleration data

These methods allow the real-time assessment of the vehicle movement efficiency on-site. A model was used to calculate energy consumption, with the following assumptions: the mass of the truck, its coordinates, and the acceleration values were recorded for each point in the 3D space (Figure 23); the forces, accelerations, and velocities intersect at a single point of mass; the coordinates are calculated for every single point of the mass of the modeled body.

Figure 23. Model of the AGV.

In the model, the total mass m_t consists of the mass of the truck and the mass of the container on top of it. The total mass changes over time with different containers. At some point in time, two containers can be placed on the truck (TEU containers). For example, Figure 24 demonstrates the changes in the total mass during a single cycle of the truck in the terminal obtained by direct observation. We can see that the truck waited up to 300 seconds for the crane to load the container. The first 20 feet of the container was unloaded

from the truck in the stack by the end of the 440th second. The second 20 feet container was unloaded from the truck by the end of the 640th second and the truck went back to the crane by the end of the 800th second, which concludes the full cycle.

Figure 24. Example of the total mass change during a single cycle in the terminal.

Next, we present the energy consumption model necessary for the estimation of the energy losses during these full cycles in the terminal. The model uses the calculated rolling (0.0098) and air (1.69) resistance coefficients. To calculate these coefficients, additional measurements were made with the truck, and the measuring equipment during the experimental phase. Detailed methodical explanation is presented in Section 3.2.4.

The following equation (1) presents the energy consumption of the truck that is required for acceleration or maintain constant velocity:

$$E_{mov} = \int_{t_s}^{t_e} P_{mov} dt, \tag{1}$$

where t_s – the starting time point t of the truck work cycle (ship-stack-ship), t_e– the ending time point t of the truck work cycle (ship-stack-ship). Truck movement power P_{mov} is calculated using the following equation:

$$P_{mov} = \begin{cases} F_T(t) \cdot |v(t)|, & \text{when } a_{horz} > 0 \\ 0, & \text{otherwise} \end{cases}, \tag{2}$$

where $v(t)$ – the velocity of the total mass body at the exact time, $a_{horz}(t)$ – the acceleration value of the body (explained below in (5)). The total resistance force $F_T(t)$ of the movement of the body is calculated for each time point t:

$$F_T(t) = F_{in}(t) + F_{air}(t) + F_{roll}(t). \tag{3}$$

58

The inertial force $F_{in}(t)$ resisting the movement of the body at a given time t is calculated by Newton's second law:

$$F_{in}(t) = m_t(t) \cdot a_{horz}(t), \tag{4}$$

where $m_t(t)$ – total mass of the body at each time t, $a_{horz}(t)$ is the truck acceleration at each time t that is calculated by summing up the two accelerations in the plane of movement of the truck:

$$a_{horz}(t) = \sqrt{a_{long}(t)^2 + a_{lat}(t)^2} \cdot \text{sign}\left(a_{long}(t)\right), \tag{5}$$

where $a_{long}(t)$ – the acceleration of the truck at a specific point in time is measured along the longitudinal axis of the AGV (Figure 23), $a_{lat}(t)$ – the measured acceleration of the truck at a specific point in time, perpendicular to the movement axis of the truck.

The vertical acceleration $a_{vert}(t)$ running perpendicular to the movement axis of the truck and the plane of movement. This acceleration was not used in the calculation of the energy cost estimation model.

The air resistance force $F_{air}(t)$ acting on a moving truck at a specific time is calculated as:

$$F_{air}(t) = c_a A \frac{\rho}{2} (3.6 \cdot v(t))^2, \tag{6}$$

where c_a – air resistance coefficient, A – truck air resistance area m^2, ρ – air density at normal conditions kg/m^2.

The rolling resistance force $F_{roll}(t)$ acting on the moving truck at the specified time is calculated as:

$$F_{roll}(t) = m_t(t)gf_r, \tag{7}$$

where g – gravitational acceleration (9.81 m/s2), f_r – rolling resistance coefficient.

The energy consumption E_{br} of the truck for active braking is calculated according to:

$$E_{br} = \int_{t_s}^{t_e} P_{br} dt. \tag{8}$$

This energy is lost by converting it to heat in the engine or/and brakes. It can be recovered using an electric motor – generator. Break power P_{br} (W) is calculated as:

$$P_{br} = \begin{cases} F_T(t) \cdot v(t), \text{when } a_{horz} < 0 \wedge F_T(t) < 0 \\ 0, \text{otherwise} \end{cases}. \tag{9}$$

The energy consumption model presented above was calculated by numerical integration using the rectangular method. The integration step was determined by the recording frequency of the recorded data, which was 10 ms. Energy consumption was calculated only for those periods when the truck was moving. The data which was recorded when the truck was not moving was excluded from the calculations to reduce the errors caused by measurement noise, in energy calculation.

The following assumptions have been made in the calculation of fuel consumption. The fuel consumption of a truck consists of two parts: fixed to maintain the efficiency of the truck, and variable (to overcome forces resisting movement to increase or maintain a constant velocity); in the variable part, the relationship between the power supplied to the truck wheels and the fuel consumption of the engine at that time is linear.

Constant fuel consumption (l/s) component at a specific point in time is:

$$c_p(t) = p_f b(t), \tag{10}$$

where p_f is the constant component coefficient. The binary factor $b(t)$ determines whether the engine is running at a specific time:

$$b(t) = f(x) = \begin{cases} 1, & \text{when the engine is ON} \\ 0, & \text{otherwise} \end{cases}. \tag{11}$$

A variable component l/s/W of fuel consumption at a particular point in time:

$$c_d(t) = d_f P_{mov}(t), \tag{12}$$

where d_f — constant component coefficient and fuel consumption (l/s) at a specific point in time is:

$$c_t(t) = c_p(t) + c_d(t). \tag{13}$$

The component factors are calculated from the truck's measurement data: masses, accelerations, velocities, and total fuel consumption during the measurement period C_t (l).

By integrating the elements of (13) during the measurement period (from t_s to t_e) we get the total fuel consumption:

$$\int_{t_s}^{t_e} c_p(t)dt + \int_{t_s}^{t_e} c_d(t)dt = \int_{t_s}^{t_e} c_t(t)dt \tag{14}$$

or

$$\int_{t_s}^{t_e} p_f b(t)dt + \int_{t_s}^{t_e} d_f P_{mov}(t)dt = \int_{t_s}^{t_e} c_t(t)dt. \tag{15}$$

As a result, we get:

$$p_f \int_{t_s}^{t_e} b(t)dt + d_f E_{mov} = C_t, \tag{16}$$

where p_f and d_f, there are two unknowns. Other elements are derived from the measurement results. A two-equation system was created to find unknowns by using data from two separate measurements (indices 1 and 2):

$$\begin{cases} p_f \int_{t_s}^{t_e} b_1(t)dt + d_f E_{mov1} = C_{t1} \\ p_f \int_{t_s}^{t_e} b_2(t)dt + d_f E_{mov2} = C_{t2} \end{cases}. \tag{17}$$

System (17) in matrix form:

$$A = \begin{bmatrix} \int_{t_s}^{t_e} b_1(t)dt & E_{mov1} \\ \int_{t_s}^{t_e} b_2(t)dt & E_{mov2} \end{bmatrix}, B = \begin{bmatrix} C_{t1} \\ C_{t2} \end{bmatrix}. \tag{18}$$

Now we can write:

$$A \begin{bmatrix} p_f \\ d_f \end{bmatrix} = B. \tag{19}$$

The coefficients are calculated as:

$$\begin{bmatrix} p_f \\ d_f \end{bmatrix} = A^{-1}B. \tag{20}$$

To calculate fuel and energy consumptions, it is necessary to have the components of the resistance to the movement of the truck. The calculation methodology of these components is presented in Section 3.2.4. To find these components, experimental field measurements were performed to determine the necessary data for the calculations. To calculate the energy usage required to transport the container, it is necessary to self-assess the coefficients of aerodynamic and total resistance to the movement of the truck. The methodology for determining these coefficients experimentally is given below.

The coefficient of total rolling resistance f, is determined when the truck rolls freely on a level road surface in still air. During the experiment, two runs were performed: at a high initial velocity v_{a1}, and at low initial velocity v_{a2}. In both cases, the duration of time t_1, t_2 were measured until the velocity of movement of the truck decreases to the minimum: v_{b1}(during the first ride), v_{b2} (during the second run).

This methodology can be applied up to velocities $v_{a1} = 30$ km/h. The determination of aerodynamic drag coefficient c_d had the same procedures as for determining rolling resistance. This methodology also applies to velocities up to $v_{a1} = 30$ km/h.

The total rolling resistance coefficient is calculated according to:

$$f_r = \frac{28.2 \cdot (a_2 \cdot v_1^2 - a_1 \cdot v_2^2)}{1000 \cdot (v_1^2 - v_2^2)}, \tag{21}$$

where v_1 – average velocity is determined as:

$$v_1 = \frac{v_{a1} + v_{b1}}{2}, \tag{22}$$

where v_{a1} – initial set velocity, km/h, v_{b1} – minimal set velocity, km/h, a_1 – average acceleration is calculated as:

$$a_1 = \frac{v_{a2} - v_{b1}}{t_1}, \tag{23}$$

where t_1 – time of the experimental drive test, v_2 – average velocity km/h is calculated as:

$$v_2 = \frac{v_{a2} + v_{b2}}{2}, \tag{24}$$

where v_{a2} – normal set velocity, km/h, v_{b1} – minimum set velocity km/h, a2 – average acceleration, and calculated as:

$$a_1 = \frac{v_{a2} - v_{b2}}{t_2}, \tag{25}$$

where t_2 – time of the experimental drive test.

The aerodynamic drag coefficient is calculated according to the expression:

$$c_a = \frac{6 \cdot m \cdot (a_1 - a_2)}{A \cdot (v_1^2 - v_2^2)}, \tag{26}$$

where A – the area of the truck with the container, m^2, m – total mass of the truck kg is calculated as:

$$m = m_t + m_{kont} + m_{kr}, \tag{27}$$

where m_t – mass of the empty truck (ready for operation), m_{kr} – mass of the cargo kg, m_{kont} – mass of the empty container kg.

Based on these methodologies the real field experiment was performed (see in Sections 3.1.4 and 3.2.4) to determine the rolling resistance and air drag coefficients, which were used in the energy (fuel) consumption model and energy (fuel) consumption calculation.

2. 3. 2. Development of a crane control system prototype

New Quay crane control methods require the adoption of novel ICT technological solutions and testing environments, attempting to solve the

container sway problems caused by a complex set of effects from the operational environment. The proposed method includes a prediction of these parameters by evaluating the nature and minimizing the effects of the sway on the handling process. The basic structure of the developed laboratory prototype is presented in Figure 25.

Figure 25. The main system components of the quay crane prototype.

The laboratory crane is fixed by a relatively flexible connection to the laboratory ceiling. The lower arms of the boom face the guideways for the horizontal trolley movement. The trolley top is equipped with a sensor net for trolley movements and position measurement. In the lower part, the pulleys are used for lifting a spreader holder. A sensor network is also installed at the top of the spreader, recording its swing angle, speed and position. The spreader and the lifting mechanism are controlled through the main unit, which is equipped with transmission gear and an electronic automatic control system installed. This system consists of a control module, motors, trolley and clamp speed sensors and a power supply. After performing virtual checks of the quay crane lifting mechanism and spreader system and constructing a laboratory prototype for experimental research, it was necessary to simulate the quay crane's control system in a computer environment. The control task signal was programmed using a speed change profile that has been selected through experimental and theoretical studies. Based on the analysis of the scientific literature and the evaluation of the effectiveness of the PID

controller in this type of crane control systems, described in sub-section 1.1.3, it was decided, to select the appropriate speed profile for the input, which was combined with the PID controller for the control of the quay crane transportation process.

2. 3. 3. Crane spreader control mathematical model

The following mathematical model described the laboratory cranes spreader control sub-system, involving the PID and PI control methods developing the container anti-sway algorithm. Firstly, the converter performs conversion of the control signal to PWM signal which afterward generates the motor phase voltages U_A and U_B:

$$\begin{cases} U_A = f\big(u(t)\big) \\ U_B = f\big(u(t)\big) \end{cases}.$$

(28)

Then, the generation of voltages U_A and U_B are implemented using PWM signal modulation. The equivalent motor, which was used in the laboratory prototype, is the stepper motor. Motor equations is:

$$\begin{cases} \dfrac{di_A}{dt} = \dfrac{1}{L}(U_A - Ri_A - e_A) \\ \dfrac{di_B}{dt} = \dfrac{1}{L}(U_B - Ri_B - e_B) \\ M_v = -K_m\left(i_A - \dfrac{e_A}{R_m}\right)\sin(N_r\theta) + \\ +K_m\left(i_B - \dfrac{e_B}{R_m}\right)\cos(N_r\theta) - M_{bt}\cos(4N_r\theta) \\ \dfrac{d\theta}{dt} = \omega_v \end{cases},$$

(29)

where K_m – torque constant of the stepper motor, i_A and i_B – stepper motor coil current, e_A and e_B – the electromotive force of stepper motor, R_m – magnetization resistor, N_r – stepper motor tooth per pole, θ – single step rotation angle, M_{bt} – internal braking torque, R – winding resistance, L – winding inductance, U_A and U_B – A and B phase winding voltages.

Therefore, the S-shaped profile, as part of a single control system, can be used as a reference signal of the control system. A comprehensive mathematical model was also developed:

$$\begin{cases} \dfrac{d\varphi_g}{dt} = \omega_g, \dfrac{ds_{v\check{z}}}{dt} = v_{v\check{z}}, \\[2mm] \begin{bmatrix} \left(m_g + m_{v\check{z}}\right)\dfrac{ds_{v\check{z}}}{dt} + \\ +m_gL\dfrac{d\omega_g}{dt} + \\ +\dfrac{1}{R^2}\left(J_b + J_vU^2\right)\dfrac{dv_{v\check{z}}}{dt} \end{bmatrix} \cdot R_{dr} + M_{fr} = M_vU\eta \\[2mm] m_gL\dfrac{dv_{v\check{z}}}{dt} + m_gL^2\dfrac{d\omega_g}{dt} + m_gLg\varphi_g = 0. \\[2mm] J_v\dfrac{d\omega_v}{dt} = -B\omega_v + M_v \end{cases}, \qquad (30)$$

where η - the efficiency of the mechanical transmission, φ_g – the angle of the spreader (gripper) swinging, ω_g – the angular velocity of the spreader (gripper) swing, $s_{v\check{z}}$ – trolley displacement, $v_{v\check{z}}$ – trolley speed, m_g – the mass of the spreader with the load, $m_{v\check{z}}$ – the weight of the trolley, L – the length of the cable rods, R_{dr} – drum radius, J_b – moment of drum inertia, J_v – moment of inertia of the electric motor, U - reduction gear ratio, M_{fr} – friction moment, M_v – engine moment, indices: $v_{\check{z}}$ – trolley; g – spreader (gripper); s – pulley; v – motor, B – motor rotation damping.

Based on the crane lifting mechanism and spreader holder control system, the model was transformed into the Matlab Simulink environment computational structure presented in Figure 26.

Figure 26. Block diagram of lifting mechanism mechanical subsystem (MATLAB Simulink).

Where $M_{v.red}$ – gear reduced motor torque, M_d – dynamic torque of plant, $a_{v\check{z}}$ – trolley linear acceleration, ε_g – angular acceleration of spreader, s – Laplace operator.

In addition, in this model, a computational structure was developed to calculate linear kinematic parameters of cargo, linear load variation, speed and displacement. The crane lifting mechanism and the trolley's mechanical subsystem unit consist of two inputs and twelve exits for monitoring the system. Outputs describe the kinematic characteristics of the trolley and the

load. Inputs are provided for the momentum of the frictional force and the torque input.

2. 4. Section conclusion

1. The developed LoRaWAN network topology for the terminal operations is a crucial part of the decision support system because it allows developing a quality link for two-way communication between all network participants (nodes). A security mechanism is proposed to be used with the existing LoRa network to ensure the safety of the operation and data transmissions with double security on MAC and applications layers, suitable for individual cargo-handling processes. This communication technology was proposed for container handling process data synchronization, using a newly developed LoRa gateway structure. The proposed solution includes physical prototypes of the network equipment and a developed two-layer (Application and MAC) security mechanism in LoRaWAN, encrypted using the AES-128 algorithm by AppKey (Figure 14).

2. The proposed methodology and developed numerical models provide a way to calculate the momentum fuel consumption, necessary for the near real-time decision support. It allows us to monitor the entire AGV park in the terminal and control their movement based on the fuel consumption criteria. These control parameters are constantly updated in the system (on the server side). The decision support module uses it as a primary criterion to choose the appropriate AGV and Quay crane for each operation, transmitting the control commands to the moving AGVs on-site and receiving their fuel consumption data for further knowledge extraction and decisions. Therefore, a near real-time two-way secure and agile communication was established within the premises of the seaport containers terminal, relying on the optimized decisions for the Green Port initiative, including the use of ICT modules (LoRaWAN communication, Software agent), suitable for speeding up and securing the handling procedures.

3. EXPERIMENTAL INVESTIGATION AND DISCUSSIONS

3. 1. The description of the experimental use cases

In this section, the performed experiments are discussed, providing insights into technologies used for data acquisition, the technological processes and various other key aspects. This section explains the conditions of the experiments and the environmental impact of the surrounding container terminal. Use cases of the experimental investigation are based on the research findings, mentioned in Section 1, and according to the methodology described in Section 2. In the following sub-sections, 4 experimental use-cases are presented with brief descriptions.

3. 1. 1. Use-case 1: Experimental investigation of the quay crane control algorithm using the developed laboratory scaled prototype

This experiment was conducted to evaluate the proposed crane control algorithm to minimize the sway of the container during its transportation from point A to point B in accordance with the scale of the prototype. Figure 27 demonstrates the crane prototype scheme used for the testing of the algorithms.

Figure 27. Crane prototype scheme used in the experimental study in the laboratory.

This experiment was done in a laboratory environment, presented in sub-section 2.3.2. Weather conditions were not taken into consideration or modeled during the experiment. The scaled container was transported 1.9 meters in length. The algorithms from sub-section 2.3.3 were used to control the sway of the scaled container by controlling the speed of the scaled spreader. These experiments were carried out to ensure the effectiveness of the designed algorithms and to choose the best PID and PI control parameters and coefficients. The results of these experimental investigations are presented in sub-section 3.2.1.

3. 1. 2. Use-case 2: Experimental study of the data acquisition equipment used on the quay cranes.

The aim of this experimental research was to test the real working conditions of the quay cranes, the operators' work and conditions, the efficiency of the spreader and the unnecessary forces accumulated during the container handling operations. In recent years, researchers have worked closely with electrically powered terminal trucks and cranes [107], [108]. To assess the need for synchronization, this experimental research was performed at Klaipėda seaport. During the research, the quay crane carried out container handling operations, during which the statistical data was collected. Data was collected from 204 handling operations (full cycles). These full cycles include container transportation from the ship to the truck and from the truck to the ship. MK2 data logger hardware was used for these experimental measurements (Figure 28).

Figure 28. The data acquisition equipment used for experimental measurements at Klaipėda seaport.

When determining the dynamic parameters of the object under investigation (in this case – the container), data about its acceleration, speed, position in space, were measured and recorded. For this purpose, a DL1 - MK2 data logger (Race Technology, UK), a three-way accelerometer (guaranteed 2g minimum full scale on both axes; resolution of 0.005g; optional 6g sensor available as a factory option) vibration measurements (vibration factory tested

at 25g, 50Hz sinusoid for 5 minutes), was used to record and store vehicle motion dynamics parameters. For positioning, the meter is connected to a GPS antenna (GPS – module outputs position, speed, position accuracy and speed accuracy every 200ms with no interpolation; GPS tracking loops optimized for applications up to about 4g; tracking of all satellites in view). Based on the time course of the vehicle and the acceleration readings, the device measures the speed of the test object with an accuracy of 0.16 km/h, with a measurement error of up to 1%. Longitudinal and transverse accelerometers record accelerations up to 20 m/s2 and measurement error up to 0.05 m/s2.

This research aimed to experimentally prove the inefficiency of the current procedures and technological solutions. Collected data includes the duration of the separate handling procedures and general statistical information. These experimental results are discussed in sub-section 3.2.2.

3. 1. 3. Use-case 3: Experimental study of on-site quay cranes using data acquisition equipment

In the experimental research DL1 - MK2 data logger/analyzer was used to acquire and transfer statistical data (Figure 28). It uses a three-axis accelerometer. Dynamical characteristics were examined, including acceleration, speed and position. A GPS antenna was used to increase the accuracy. Movement speed detection accuracy was set to 0.16 km/h due to technological reasons and data logging accuracy was set to 1% due to irregularities in the electronics. The mounting point was set on the spreader, shown in Figure 29.

This position was chosen as more reliable and safer due to constant movements and obstructions, unnecessary hits in all areas. Battery life was not an essential part of the equipment. Its full capacity lifetime was enough to function on a regular basis for the entire period of experimentation (8000 mAh). DL1 – MK2 data logger chosen because it allows all the data to be referenced to not just time, but also a position during 3D movement. This allows the data to be interpreted in a strict understandable way, referenced clearly to the actual position and time stamp.

Braking points and gripper usage was analyzed with the built-in three-axis accelerometer enhanced for high downforce applications. It is capable of detecting minute changes with a 100Hz update rate on all attached sensors and accelerometer channels. It also provides 8 analog channels (with 0-20 V battery voltage) for sensor inputs ready for additional measurements and 2 CAN channels with up to 1 M baud rate with 14 CAN filters per channel (CAN 2.0 compatible).

Figure 29. Demonstration of the Data Acquisition sensory hardware placement on the crane spreader.

Logger itself has IP50 environmental protection, but due to the harsh working environment, it was decided to add additional protection via the secured hard plastic mounting case. Maximum power consumption set to 1.6 W. The aim of this experiment is to perform the data acquisition process and to show the exact placement of the data logging equipment. The results of these experimental cases are presented and discussed in Section 3.3.3.

3. 1. 4. Use-case 4: Experimental study of container truck movement and fuel consumption

This section describes how the experiment was conducted, what parameters were measured, and what was evaluated. Based on the presented methodology and the mathematical model, the provided equations can be used to calculate the energy consumption required to transport a container by a truck in the container terminal. Experimental studies were aimed to perform parameter identification of the model, i.e., to determine the coefficients of resistances required for the calculations.

The methodology (mentioned in Section 2.3.1) of the experiment was developed and the experimental studies of energy consumption were performed to compare with the results of the analytical calculations. The mentioned measurement (Figure 28) equipment was used during the data collection from the moving trucks. The equipment was mounted on the roof

of the truck using magnets. The equipment mounting position is presented in Figure 30 and Figure 31.

Figure 30. Demonstration of the trucks being used and the mounting point chosen for the experiments.

At the start of the experiment, the current fuel level was observed. The fuel level was checked every half an hour during the entire experiment. After an undefined amount of time during the operations, the vehicle was filled with fuel. The operators checked the fuel levels before and after the refuel, observing the displayed amount of fuel from the fuel pumps for more accurate results. Experimental measurements of non-autonomous container handling in the port territory were performed. Experimental measurements of the movement of the trucks with the containers from the ships to the stack were performed using modern measuring instruments. A total of 160 full cycles of the truck were analyzed.

Figure 31. Demonstration of the sensory unit placement on the roof of the truck.

The aim of this research is to experimentally test the developed fuel consumption methodology, its accuracy working in combination with the GPS equipment and the acceleration data. Detailed results and discussion of these experimental cases are presented in Section 3.3.4.

3. 2. The results of experimental research: quantitative analysis

3. 2. 1. Investigation of the quay crane control algorithm using the developed laboratory scaled prototype

The developed control algorithm was tested using a mathematical model implemented in MATLAB Simulink which is designed to determine the parameters of the PID controller, aimed to minimize load swinging in the trolley. Many literature reviews have been made (mentioned in Section 1.1.3) on this topic and many methods have been examined for adjusting the PID controller. In addition, some findings were also applied to our experimental test-bed, taking into account the complexity of the system and the hanging load, whose swinging is minimized. In our example, the research findings did not produce the desired results, and it was decided to combine the controller empirical and experimental results, by determining the controller coefficients resulting in minimal sway during the grabbing and the transportation procedures.

The proposed procedure of PID and PI controllers' parameters determination was divided into two steps. Firstly, the PID controller parameters were determined without auxiliary feedback to find the minimum value of the integral square error of trolley velocity and were obtained by modeling for initial calculations. Then the auxiliary feedback was activated.

Using MATLAB simulation, the PI controller parameters were determined, calculating the minimum integral criterion of the square error of spreader oscillation velocity (detail information provided in the author's publication). The first step of controller (PID) parameter estimation was carried out without feedback (crane trolley velocity and load variation linear velocity). The proportional part K_{p1}, T_{i1} – is the integral part, T_{d1} – the coefficients of the differential part. In the second simulation, the minimum square error tolerance has been set, but this is explained by the fact that the trolley does not reach the set speed (0.2 m/s) due to low amplification and therefore, by increasing the proportional part of K_{p1}, this deviation decreases. Therefore, $K_{p1} = 0.2$ was selected for another search and the PID controller integral component of the factor was determined. This step is used to minimize the steady state error of the trolley's speed, as increasing the coefficient of the integrative component increases the system response speed, and therefore the load swinging is much higher. According to the simulation results with only one feedback, the following parameters of the PID controller were obtained: $K_{p1} = 0.6$, $K_{i1} = 13$, and $K_{d1} = 0.01$. Using these parameters, the transition process of the crane trolley and load variation rates are presented in Figure 32.

Figure 32. S-shape velocity profile (green), trolley velocity (blue) and spreader oscillation velocity (red) graphs with PID controller and one feedback.

The second step was performed for the auxiliary feedback control loop with the PI controller designed to suppress container swinging. According to the results, it was determined that the additional PI system for reducing the intensity of cargo volatility has a higher error only with the proportional controller. This is a result of the integral part of the PI controller and the square error is increasing when the K_{p2} coefficient is being increased.

According to the simulation data and modeling results, the following PID and PI coefficients were chosen: PID: $K_{p1} = 0.6$, $K_{i1} = 13$, $K_{d1} = 0.01$, and

additional PI controller: $K_{p2} = 0.2$, $K_{i2} = 2$. The coefficients were calculated based on the trolley's integral square error minimal value in the PID and PI control system; the square integral error of the load swinging varies from this value every 3 percent. These control parameters are the initial data of the PID and PI controller for experimental evaluation.

These optimal parameters are suitable for the case studied for operation synchronization evaluations; therefore, the PID and PI parameters should vary and be adaptable. Such investigation is planned for future research. The experimental laboratory physical model was designed to analyze the theoretical and simulation findings. Results suggest that during the loading process using the S-shaped velocity profile in dynamic mode as control system input provides a possibility to obtain the most suitable solution for the transport modes of a specific container. The results of comparative and experimental studies show that the proposed autonomous quay crane's control algorithm, with a PI sub-system for decreasing container swinging during loading, can be used to accelerate the handling process as well as data for operation synchronization purposes.

3. 2. 2. **Statistical analysis of the quay crane and truck operations**

After processing the data collected during the experimental measurements, the entire loading process was divided into stages to identify which technological loading processes take the longest. The purpose of this experiment was to identify problematic operations in the loading process when scheduling a synchronization task, thereby justifying the need for synchronization. By synchronizing individual port facilities (such as terminal trucks and quay cranes) and by planning cargo operations accordingly, it is possible to minimize the impact of these problem areas on the loading time. These stages and summarized experimental results are given in the table below. The number of cycles n=102 was measured (from ship-to-shore).

Table 3. Quay crane handling operations and their durations.

Stage of loading	Mean	Min	Max	Standard deviation	Variation coeff. %
1. Start of lifting (hooking)	2.43	0.62	11.47	1.84	76.01
2. Vertical lifting	4.68	1.04	13.47	3.32	70.89
3.Diagonal lifting	5.14	0.79	9.84	1.97	38.28
4. Horizontal transportation	6.34	2.05	19.03	3.46	54.68
5. Diagonal lowering	6.36	2.72	23.97	3.05	47.90
6. Vertical lowering	7.25	1.66	19.13	2.86	39.42

7. Placing on vehicle	5.43	2.36	20.43	2.99	55.16
Total (Ship-to-shore)	37.63	11.24	117.34		

Experimental measurements were made when the cargo was shipped from the ship to the shore. Depending on the loading process, the operations were divided into 7 stages: 1. Start of lifting (hooking); 2. Vertical lifting; 3. Diagonal lifting; 4. Horizontal transportation; 5. Diagonal lowering; 6. Vertical lowering; 7. Placing on a terminal truck. The overall loading cycle in the ship-to-shore process was also evaluated. The summarized results of experimental studies show that the entire duration of the ship-to-shore cycle of the loading process during the transfer of cargo from the ship to the shore is in accordance with the statistical Log-normal distribution law.

The Log-normal distribution law hypothesis was tested by Pearson's Chi-square criterion. The histogram of the experimental loading times determined during experimental measurements is shown in Figure 33-A. After analyzing the loading process measurements in stages, steps 6 and 7 were chosen for further analysis, i.e., vertical lowering and positioning on the vehicle. These stages determine the crane-to-vehicle alignment to optimize the loading process and make it continuous. In Figure 33-B, the empirical distribution of the vertical lowering time is presented.

A.   B.

Figure 33. Distribution of the duration of the processes of the crane.

We can see that the vertical lowering mean time of the container t is equal to 7.3 s., and the vertical lowering height mean value is 8.8 m., considering the standard deviation as 4.5 m. The hypothesis of lowering Time Distribution by Normal law was tested by Pearson's Chi-square criterion. Experimental results show that the average weight of the container load during the experimental measurements is 22.2 tons and the standard deviation is 10.2 tons, coefficient of variation is 0.46. In Figure 34-A the distribution of the

loading phase duration when the load is placed on the terminal truck and detached is presented.

As we can see, shorter intervals predominate, they represent about 50 percent of the total (n=102) measurement results. The average duration is about 5.43 seconds, however, container placement can take up to 20 seconds. Duration of this step could be optimized by automation of loading process and this process could be about 2 seconds, as experimental results show. The purpose of the synchronization task is to make the vehicle arrive exactly when the load is lowered during the loading process. Therefore, experimental measurements were carried out when the equipment was mounted on container transport. The trajectory of the terminal truck in the port area and its waiting time at the crane were measured (Figure 34B).

A.   B.

Figure 34. Distribution of the duration of the processes of the trucks.

The results show that the waiting time of the vehicle at the container crane varies from 4 seconds to 34 minutes (2096 s). The average waiting time is 229 seconds. with a standard deviation of 346 seconds. This process is extremely unstable with a coefficient of variation of more than 150%. During the experimental measurements, the cargo was also evaluated (when mounting the equipment on the gripper, i.e., the closest point to the container). The velocities and accelerations of the moving load were measured. After processing the findings, we selected the best result, namely the experimental result of the fastest lowering of the load (Figure 35).

Figure 35. Statistical analysis of the results.

The results show that the investigated case of load lowering vertically was done in 1.9 seconds. The lowering speed of this situation is given in Figure 35-A. Here, speed values are negative because the load is lowered. We also watched the fluctuations of the load that influence the full automation of the process. The load fluctuations in the horizontal plane during lowering are shown in Figure 35-B. As one can notice, the container sways in a 10 cm boundary. This value suggests that the cargo is lowered stably and no outer forces affect the sway (wind gusts or operator mistakes).

The experimental results show the need for more sophisticated control of the crane-container terminal truck system, but to work in a real situation and try to improve the performance is difficult due to the intervention into the port operation. Therefore, that mathematical model for lowering the container was developed to serve as a tool for control system development.

Experimental measurements "in situ" of container lowering to the terminal truck have been investigated in detail and statistical analysis of the new experimental results carried out. Experimental measurements showed that the variance coefficient reached up to 150% during the final handling operation. These operation durations varied between 2.36 to 20.43 seconds, with a mean value of 5.43 seconds. The entire lowering cycle variation coefficient reached 55.16%. A shorter time boundary shows that the handling process is optimizable up to two times by scheduling the operations between quay crane and terminal truck operators and using specialized algorithms for lowering process control for each case. This could provide more stability to port operations and make processes and procedures more agile for long-term planning. Based on these findings, a methodology for crane and terminal truck, and AGV synchronization in near real-time was prepared. This methodology could be used to bridge the scheduling mechanisms into a single real-time synchronization system.

3. 2. 3. **Analysis of the container transportation operations**

During the experimental measurements, the number of container loading and unloading measurements was set to 278, due to port operations strict rules and cooperation agreements for the measurement period. Crane operators were warned that measurements would be made during their working hours to avoid legal problems. During the meeting with the working crane operators and truck drivers (who are also AGV operators), discussions were held to address the importance of these measurements and to see the vector of improvement. Some of the crane operators even expressed appreciation of the research. Figure 36 provides casual measurements from the loading and unloading procedures.

Figure 36. Spreader position detection and movement points during the container unloading operation from the ship.

Each measurement had its deviation and irregularity, considering the operator's "best choice" scenario set by the operational manual. Figure 36 demonstrates the positional movement of the container unloading procedure. Each container varied in mass, therefore, the average mass of 20 metric tons at this exact measurement, the mass of the container measured at 19220 kg. Figure 36, Figure 37 and Figure 38 demonstrate the 7 stages of operational consideration described in Table 3. Figure 37 demonstrates the actual speed values during these 7 stages for the process, described in Figure 36. Figure 38 demonstrates spreader and container sway oscillation values.

These values are of high importance, because higher values correlate with the actual speed of the operation during the 7th stage by lowering the speed of container positioning on the transport means or AGV. The overall transportation process is then prolonged to compensate for the sway and keep up with the work standard for the safety of cargo and security of operation. These operations are mostly synchronized with the on-site AGV operators and working standards to keep up with the ship unloading procedure. Yet, due to technological reasons, delays occur on a daily basis.

Figure 37. Demonstration of spreader speed actual values during the 7 stages of operation.

Initial results suggest that the operator did not maintain the same speed during the horizontal transfer of the container. The operator made sudden joystick control movements to stop the transportation process for a short period. Figure 37 demonstrates the ladder shape of the speed values, which correlates with the initial suggestion. This is due to the operator's mistake, lack of experience and unsynchronized actions between AGV or truck and the crane. Each ladder produces additional oscillation, which is kept up to the final 7th stage.

Figure 38. Demonstration of spreader and container sway oscillation during the 7 stages of operation.

The operational standard regulates the maximum speed of the spreader movement. Due to these factors, each container was transported with an average of 8.1 seconds delay for the 278 measurements and the average speed of operation was calculated as 40.4 seconds. This indicates that the working efficiency of the operation is only 80%. Each crane is capable of delivering many more containers if the operator movement were controlled by an AI system with pre-defined algorithms for optimal movement of containers with different masses and environmental conditions.

The containers handling operational actions of the Klaipėda port were analyzed in detail. The use-case study proved possible to deploy and use information systems in harsh conditions to gather valuable statistical knowledge. It was detected that each operator made control mistakes when handling cargo, which in return delayed overall port operations.

3. 2. 4. Analysis of container truck movements and the fuel consumption

The real field experiments were performed using data acquisition equipment described before (see Figure 28), in case to analyze container truck movements in the terminal area. The results of the actual truck routes as the relationship between travel distance and travel time in the port area are presented in Figure 39.

Figure 39. Relationship between the duration of a truck ride in the port area and the distance traveled.

The equation of the linear regression is Y=1082.18+0.3x, where Y is the traveling distance (m), x is the time in seconds. The value of correlation coefficient r is 0.32, the coefficient of determination R2 is very low. These results show that the traveling distance and duration are scattered. As we can see from Figure 39, the distance in a range from 1200 m to 1400 m the truck travels in 200 – 1200 seconds. The duration can vary up to 10 times.

The distribution of traveling time is presented in Figure 40. As we can see from these data in the case of non-autonomous loading, the duration of transportation at the quay can vary from 253 to 2600 seconds. From the available data, it can be seen that the travel route is often longer than necessary, so generally speaking, managing the information and the overall data flows between the transport means of the loading process could optimize the transporting traveling time. Statistical analysis of the measured data was performed according to the Chi-square method. It was found that the total driving time "crane-stack-crane" is distributed according to the log-normal law.

Figure 40. Distribution of the duration of truck movement in the port area.

The statistical analysis of the traveling time of the measured data (see Figure 40) shows that over 67% of the traveling durations do not last more than 650 seconds. However, about 35% of the traveling duration lasts more than 650 seconds due to disturbances and causes irrational use of energy.

The results of the measured travel distance in the port area are presented in Figure 41.

Figure 41. Distribution of distances traveled in the port territory.

As we can see from the obtained traveling distance and duration data, they are very scattered. The distance within a range from 1200 to 1400 m the truck travels in 200 – 1200 seconds. The duration can vary up to 10 times. The average travel distance is 1289 m and the standard deviation is about 347 m. The highest values of travel distance reach up to 2890 m. This indicates that the vehicle is traveling on an irrational trajectory (Figure 41).

Figure 42. The trajectory of the truck in the terminal (b – beginning; e – end).

The duration of transportation in the port area can be reduced by synchronizing the work of vehicles, automating the entire loading and transportation process in the port, thus using energy resources efficiently and ensuring less pollution. This is especially true when the port is in an urban area.

Further in this section, we provide detailed measurements of the truck's movement in the port to identify transport disturbances, truck, or crane downtime due to uncoordinated operating modes of the loading equipment. The most common trajectory length traveled by truck is shown in Figure 42.

The truck drove off from the ship after the container loading procedure, then it was unloaded near the stack and returned to the container loading spot near the ship. In the following figure, the sections of the curved trajectory are marked with the beginnings ".b" and the endings as ".e". As mentioned before, the position of the truck was measured using GPS equipment. As the GPS information is transmitted by the radio signals and the working environment is full of metal constructions, we received a lot of interferences during the experiments, thus causing the measured trajectory distortions.

Figure 43 demonstrates the change of mass during a single route cycle of the truck with loaded containers presented in Figure 42.

Figure 43. Track mass variation during the container transportation cycle.

Figure 44 demonstrates the measured velocity of the truck routing the cycle. The velocity of the truck was non-uniform, inconstant, and changed radically with each new turn.

Figure 44. Truck velocity during a single transportation cycle.

Figure 45 shows the sudden and uneven changes of accelerations along the truck movement direction (longitudinal acceleration). It presents possible reasons for the increased fuel consumption. Maximum accelerations occur during truck acceleration and deceleration.

Figure 45. The changes of accelerations along the truck movement direction (longitudinal acceleration).

The instantaneous powers that were calculated using the defined model are shown in Figure 46. The presented results show a rather exaggerated velocity increase at several moments – a source of increased fuel consumption. If the electric autonomous guided vehicle (AGV) were to run on the same profile, its electric motor-generator must be of considerable power (> 100 kW) to be able to absorb the energy recovered during the braking cycles. The red line shows the power during the active braking of the truck. In the case of an internal combustion engine, the mentioned braking energy is converted into heat, but with the installation of an electric motor-generator, it can be recovered into electrical energy.

Figure 46. Instantaneous truck moving power (acceleration and continuous power for driving) and braking power.

Figure 47 demonstrates the fuel consumption required to accelerate or maintain a constant track velocity. The fuel consumption is calculated according to the methodology presented in Section 2.3.1.

Figure 47. Calculated fuel consumption during a single-cycle drive of the loaded truck.

In Figure 47 it is shown that during the acceleration the fuel consumption momentary exceeds 0.004 l/s. Also, in downtime (periods of 0–90 seconds, 130–200 seconds, etc.), the fuel consumption of the truck reaches a significant value > 0.001 l/s. We can assume that such a sudden increase in truck velocity increases the overall fuel consumption. It can also be observed that in this work cycle there are downtimes when the truck is not moving which could be partially eliminated by synchronizing the operations with other machinery on-site. During this cycle, the energy resources can be saved by adjusting the driving and acceleration characteristics.

Performed measurements were taken during 160 truck work cycles around the terminal. After processing the measurement data for all cycles, it was discovered that the truck usually covered about 1.3 km of the road during its operating cycle. The truck is often queuing or waiting for the operation to start at the ship's crane or container crane when loading. Figure 48 shows exactly the amount of fuel being consumed.

Figure 48. Histogram of truck fuel consumption at downtimes.

During those downtimes, the truck wastes 0.13 l of fuel on 22% of the loading cycles. The distribution law of gamma probability densities can be applied to the data (by Chi-square test: $p = 0.32$). These losses could be avoided by applying optimal synchronization of cargo-handling processes and by integrating the electric drivetrain for the trucks.

This proposed calculation methodology allows calculating the current fuel consumption based on the real-time acceleration data. Fuel consumption could be reduced by applying the necessary methodology for synchronization of the AGV cargo-handling processes, as a result of which, the truck would increase the velocity evenly in the fuel economy area. Synchronization would also solve the problem of truck fuel wastage in downtimes. These calculations allow estimating the potential benefits from applying the best synchronization tools to benefit the overall cargo handling processes in container terminals around the world.

3. 3. Experimental investigation of proposed methodology and algorithm in container terminal area

3. 3. 1. Description of the experimental environment – characteristic of the container terminal

The following experiment was performed in the container terminal at Klaipėda Port. The terminal infrastructure consists of quays, container storage sites and loading equipment. The main characteristics of the terminal and the terminal capacity are presented below:
- Length of the quays is 1088 m.
- Depth at the quays around 14.00 m.
- Maximum draught at the quays for the ships is 13.20 m.

- Maximum length of the allowed vessels is 337 m.
- Storage site capacity – 20000 TEU.
- Number of refrigerated containers is 657.

Currently, the container terminal is capable of transloading more than 600000 TEU per year. Container ships of 3000–9178 TEU capacity are served in the terminal. The main cargo handling equipment in the container terminal is listed below:

- STS cranes (51 t load capacity, 65 t for 2x TEU containers) – 4 units.
- Mobile container crane Liebherr LHM 500 (104 t) – 1 unit.
- Mobile container cranes Liebherr LHM 400 (104 t) – 1 unit.
- RTG (Rubber Tired Gantry) 40 t, Konecranes for containers placement in the stacks – 7 units.
- Containers fork lifters Linde and Ferrari for the stacks – 5 units.
- Terminal trucks Terberg are used at the terminal – 19 units.

STS crane can be seen in Figure 49. As mentioned earlier, four STS cranes used in the terminal are often found in the literature. Also, the terminal area used for the experimental study is seen in the figure.

Figure 49. The photo of a STS crane in the container terminal area.

Container trucks used in the experimental study are presented in Figure 50. LoRaWAN was attached to each of the trucks for data acquisitions.

Figure 50. The photo of container trucks in the container terminal area.

The provided figures describe the harsh environment where the wireless communication system was used and, in theory, could be used in future products. This environment is full of metal obstructions, which decreases the strength of the transferred signals.

3.3.2. Description of LoRaWAN equipment used in the experimental study

For experimental research, LoRaWAN hardware consisting of the gateway and the node was constructed and used. The gateway is presented in Figure 51. The node was installed inside a secure case with data acquisition equipment (Figure 28).

Figure 51. LoRaWAN gateway equipment used for experiments.

LoRaWAN gateway consists of the main controller, LoRa communication module, an antenna, LAN port and antenna surge protectors. All this equipment is installed in an industrial type IP 54 enclosure box. An antenna was mounted outside the box for better signal strength characteristics. The structure of this gateway is presented in Figure 52.

Figure 52. Structure of LoRaWAN gateway.

Before the LoRaWAN system was tested in the real environment, it was tested in lab conditions and the terminal with a stationed truck. An adaptive environment was used and the results gained are presented in Figure 53.

Figure 53. Monitoring the environment of LoRaWAN gateway.

The LoRaWAN gateway testing software was developed as an end-user data visualization tool. Gateway bandwidth was examined by sending test data packets. The equipment showed no packet losses and system stability was achieved. The LoRaWAN network system collected additional information, such as system load, memory/swap/HDD/CPU usage, uptime, IN/OUT interface traffic, CPU temperature, the temperature and humidity inside the GW box, the total number of received LoRa packets, the number of received LoRa packets per minute. Figure 54 demonstrates the LoRaWAN node communication with the gateway scenario and its visualization from the end-user perspective.

Figure 54. Sensor data transfer experimental study using LoRaWAN (temperature and humidity).

During the LoRaWAN node communication, the test data packets were sent to the gateway. During these data transfer experiments, signal strength, signal-to-noise ratio, and testing data were measured and received (in this we used temperature and humidity sensors). The experiments were successfully completed.

LoRaWAN node transmits data packets that have a specific structure. This structure is presented in Table 4.

Table 4. Packet structure of LoRaWAN node.

Type	Data	Description
time	TIMESTAMP	Timestamp receive frame
uint64	DEV_ADDR	Device address

double	RSSI	Received signal strength indication
string	PHY_PAYLOAD	Payload from message

Data packets sent by the LoRaWAN gateway to the nodes have their own structure which is presented in Table 5.

Table 5. Packet structure of LoRaWAN gateway.

Type	Data	Description
time	TIMESTAMP	Timestamp receive frame
macaddr	INCIDENT_DEV_ADDR	Device address
uint32	ALERT_CODE	Alert code
string	PHY_PAYLOAD	Payload message
double	RSSI	Received signal strength indication
double	BASE_RSSI	Base RSSI value is defined by the first received message from device to detector
double	VARIANCE	Define variance

The main structure of the data packets received by the gateway consists of timestamp received frame, device address, alert code, payload message, received signal strength indication. The base RSSI value is defined by the first received message from device to detector, define variance. The payload includes information dedicated to each node.

3. 3. 3. The description of the experimental study

During the experimental case study, the LoRaWAN system was mounted on a moving AGV. The developed wireless data logging system was used to collect the parameters in real-time described in 3.1.2. During the experiment, several positions of system placement were discussed with the operators on-site. Obvious positions were considered taking into account the security measures, the harsh working conditions (possibility to damage the system during cargo handling operations) and the possibility to have easy access to mount or change the equipment. The best possible scenario was to mount the system on the top of the cabin of the truck (Figure 30 and Figure 31).

Next, the system was initiated from the cabin using connected laptop equipment. Similar equipment was used in a secure location near the quay crane, simulating the access point of the network. This was done to ensure the stability and work-ready conditions of the software and wireless connection. Updates were performed for the sensory units of the node. The truck moved in the usual manner across the terminal with the loaded cargo. The following movement path describes the average movement pattern (Figure 55).

Figure 55. The use case of the LoRaWAN experimental study.

In sub-section 3.3.4 comparison of the gathered results with the currently adopted method is presented. We have chosen to place the antenna of the gateway on the highest point available – the main building with the local server, which is close to the moving trucks. Due to some limitations working in the terminal area, the more appropriate areas were not acceptable. These limitations can decrease the efficiency of the system for data collection using LoRaWAN networking technology in the port area. According to this scenario an experimental study was performed and results achieved, and are described briefly in Section 3.3.5.

3. 3. 4. Statistical comparison of the proposed data synchronization method versus the current method

The statistical analysis of the measured total durations of the cargo handling procedures (Table 6) shows that using the current method (cooperation between operators) it takes 37.6 seconds to unload a container from the ship to AGV. While this operation is performed, either AGV is already waiting (186.7 on average), or it arrives almost on time (min 4.2 s). In our experimental case study, we have excluded transportation of empty containers to the storage area and kept only transportation to the main stacks, also shown in Figure 56. It takes around 600.4 seconds on average to transport the container to the stack, while it takes only 153.2 seconds to the nearest stack. These durations depend heavily on the selected route of the AGV and the target location.

93

Table 6. Comparison of the proposed data synchronization method.

Stage of loading	Mean	Min	Max
1. STS crane operations	32.2	8.9	96.9
2. Placing on vehicle	5.4	2.6	20.4
3. Total (ship-to-AGV) current method (1+2)	37.6	11.5	117.3
4. AVG waiting	186.7	4.2	467.1
5. AGV transportation	562.8	141.7	890.1
6. Total (ship-to-stack) current method (3+5)	600.4	153.2	1007.4
7. Total (ship-to-stack) process data synchronization method (6-4)	413.7	149.0	540.3

The proposed process data synchronization method eliminates the AGV waiting times, synchronizes the operator's actions and influences other handling process durations. Computational results suggest that it is possible to diminish the AGV waiting times and thus minimize the total container handling process duration up to 413.7 seconds on average, resulting in a 31% improvement over the current method.

3. 3. 5. Experimental results and discussions

Experimental measurements and corresponding calculations were made to verify the LoRaWAN technical equipment (gateway and nodes) and their capabilities in a real port environment. According to the developed method, described in Section 2.2, and using the described system from sub-section 3.3.2, an experiment was performed. The purpose of the experiment was to verify that the developed methodology can be implemented using the LoRaWAN network in harsh conditions such as a container terminal. During the experiment, the nodes were placed on the trucks, carrying containers from the cranes to the stacks. They sent the collected sensory data in near real-time to the main station – gateway. LoRaWAN network architecture enriched with double encryption protocol was used. Container truck movement and acceleration data was acquired. Only one main data collection station was used in the experiment on top of the main building, despite the harsh conditions – metal obstructions which shield the signals, influencing data transmission. During the experiment, the signal strength was measured – RSSI (Received signal strength indicator – dBm). The measurement of the RSSI was made continuously, the data packets were formed by the nodes with a delay of 100 ms. Signal strength measurements are presented in Figure 56.

Figure 56. Visualization of experimental results of signal strength.

The resulting visualization clearly shows that LoRaWAN nodes were accessible all the time during all the working cycles of the truck (STS-stack-STS). According to the position of the LoRaWAN gateway, the received signal was the strongest at the main station on top of the building. Due to the harsh environment, the strength of the signal further away from the central station decreased to over 80-82 dBm. However, this is not a critical threshold. According to these results, one base station can serve the entire territory. The full results of this test are presented in Figure 57. It shows a distribution of the signal strength versus the distance from the gateway.

Figure 57. Experimental results analyzing the RSSI vs distance with the moving node.

However, to ensure uninterrupted data collection, the feasibility of installing at least two gateways in the terminal area should be assessed, that

will overlap and fill possible signal loss gaps. Such infrastructure will not be costly and not hard to install. Such a system will be much cheaper compared to the other. In comparison, it would take more than 10 Wi-Fi gateways to fill such territory, even using the latest 5G technologies. The proposed solution is much more effective, as it requires small data packets to be sent from each measurement point, and the transfer is not crucial as well. LoRaWAN technology fits well for such use cases and is fully compatible with the proposed methodology described in Section 2.1.

3. 4. Section conclusion

1. In this section, the experimental study is provided, describing the technical means used for data acquisition and transfer in the container terminal of Klaipėda Port. LoRaWAN network architecture was used with security mechanisms to ensure that the system would work in a real environment using sensory data and safety protocols. A communication efficiency experiment was performed using moving trucks with attached LoRa nodes, collecting sensory information about the position of the trucks, their speed and accelerations. The results show that the proposed long-range LoRaWAN networking technology is adaptable in the harsh environment of the container terminal and can be used for data synchronization among moving nodes. These nodes were placed on the moving trucks and no insignificant signal losses were observed during the cargo handling procedures. Placement of other technical means to acquire the same signals and same data from the trucks is possible, but such infrastructure would cost more to deploy and maintain during a long operational period. To cover the whole terminal, it is suggested that two base stations (gateways) on opposite sides of the terminal should be used for better signal coverage. The harsh environment of the terminal, taking into account the shielding of the signals by the metal obstructions, e.g., containers in the stacks, can cause additional problems for the other conventional system with higher bandwidth (4G, 5G, Wi-Fi). The sensory data was received without any deviations and downtimes and for such a system deployment it is more than enough to optimize the truck movement and crane operations, synchronizing the processes using limited sensory data at full.
2. Computational results suggest that it is possible to diminish the AGV waiting times and thus minimize the total container handling process duration up to 413.7 seconds on average, resulting in a 31% improvement over the current method.

3. LoRaWAN technology is not new in the research community, but its adoption in new areas to solve unconventional problems and its optimization to suit the needs of the industry is a complex interdisciplinary challenge to informatics and transport engineers as demonstrated in the previous sections.

CONCLUSIONS

1. The performed literature review in the areas of container terminal optimization, control of quay crane and cargo handling processes, AGV navigation, route planning, wireless and smart technologies show that current systems and algorithms are not enough to solve the synchronization problems or to increase the efficiency of the container handling process. The existing planning systems do not evaluate real-time data for processes synchronization, which leads to lowered effectiveness of the procedures. To synchronize the movement data between trucks and quay cranes LoRa technology was chosen due to its unique properties dealing with long-range communication tasks in harsh environments, optimal for port operations. LoRaWAN networks provide higher interference immunity compared to other wireless communication technologies (SIGFOX, LTE-Cat 1, LTE-M, NB-LTE) while maintaining optimal battery usage using sleep mode and high link threshold values. The used modulation and bandwidth are optimal for sensory data transmission in port operations with an unlimited number of messages while maintaining 290 bps–50 Kbps data rates. The adoption of the new data synchronization system requires new infrastructure deployment, yet, it is problematic to apply these new technologies in the harsh environment of the container terminal. Therefore, it was concluded that to solve these problems it is necessary to use LoRa technology for secure and reliable connections for handling processes synchronization.

2. A new method for processes data synchronization between port trucks and quay cranes was developed, including assignment, positioning and data exchange algorithms, decision support modules, and LoRaWAN network topology with double security on MAC and applications layers that are suitable for individual cargo-handling processes:

   A. The concept of container handling process data synchronization between two nodes (AGV and quay crane) was proposed, including the use of ICT modules (LoRaWAN communication, Software agent). Additionally, to speed up the data acquisition and process control, two modules were proposed in both nodes (Data collection and Decision support). This method is suitable for speeding up and securing the handling procedures, reducing downtimes of the trucks, and ensuring optimal vehicle energy consumption for the entire operational cycle, according to the EU Directive 2018/410 for the "green" port guides.

   B. Wireless communication technology was proposed for container handling process data synchronization, using a newly developed LoRa

gateway structure. The proposed solution includes physical prototypes of the network equipment and a developed two-layer (Application and MAC) security mechanism in LoRaWAN protocol, encrypted using the AES-128 algorithm by AppKey.

3. Comparative and experimental research results show:
   A. Computational results suggest that it is possible to diminish the AGV waiting times and thus minimize the total container handling process duration up to 413.7 seconds on average, resulting in a 31% improvement over the current method.
   B. The proposed long-range LoRaWAN networking technology is adaptable in the harsh environment of the containers terminal and can be used for data synchronization among moving nodes. The average signal strength in the port environment was -77.49 dBm, and the maximum signal strength drop not exceed the threshold. If the threshold of -120 dBm is not reached, then the signal loss is not critical at the terminal. The results suggest that by using only a single gateway it is possible to cover medium size container terminal for data acquisition from all nodes. The number of LoRa nodes can be increased to cover even the largest port areas like Rotterdam but to make it happen simply more gateways must be used.

4. Future research will be aimed at the evaluation of complex decision support methods to improve the operator actions, developing state of the art in process control and prediction using novel AI algorithms (machine learning, deep learning and neural networks). This will help improve the crane operator's work by providing real-time situation information, not only predicting an action but also making process data synchronization more accurate in long-term planning. The performed research and future planned activities are based on the Lithuanian Smart Specialization Strategy (RIS3) priority – transport, logistics and ICT.

BIBLIOGRAPHY AND REFERENCES

[1]   L. A. Tuan, H. M. Cuong, P. Van Trieu, L. C. Nho, V. D. Thuan, and L. V. Anh, "Adaptive neural network sliding mode control of shipboard container cranes considering actuator backlash," *Mech. Syst. Signal Process.*, vol. 112, pp. 233–250, 2018, doi: 10.1016/j.ymssp.2018.04.030.

[2]   I. Golovin and S. Palis, "Robust control for active damping of elastic gantry crane vibrations," *Mech. Syst. Signal Process.*, vol. 121, 2019, doi: 10.1016/j.ymssp.2018.11.005.

[3]   M. Sha *et al.*, "Scheduling optimization of yard cranes with minimal energy consumption at container terminals," *Comput. Ind. Eng.*, vol. 113, pp. 704–713, 2017, doi: 10.1016/j.cie.2016.03.022.

[4]   European Commission, "The European Green Deal: Communication from the Commission to the European Parliament, the European Council, the Council, the European Economic and Social Committee and the Committee of the Regions," p. 24, 2019, doi: 10.2307/j.ctvd1c6zh.7.

[5]   N. Sun, Y. Wu, H. Chen, and Y. Fang, "An energy-optimal solution for transportation control of cranes with double pendulum dynamics: Design and experiments," *Mech. Syst. Signal Process.*, vol. 102, 2018, doi: 10.1016/j.ymssp.2017.09.027.

[6]   M. Kermani, G. Parise, L. Martirano, L. Parise, and B. Chavdarian, "Optimization of Peak Load Shaving in STS Group Cranes Based on PSO Algorithm," 2018, doi: 10.1109/EEEIC.2018.8494467.

[7]   A. A. Elbadawy and M. M. G. Shehata, "Anti-sway control of marine cranes under the disturbance of a parallel manipulator," *Nonlinear Dyn.*, vol. 82, no. 1–2, pp. 415–434, 2015, doi: 10.1007/s11071-015-2165-3.

[8]   M. A. Majid, W. S. W. Ibrahim, S. Mohamad, and Z. A. Bakar, "A comparison of PID and PD controller with input shaping technique for 3D gantry crane," *Proc. - 2013 IEEE Conf. Syst. Process Control. ICSPC 2013*, no. December, pp. 144–148, 2013, doi: 10.1109/SPC.2013.6735121.

[9]   M. E. Taner, O. Kulak, and M. U. Koyuncuoğlu, "Layout analysis affecting strategic decisions in artificial container terminals," *Comput. Ind. Eng.*, vol. 75, no. 1, 2014, doi: 10.1016/j.cie.2014.05.025.

[10]   T. T. Wong, C. H. H. Tang, and M. Mailah, "Robust active heave compensated winch-driven overhead crane system for load transfer in marine operation," *ICIAS 2012 - 2012 4th Int. Conf. Intell. Adv. Syst. A Conf. World Eng. Sci. Technol. Congr. - Conf. Proc.*, vol. 1, pp. 111–116, 2012, doi: 10.1109/ICIAS.2012.6306170.

[11]   T. T. Wong, C. H. H. Tang, and M. Mailah, "Winch driven active heave compensation for load transfer in overhead crane system," *ICIAS 2012 - 2012 4th Int. Conf. Intell. Adv. Syst. A Conf. World Eng.*

Sci. Technol. Congr. - Conf. Proc., vol. 1, pp. 34–39, 2012, doi: 10.1109/ICIAS.2012.6306154.

[12] M. Zhang, Y. Zhang, H. Chen, and X. Cheng, "Model-independent PD-SMC method with payload swing suppression for 3D overhead crane systems," *Mech. Syst. Signal Process.*, 2019, doi: 10.1016/j.ymssp.2019.04.046.

[13] H. I. Jaafar, Z. Mohamed, A. F. Z. Abidin, and Z. A. Ghani, "PSO-tuned PID controller for a nonlinear gantry crane system," *Proc. - 2012 IEEE Int. Conf. Control Syst. Comput. Eng. ICCSCE 2012*, pp. 515–519, 2013, doi: 10.1109/ICCSCE.2012.6487200.

[14] H. I. Jaafar, M. F. Sulaima, Z. Mohamed, and J. J. Jamian, "Optimal PID controller parameters for nonlinear gantry crane system via MOPSO technique," *Proc. - 2013 IEEE Conf. Sustain. Util. Dev. Eng. Technol. IEEE CSUDET 2013*, pp. 86–91, 2013, doi: 10.1109/CSUDET.2013.6670992.

[15] T. Eglynas, M. Bogdevičius, A. Andziulis, and M. Jusis, "Trolley Motion Control Based on S-shaped Velocity Profile for Quay Crane Cargo Oscillation Comparison," *Moksl. - Liet. ateitis*, vol. 9, no. 3, 2017, doi: 10.3846/mla.2017.1034.

[16] K. H. Rew, C. W. Ha, and Y. S. Kim, "A practically efficient method for motion control based on asymmetric velocity profile," *Int. J. Mach. Tools Manuf.*, vol. 49, no. 7–8, pp. 678–682, 2009, doi: DOI 10.1016/j.ijmachtools.2009.01.008.

[17] R. Béarée, "New Damped-Jerk trajectory for vibration reduction," *Control Eng. Pract.*, vol. 28, pp. 112–120, Jul. 2014, doi: 10.1016/j.conengprac.2014.03.010.

[18] G. Lal Kumawat, D. Roy, R. De Koster, and I. Adan, "Stochastic Modeling of Parallel Process Flows in Intra-logistics Systems: Applications in Container Terminals and Compact Storage Systems," *Eur. J. Oper. Res.*, 2020, doi: 10.1016/j.ejor.2020.08.006.

[19] D. Roy and R. de Koster, "Stochastic modeling of unloading and loading operations at a container terminal using automated lifting vehicles," *Eur. J. Oper. Res.*, vol. 266, no. 3, pp. 895–910, 2018, doi: 10.1016/j.ejor.2017.10.031.

[20] S. Karakas, A. Z. Acar, and M. Kirmizi, "Development of a multidimensional performance evaluation model for container terminals at Marmara Sea," *Res. Transp. Bus. Manag.*, no. May, p. 100498, 2020, doi: 10.1016/j.rtbm.2020.100498.

[21] M. J. Basallo-Triana, C. Vidal Holguín, and J. J. Bravo Bastidas, "Planning and design of a chassis container terminal," *IFAC-PapersOnLine*, vol. 52, no. 13, pp. 2578–2583, 2019, doi: 10.1016/j.ifacol.2019.11.595.

[22] Y. Yang, M. Zhong, Y. Dessouky, and O. Postolache, "An integrated scheduling method for AGV routing in automated container terminals," *Comput. Ind. Eng.*, vol. 126, no. October, pp. 482–493,

2018, doi: 10.1016/j.cie.2018.10.007.

[23] M. Zhong, Y. Yang, Y. Dessouky, and O. Postolache, "Multi-AGV scheduling for conflict-free path planning in automated container terminals," *Comput. Ind. Eng.*, vol. 142, no. June 2019, p. 106371, 2020, doi: 10.1016/j.cie.2020.106371.

[24] X. Hu, J. Guo, and Y. Zhang, "Optimal strategies for the yard truck scheduling in container terminal with the consideration of container clusters," *Comput. Ind. Eng.*, vol. 137, no. September, p. 106083, 2019, doi: 10.1016/j.cie.2019.106083.

[25] L. Zhen, H. Hu, W. Wang, X. Shi, and C. Ma, "Cranes scheduling in frame bridges based automated container terminals," *Transp. Res. Part C Emerg. Technol.*, 2018, doi: 10.1016/j.trc.2018.10.019.

[26] A. Malekahmadi, M. Alinaghian, S. R. Hejazi, and M. A. Assl Saidipour, "Integrated continuous berth allocation and quay crane assignment and scheduling problem with time-dependent physical constraints in container terminals," *Comput. Ind. Eng.*, vol. 147, no. July, p. 106672, 2020, doi: 10.1016/j.cie.2020.106672.

[27] U. Clausen, J. Kaffka, and F. Meier, "CONTSIM–Container Terminal Management with Simulation," *Procedia - Soc. Behav. Sci.*, vol. 54, pp. 332–340, 2012, doi: 10.1016/j.sbspro.2012.09.752.

[28] S. Kavakeb, T. T. Nguyen, K. McGinley, Z. Yang, I. Jenkinson, and R. Murray, "Green vehicle technology to enhance the performance of a European port: A simulation model with a cost-benefit approach," *Transp. Res. Part C Emerg. Technol.*, vol. 60, pp. 169–188, 2015, doi: 10.1016/j.trc.2015.08.012.

[29] E. COMMISSION, "Annex to Motorways of the Sea Detailed Implementation Plan," 2018.

[30] H. Benamara, "Role of International Shipping," in *UNCTAD Multilayer Expert Meeting on transport, Trade Logistics and Trade Facilitation 21-23 November 2018, Geneva*, 2018, no. November, p. 13p.

[31] C. Speier, J. M. Whipple, D. J. Closs, and M. D. Voss, "Global supply chain design considerations: Mitigating product safety and security risks," *J. Oper. Manag.*, vol. 29, no. 7–8, pp. 721–736, Nov. 2011, doi: 10.1016/j.jom.2011.06.003.

[32] G. Tang, M. Qin, Z. Zhao, J. Yu, and C. Shen, "Performance of peak shaving policies for quay cranes at container terminals with double cycling," *Simul. Model. Pract. Theory*, vol. 104, no. April, p. 102129, 2020, doi: 10.1016/j.simpat.2020.102129.

[33] J. Xin, R. R. Negenborn, and G. Lodewijks, *Trajectory planning for AGVs in automated container terminals using avoidance constraints: A case study*, vol. 19, no. 3. IFAC, 2014.

[34] K. S. Hong and Q. H. Ngo, "Dynamics of the container crane on a mobile harbor," *Ocean Eng.*, 2012, doi: 10.1016/j.oceaneng.2012.06.013.

[35]   K. Zheng, Z. Lu, and X. Sun, "An Effective Heuristic for the Integrated Scheduling Problem of Automated Container Handling System Using Twin 40' Cranes," *2010 Second Int. Conf. Comput. Model. Simul.*, no. 1990, pp. 406–410, Jan. 2010, doi: 10.1109/ICCMS.2010.290.

[36]   F. Alasali, S. Haben, and W. Holderbaum, "Stochastic optimal energy management system for RTG cranes network using genetic algorithm and ensemble forecasts," *J. Energy Storage*, 2019, doi: 10.1016/j.est.2019.100759.

[37]   V. Papaioannou, S. Pietrosanti, W. Holderbaum, V. M. Becerra, and R. Mayer, "Analysis of energy usage for RTG cranes," *Energy*, 2017, doi: 10.1016/j.energy.2017.02.122.

[38]   D. Liu and Y. E. Ge, "Modeling assignment of quay cranes using queueing theory for minimizing CO_2 emission at a container terminal," *Transp. Res. Part D Transp. Environ.*, 2018, doi: 10.1016/j.trd.2017.06.006.

[39]   K. Bichou, "An empirical study of the impacts of operating and market conditions on container-port efficiency and benchmarking," *Res. Transp. Econ.*, 2013, doi: 10.1016/j.retrec.2012.11.009.

[40]   A. Arena, W. Lacarbonara, and A. Casalotti, "Payload oscillations control in harbor cranes via semi-active vibration absorbers: Modeling, simulations and experimental results," 2017, doi: 10.1016/j.proeng.2017.09.136.

[41]   Š. Ileš, J. Matuško, and F. Kolonić, "Sequential distributed predictive control of a 3D tower crane," *Control Eng. Pract.*, 2018, doi: 10.1016/j.conengprac.2018.07.001.

[42]   R. I. Verdés Kairuz, L. T. Aguilar, A. F. de Loza, and J. E. Andrade García, "Robust Positioning Control Law for a 3D Underactuated Crane System," *IFAC-PapersOnLine*, 2018, doi: 10.1016/j.ifacol.2018.07.319.

[43]   B. Li, H. Liu, D. Xiao, G. Yu, and Y. Zhang, "Centralized and optimal motion planning for large-scale AGV systems: A generic approach," *Adv. Eng. Softw.*, vol. 106, pp. 33–46, 2017, doi: 10.1016/j.advengsoft.2017.01.002.

[44]   C. Güven and D. T. Eliiyi, "Trip allocation and stacking policies at a container terminal," *Transp. Res. Procedia*, vol. 3, no. July, pp. 565–573, 2014, doi: 10.1016/j.trpro.2014.10.035.

[45]   Z. Sun, N. Wang, Y. Bi, and J. Zhao, "A DE based PID controller for two dimensional overhead crane," *Proc. 34th Chinese Control Conf.*, no. 1, pp. 2546–2550, 2015.

[46]   F. Panuncio, W. Yu, and X. Li, "Stable neural PID anti-swing control for an overhead crane," *IEEE Int. Symp. Intell. Control - Proc.*, pp. 53–58, 2013, doi: 10.1109/ISIC.2013.6658616.

[47]   M. J. Stojčić, "DESIGN AND IMPLEMENTATION OF A DIGITAL POSITIONING SYSTEM WITH CONTROLLED JERK," *Facta Universitatis, Series: Automatic Control and Robotics*, vol. 13, no. 3.

. 159–168, Dec. 2014.

[48] C. Yang, Z. Zhang, and Q. Zhao, "Study on Intelligent Control of Two-Dimensional Precision Positioning System," in *2008 International Conference on Computer Science and Software Engineering*, 2008, vol. 4, pp. 835–838, doi: 10.1109/CSSE.2008.1211.

[49] C. Liu, H. Zhao, and Y. Cui, "Research on Application of Fuzzy PID in Collective Pitch Control System," *2011 Int. Conf. Control. Autom. Syst. Eng.*, pp. 1–4, 2011, doi: 10.1109/ICCASE.2011.5997553.

[50] N. Lv, H. Li, M. Li, and M. Hou, "Based on PID Control Optimization Of Synchronous Motor Control," *Conf. Meas. Inf. Control*, pp. 2111–2114, 2012.

[51] T. Eglynas, M. Jusis, S. Jakovlev, A. Senulis, A. Andziulis, and S. Gudas, "Analysis of the efficiency of shipping containers handling/loading control methods and procedures," *Adv. Mech. Eng.*, vol. 11, no. 1, 2019, doi: 10.1177/1687814018821229.

[52] T. Le-Anh and M. B. M. De Koster, "A review of design and control of automated guided vehicle systems," *Eur. J. Oper. Res.*, vol. 171, no. 1, pp. 1–23, 2006, doi: 10.1016/j.ejor.2005.01.036.

[53] J. He, C. Tan, and Y. Zhang, "Yard crane scheduling problem in a container terminal considering risk caused by uncertainty," *Adv. Eng. Informatics*, vol. 39, no. October 2018, pp. 14–24, 2019, doi: 10.1016/j.aei.2018.11.004.

[54] J. Cao, Q. Shi, and D. H. Lee, "Integrated quay crane and yard truck schedule problem in container terminals," *Tsinghua Sci. Technol.*, vol. 15, no. 4, pp. 467–474, 2010, doi: 10.1016/S1007-0214(10)70089-4.

[55] T. G. Crainic and K. H. Kim, "Intermodal Transportation," vol. 14, no. 06, pp. 467–537, 2007, doi: 10.1016/S0927-0507(06)14008-6.

[56] B. G. Zweers, S. Bhulai, and R. D. van der Mei, "Optimizing pre-processing and relocation moves in the Stochastic Container Relocation Problem," *Eur. J. Oper. Res.*, vol. 283, no. 3, pp. 954–971, 2020, doi: 10.1016/j.ejor.2019.11.067.

[57] Y. Xie and D. P. Song, "Optimal planning for container prestaging, discharging, and loading processes at seaport rail terminals with uncertainty," *Transp. Res. Part E Logist. Transp. Rev.*, vol. 119, no. October, pp. 88–109, 2018, doi: 10.1016/j.tre.2018.09.008.

[58] Q. Zeng, Y. Feng, and Z. Yang, "Integrated optimization of pickup sequence and container rehandling based on partial truck arrival information," *Comput. Ind. Eng.*, vol. 127, no. October 2018, pp. 366–382, 2019, doi: 10.1016/j.cie.2018.10.024.

[59] C. Zhou, B. K. Lee, and H. Li, "Integrated optimization on yard crane scheduling and vehicle positioning at container yards," *Transp. Res. Part E Logist. Transp. Rev.*, vol. 138, no. June 2019, p. 101966, 2020, doi: 10.1016/j.tre.2020.101966.

[60] D. Muravev, H. Hu, A. Rakhmangulov, and P. Mishkurov, "Multi-agent optimization of the intermodal terminal main parameters by

using AnyLogic simulation platform: Case study on the Ningbo-Zhoushan Port," *Int. J. Inf. Manage.*, no. April, p. 102133, 2020, doi: 10.1016/j.ijinfomgt.2020.102133.

[61]   H. Lu and S. Wang, "A study on multi-ASC scheduling method of automated container terminals based on graph theory," *Comput. Ind. Eng.*, vol. 129, no. January, pp. 404–416, 2019, doi: 10.1016/j.cie.2019.01.050.

[62]   C. Zhang, H. Guan, Y. Yuan, W. Chen, and T. Wu, "Machine learning-driven algorithms for the container relocation problem," *Transp. Res. Part B Methodol.*, vol. 139, pp. 102–131, 2020, doi: 10.1016/j.trb.2020.05.017.

[63]   C. Caballini, M. D. Gracia, J. Mar-Ortiz, and S. Sacone, "A combined data mining – optimization approach to manage trucks operations in container terminals with the use of a TAS: Application to an Italian and a Mexican port," *Transp. Res. Part E Logist. Transp. Rev.*, vol. 142, no. June, p. 102054, 2020, doi: 10.1016/j.tre.2020.102054.

[64]   I. Rekik and S. Elkosantini, "A multi agent system for the online container stacking in seaport terminals," *J. Comput. Sci.*, vol. 35, pp. 12–24, 2019, doi: 10.1016/j.jocs.2019.06.003.

[65]   H. H. Götting, "Automation and Steering of Vehicles in Ports," *Port Technology International 10*, pp. 101–111, 2000.

[66]   R. Demuth, "Frequency Generator HG G-57400ZE," *Götting KG*, 2017. .

[67]   A. Vale, R. Ventura, P. Lopes, and I. Ribeiro, "Assessment of navigation technologies for automated guided vehicle in nuclear fusion facilities," *Rob. Auton. Syst.*, vol. 97, pp. 153–170, 2017, doi: 10.1016/j.robot.2017.08.006.

[68]   I. F. A. Vis, "Survey of research in the design and control of automated guided vehicle systems," *Eur. J. Oper. Res.*, vol. 170, no. 3, pp. 677–709, 2006, doi: 10.1016/j.ejor.2004.09.020.

[69]   A. Dhanvijay and M. M. Raut, "Intelligent Autonomous Automated Guided Vehicle," *Int. J. Innov. Res. Electr. Electron. Instrum. Control Eng.*, vol. 4, no. 12, pp. 97–100, 2016, doi: 10.17148/IJIREEICE.2016.41219.

[70]   S. Lu, C. Xu, R. Y. Zhong, and L. Wang, "A RFID-enabled positioning system in automated guided vehicle for smart factories," *J. Manuf. Syst.*, vol. 44, pp. 179–190, 2017, doi: 10.1016/j.jmsy.2017.03.009.

[71]   A. Y. . Nee, Y. Suzhu, M. Zarinejad, J. Wei, W. Zhou, and S. Subbiah, *Handbook of Manufacturing Engineering and Technology*. 2015.

[72]   S. Lu, C. Xu, R. Y. Zhong, and L. Wang, "A passive RFID tag-based locating and navigating approach for automated guided vehicle," *Comput. Ind. Eng.*, no. xxxx, pp. 0–1, 2018, doi: 10.1016/j.cie.2017.12.026.

[73]   H. Martínez-Barberá and D. Herrero-Pérez, "Autonomous navigation of an automated guided vehicle in industrial environments," *Robot.*

Comput. Integr. Manuf., vol. 26, no. 4, pp. 296–311, 2010, doi: 10.1016/j.rcim.2009.10.003.

[74] K. Jung, J. Kim, J. Kim, E. Jung, and S. Kim, "Positioning accuracy improvement of laser navigation using UKF and FIS," *Rob. Auton. Syst.*, vol. 62, no. 9, pp. 1241–1247, 2014, doi: 10.1016/j.robot.2014.03.016.

[75] C. Kirsch and C. Röhrig, "Global localization and position tracking of an Automated Guided Vehicle," *IFAC Proc. Vol.*, vol. 18, no. PART 1, pp. 14036–14041, 2011, doi: 10.3182/20110828-6-IT-1002.01245.

[76] S. . Kalaimagal and R. . Sivaramakrishnan, "Navigation Of Autonomous Ground Vehicle Using Gps System," *Int. J. Eng. Res. Technol.*, vol. 1, no. 7, pp. 1–6, 2012.

[77] M. Joerger, J. Christ, R. Duncan, and B. Pervan, "Integrated design of an AGV for improved GPS-based path-following performance," *Int. J. Veh. Des.*, vol. 42, pp. 263–286, 2006.

[78] M. Yeoman, "No Title," *RFID Tag Read Range and Antenna Optimization*, 2014. https://www.comsol.com/blogs/rfid-tag-read-range-antenna-optimization/ (accessed Jan. 15, 2021).

[79] J. F. Sekaran, H. Kaluvan, and L. Irudhayaraj, "Modeling and Analysis of GPS–GLONASS Navigation for Car Like Mobile Robot," *J. Electr. Eng. Technol.*, vol. 15, no. 2, 2020, doi: 10.1007/s42835-020-00365-1.

[80] G. W. Roberts, X. Tang, and C. Brown, "A review of satellite positioning systems for civil engineering," *Proc. Inst. Civ. Eng. Civ. Eng.*, vol. 168, no. 4, 2015, doi: 10.1680/cien.15.00013.

[81] J. A. Arnold, "Navigating the future," *Public Roads*, vol. 59, no. 2, 1995, doi: 10.22459/ntf.06.2017.

[82] S. Jung, "Self-Organizing Clusters for Routing Algorithm by Diffusing an Interest in Wireless Sensor Networks," *5th ACIS Int. Conf. Softw. Eng. Res. Manag. Appl. (SERA 2007)*, pp. 702–710, Aug. 2007, doi: 10.1109/SERA.2007.118.

[83] A. M. Martín-Soberón, A. Monfort, R. Sapiña, N. Monterde, and D. Calduch, "Automation in Port Container Terminals," *Procedia - Soc. Behav. Sci.*, 2014, doi: 10.1016/j.sbspro.2014.12.131.

[84] H. Cho, "Design and Implementation of an Active RFID System Platform," 2005.

[85] M. Yu and S. Wang, "Study on Scheduling System Based on Multi-Agent of Container Terminal," *2006 10th Int. Conf. Comput. Support. Coop. Work Des.*, pp. 1–6, May 2006, doi: 10.1109/CSCWD.2006.253056.

[86] "A Study on the Advance Transportation System for Inter Terminal Transshipment: Focused on the Busan New Port," *J. Korean Navig. Port Reserch*, vol. 44, no. 4, 2020, doi: 10.5394/KINPR.2020.44.4.298.

[87] R. Ramesh and K. Usha Kiran, "Design and analysis of dual band

MIMO antenna system for GPS and IoT wireless applications," *Int. J. Innov. Technol. Explor. Eng.*, vol. 8, no. 5, 2019.

[88] M. F. M. Yazair *et al.*, "Suitability analysis for DGPS radio beacon establishment at port klang Malaysia," *Int. J. Eng. Adv. Technol.*, vol. 8, no. 6 Special Issue 3, 2019, doi: 10.35940/ijeat.F1077.0986S319.

[89] B. Gunes, G. Kayisoglu, and P. Bolat, "Cyber security risk assessment for seaports: A case study of a container port," *Comput. Secur.*, vol. 103, p. 102196, Apr. 2021, doi: 10.1016/j.cose.2021.102196.

[90] I. de la Peña Zarzuelo, M. J. Freire Soeane, and B. López Bermúdez, "Industry 4.0 in the port and maritime industry: A literature review," *J. Ind. Inf. Integr.*, vol. 20, p. 100173, Dec. 2020, doi: 10.1016/j.jii.2020.100173.

[91] C. Chapman, "Locking down the infrastructure: Internet, Wi-Fi, wired, VPN, WAN, and the core," in *Network Performance and Security*, Elsevier, 2016, pp. 39–83.

[92] M. Široka, S. Piličić, T. Milošević, I. Lacalle, and L. Traven, "A novel approach for assessing the ports' environmental impacts in real time – The IoT based port environmental index," *Ecol. Indic.*, vol. 120, p. 106949, Jan. 2021, doi: 10.1016/j.ecolind.2020.106949.

[93] J. Muñuzuri, L. Onieva, P. Cortés, and J. Guadix, "Using IoT data and applications to improve port-based intermodal supply chains," *Comput. Ind. Eng.*, vol. 139, p. 105668, Jan. 2020, doi: 10.1016/j.cie.2019.01.042.

[94] J. Sun, Q. Yu, M. Niyazbek, and F. Chu, "5G network information technology and military information communication data services," *Microprocess. Microsyst.*, p. 103459, Nov. 2020, doi: 10.1016/j.micpro.2020.103459.

[95] A. Pant, M. Singh, and M. S. Parihar, "A frequency reconfigurable/switchable MIMO antenna for LTE and early 5G applications," *AEU - Int. J. Electron. Commun.*, vol. 131, p. 153638, Mar. 2021, doi: 10.1016/j.aeue.2021.153638.

[96] O. M. Dardeer, H. A. Elsadek, H. M. Elhennawy, and E. A. Abdallah, "Ultra-wideband bandstop filter with multiple transmission zeros using in-line coupled lines for 4G/5G mobile applications," *AEU - Int. J. Electron. Commun.*, vol. 131, p. 153635, Mar. 2021, doi: 10.1016/j.aeue.2021.153635.

[97] Y. Chen and D. Han, "Water quality monitoring in smart city: A pilot project," *Autom. Constr.*, vol. 89, pp. 307–316, May 2018, doi: 10.1016/j.autcon.2018.02.008.

[98] H. Noura, T. Hatoum, O. Salman, J.-P. Yaacoub, and A. Chehab, "LoRaWAN security survey: Issues, threats and possible mitigation techniques," *Internet of Things*, vol. 12, p. 100303, Dec. 2020, doi: 10.1016/j.iot.2020.100303.

[99] Semtech Corporation, "Why LoRa?," 2021. https://www.semtech.com/lora/why-lora (accessed Jan. 15, 2021).

[100] O. Dinu, E. Rosca, V. Dragu, M. Rosca, and A. Ilie, "Optimization of the transfer function through handling productivity control in port container terminals," *Procedia Manuf.*, vol. 22, pp. 856–863, 2018, doi: 10.1016/j.promfg.2018.03.121.

[101] C. Zhou, W. Wang, and H. Li, "Container reshuffling considered space allocation problem in container terminals," *Transp. Res. Part E Logist. Transp. Rev.*, vol. 136, no. December 2019, pp. 1–23, 2020, doi: 10.1016/j.tre.2020.101869.

[102] D. Fernandes Carvalho *et al.*, "A test methodology for evaluating architectural delays of LoRaWAN implementations," *Pervasive Mob. Comput.*, vol. 56, 2019, doi: 10.1016/j.pmcj.2019.03.002.

[103] R. S. Sinha, Y. Wei, and S. H. Hwang, "A survey on LPWA technology: LoRa and NB-IoT," *ICT Express*. 2017, doi: 10.1016/j.icte.2017.03.004.

[104] Y. Li, X. Cheng, Y. Cao, D. Wang, and L. Yang, "Smart choice for the smart grid: Narrowband internet of things (NB-IoT)," *IEEE Internet Things J.*, 2018, doi: 10.1109/JIOT.2017.2781251.

[105] B. Vejlgaard, M. Lauridsen, H. Nguyen, I. Z. Kovacs, P. Mogensen, and M. Sorensen, "Coverage and Capacity Analysis of Sigfox, LoRa, GPRS, and NB-IoT," 2017, doi: 10.1109/VTCSpring.2017.8108666.

[106] K. Mekki, E. Bajic, F. Chaxel, and F. Meyer, "Overview of Cellular LPWAN Technologies for IoT Deployment: Sigfox, LoRaWAN, and NB-IoT," 2018, doi: 10.1109/PERCOMW.2018.8480255.

[107] K. P. Park, J. H. Cha, and K. Y. Lee, "Dynamic factor analysis considering elastic boom effects in heavy lifting operations," *Ocean Eng.*, 2011, doi: 10.1016/j.oceaneng.2011.04.007.

[108] N. Bahnes, B. Kechar, and H. Haffaf, "Cooperation between Intelligent Autonomous Vehicles to enhance container terminal operations," *J. Innov. Digit. Ecosyst.*, vol. 3, no. 1, pp. 22–29, 2016, doi: 10.1016/j.jides.2016.05.002.

LIST OF PUBLICATIONS

CA WoS publications with IF:

1. T. Eglynas, S. Jakovlev., V. Jankunas, R. Diziokas, J. Janutėnienė, D. Drungilas, **M. Jusis**, E. Pocevicius, M. Bogdevičius, A.Andziulis. Evaluation of the energy consumption of container diesel trucks in a container terminal: A case study at Klaipeda port. Science Progress. Vol. 104(3), 1-25 (2021) **IF 2.774**
   Contribution: development of experimental methodology, executing experiments and analysis of the results obtained, preparation of conclusions.

2. T. Eglynas, A. Andziulis, M. Bogdevičius, J. Janutėnienė, S. Jakovlev, V.Jankūnas, A. Senulis, **M. Jusis**, M. Bogdevičius, S. Gudas. 2019. Modeling and experimental research of quay crane cargo lowering processes. Advances in Mechanical Engineering. Vol. 11(12), pp. 1–9 **IF 1.024**
   Contribution: raising an idea, development of experimental methodology, executing experiments and analysis of the results obtained, preparation of conclusions.

3. T. Eglynas, **M. Jusis**, S. Jakovlev, A. Senulis, A. Andziulis, S. Gudas. 2019. Analysis of the efficiency of shipping containers handling/loading control methods and procedures. Advances in Mechanical Engineering. Vol. 11(1) , pp. 1–12 **IF 1.024**
   Contribution: raising an idea, participation in the mathematical modeling, creation of a control algorithm, development of a quay crane control system prototype, programming, executing experiments and analysis of the results obtained, preparation of conclusions.

4. A. Andziulis, T. Eglynas, M. Bogdevičius, **M. Jusis**, A. Senulis. 2016. Multibody dynamic simulation and transients analysis of quay crane spreader and lifting mechanism. Advances in Mechanical Engineering. Vol. 8(9), pp. 1–11 **IF 0.67**
   Contribution: literature analysis, executing experiments, data analysis, preparation of conclusions.

Conference proceedings:

1. S. Jakovlev, T. Eglynas, **M. Jusis**, S. Gudas, V. Jankunas. Use Case of Quay Crane Container Handling Operations Monitoring Using ICT to Detect Abnormalities in Operator Actions. 6th International Conference on Vehicle Technology and Intelligent Transport Systems (2020), Čekija.
   Contribution: preparation of presentation material.

2. S. Jakovlev, T. Eglynas, **M. Jusis**, S. Gudas, E. Pocevicius, V. Jankunas. Analysis of the Efficiency of Quay Crane Control. The 7th IEEE Workshop on Advances in Information, Electronic and Electrical Engineering, Liepaja, Latvija 2019.
   Contribution: presenter in remote conference.
3. T. Eglynas, **M. Jusis**, S. Jakovlev, A. Senulis, P. Partila, S. Gudas. Research of Quay Crane Control Algorithm with Embedded Sway Control Sub-routine. 27th Telecommunications Forum TELFOR 2019, Serbija.
   Contribution: preparation of presentation material.
4. **M. Jusis**, T. Eglynas, A. Senulis, S. Gudas, S. Jakovlev, M. Bogdevičius. Pietryčių Baltijos konteinerių terminalų apžvalga ir krovos tendencijos. Jūros ir krantų tyrimai 2017. p. 86-90.
   Contribution: preparation of poster presentation material.

1ˢᵗ publication / 1 publikacija

Evaluation of the energy consumption of container diesel trucks in a container terminal: A case study at Klaipeda port

T. Eglynas, S. Jakovlev., V. Jankunas, R. Diziokas, J. Janutėnienė, D. Drungilas, **M. Jusis**, E. Pocevicius, M. Bogdevičius, A.Andziulis.

Evaluation of the energy consumption of container diesel trucks in a container terminal: A case study at Klaipeda port

Tomas Eglynas[1] [ID], Sergej Jakovlev[1,2], Valdas Jankunas[1], Rimantas Didziokas[1], Jolanta Januteniene[1], Darius Drungilas[1], Mindaugas Jusis[1], Edvinas Pocevicius[1], Marijonas Bogdevicius[1] and Arunas Andziulis[1]

[1]Klaipeda University, Klaipeda, Lithuania
[2]VŠB – Technical University of Ostrava, Ostrava-Poruba, Czech Republic

Abstract

Introduction: In the paper, we examine the energy consumption efficiency of specialized container diesel trucks engaged in container transportation at a seaport terminal.
Objectives: Using the container terminal at Klaipėda in Lithuania as the background for the research, we produced an improved energy consumption model for measuring the theoretical energy consumption and regeneration of diesel trucks at the terminal and provide a comparative analysis.
Methods: We created a mathematical model which describes the instantaneous energy consumption of the diesel trucks, taking into account their dynamic properties and the overall geometry of their routes—"Ship-Truck-Stack-Ship"—using the superposition principle. We investigated other critical parameters relevant to the model and provide a statistical evaluation of the transportation process using data from a case study of Klaipėda port, where we collected measurements of container transportation parameters using georeferenced movement detection and logs from wireless equipment positioned on the diesel-powered container trucks.
Results: The modeling results showed that an instantaneous evaluation of energy consumption can reveal areas in the container transportation process which have the highest energy loss and require the introduction of new management and process control initiatives to address the regulations which are designed to decrease harmful industrial emissions and encourage novel technologies and thereby increase the eco-friendliness of existing systems.

Corresponding author:
Tomas Eglynas, Klaipeda University, Herkaus Manto g. 84, Klaipeda LT-92294, Lithuania.
Email: tmse@inbox.lt

Conclusion: Based on the research results, the article can provide a reference for the estimation of diesel truck efficiency in seaport terminal operations.

Keywords
Container terminal, container truck, energy consumption, measurement, modeling, transportation

Introduction

The transport sector accounts for a quarter of the total greenhouse gas emissions produced by the European Union (EU), and this proportion is still growing as industry intensifies. To reduce the effect on the climate, it is necessary to eliminate emissions due to transport by 90% by 2050,[1] while also ensuring that on-site cargo handling services in the transport industry remain internationally competitive.[2] The most effective means of enhancing container handling operations at these terminals is in determining the most critical operations where energy loss is encountered,[3] improving the existing systems through the replacement or improvement of infrastructure,[4] and proposing complex solutions to maintain the sustainability of the transportation operations.[5] However, multidimensional performance evaluation metrics such as these require a significant investment of time, effort, sectoral expertise, and holistic knowledge which are not suitable for instantaneous evaluations of separate container handling processes. CO_2 emission calculation methods have also been used to assess the efficiency of container handling terminals.[6] Researchers[7] have designed models to simulate the quantification of carbon emissions in which the energy consumption[8–12] of container trucks is based on diesel consumption. However, these models only examine the overall efficiency of the terminal over a long period and do not provide an opportunity to examine the efficiency of individual container handling operations and infrastructure units. The tasks of scheduling container transportation routes, optimization, and synchronization of handling processes have been solved by various researchers. For example, Sha et al.[13] proposed a novel integer programming model for the optimization of yard crane scheduling and their energy consumption at container terminals. This model considered key factors such as crane movement and turning distances and the practical operational rules directly related to total energy consumption. With the growing popularity of automated guided vehicles (AGVs) at container terminals, some previous studies have focused on integrated scheduling for the coordination of handling equipment and AGV routing,[14] multi-AGV scheduling for conflict-free path planning,[15] and optimization of strategies for yard truck scheduling at container terminals[16] to minimize energy costs. Other studies[17–22] have analyzed quay cranes (QCs) and related seaport infrastructure to improve transportation operations.

Previous studies have introduced models for the estimation of energy consumption in electric vehicles (EVs),[23] investigating energy recuperation capabilities and motor overload conditions. Recent literature contains energy modeling techniques for EV energy consumption in large-scale transportation networks.[24,25] Some models provide simulations of the battery powered AGV systems used at automated

container terminals, evaluating their performance[26] according to parameters such as the number of AGVs, charging station configurations, recharging policies, etc. However, these models are not suitable for the estimation of energy consumption by container transportation at the terminal. Furthermore, diesel-powered container transportation currently prevails at seaport container terminals, and battery powered AGVs are still the machines of the future. It is therefore important to identify the energy needs to transport a container from ship to stack to minimize fuel consumption and CO_2 emissions and determine the potential energy savings through the deployment of battery powered AGVs.

In summary, previous studies have focused on the assessment of the general performance of container terminals over a long period but did not consider individual container transportation route analysis in terms of energy consumption; no specialized models for the estimation of instantaneous energy costs involved in transporting individual containers at a terminal are available. In the present article, we analyzed the technical efficiency of container handling equipment (i.e. diesel-powered container trucks) in terms of energy consumption per route (cycle)—"ship-truck-stack-ship"—using a model which evaluates instantaneous energy consumption. The results allow the total efficiency of container handling during truck operations to be increased through the use of the superposition principle. The model was verified with data collected from on-site measurements at the Klaipėda port container terminal.

Methods

In this section, we present a mathematical method which describes fuel and energy consumption based on the experimental data from on-site measurements. This method not only allows the total fuel consumption for the entire operational period to be evaluated but also the fuel consumption for each individually transported container. The model also allows a real-time estimation of the efficiency of the vehicle's on-site movements.

Energy cost estimation model

The model calculates energy consumption according to the mass of the truck, its coordinates, and its acceleration values. Specific parameters were recorded for each point in 2D space (refer to Figure 1 for the model): traction force $F(t,C)$, which changes over time and depends on fuel consumption, truck velocity $v(t)$, total resistance force $F_T(t)$, and the tangent to the trajectory $\tau(t)$ intersecting at a single point of mass. The coordinates were calculated for each point of mass in the modeled body.

The work of each truck is defined by a cycle: the truck moves from the ship to the stack and back again. During the cycle, the mass of the modeled body changes. In the model, the total mass m_1 comprises the mass of the truck plus the mass of the container it carries, and mass m_2 is the mass of the truck alone. The total mass

Figure 1. Representation of truck dynamics and container transportation in the port.

changes over time as different containers are transported. At some point in time, two containers may be placed on the truck (TEU containers). The image below (Figure 2) demonstrates the changes in total mass over a single cycle of the diesel truck at the terminal.

Figure 2 indicates that the truck waited for the crane operation for up to 300 s (in the presented case study). Two 20-foot containers were loaded at the 320th second. The first 20-foot container was unloaded from the truck into the stack by the end of the 440th second. The second 20-foot container was unloaded from the truck by the end of the 640th second, and the truck returned to the crane by the end of the 800th second, concluding the full cycle.

Evaluation of the cycle included the energy consumption model, which is necessary for the estimation of energy loss during these full cycles at the terminal. To calculate these coefficients, additional measurements were conducted with the truck and the measuring equipment during the experimental phase. An explanation of the methods applied in these experiments is presented in detail in sub-section IV.

We examined three different movement modes in the container trucks to estimate their fuel consumption: 1—acceleration; 2—movement with inertia; 3—braking process. The first mode was calculated when the truck's acceleration was positive: $\frac{da}{dt} > 0$, $a(t) > 0$. The second mode was calculated when the truck moves with inertia: $\frac{da}{dt} < 0$, $a(t) > 0$. The third mode was calculated when the truck decelerates using brakes: $\frac{da}{dt} < 0$, $a(t) \leq 0$. To calculate the energy and fuel consumption, only the first and second modes were considered. To calculate the energy and fuel consumption for the third mode, only the minimum acceleration values were used $-a(t)m_{i.}$. These modes can be used to evaluate the movement and fuel
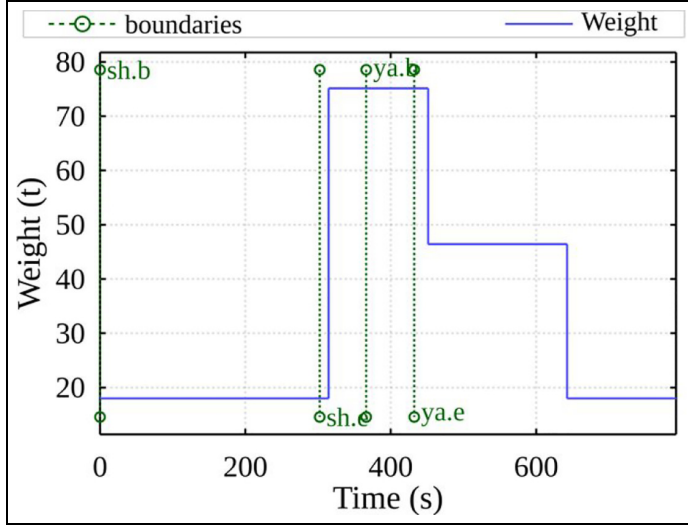
Figure 2. Example of the change in mass during a single transportation cycle at the terminal.

consumption of both loaded and unloaded trucks and present an opportunity to decrease consumption in all cycles. Therefore, the movement mode can be described according to energy consumption criteria (power).

Truck movement power P_{mov} is calculated according to:

$$P_{mov} = v\vec{\tau}^T(m_t\vec{\tau}a + \vec{\tau}F(t, C_t(t)) - \vec{\tau}F_T(t)) \cdot H(\vec{\tau}^T\vec{a})$$
$$= v(m_t a + F(t, C_t(t)) - F_T(t, v)) \cdot H(\vec{\tau}^T\vec{a}), \tag{1}$$

Where $F(t, C_t(t))$ is the traction force, $C_t(t)$ is the fuel consumption, $v(t)$ is the velocity of the total mass body at time t, τ is the unit vector tangent to the trajectory, $F_T(t, v)$ is the resistance force, $H(\vec{\tau}^T\vec{a})$ is the Heaviside function, and $a(t)$ is the acceleration value of the body mass m_t. The total mass of the body is described as:

$$m_t = (m_{truck} + m_{cont.})S_1(t) + m_{truck}S_2(t) = m_1 S_1(t) + m_2 S_2(t), \tag{2}$$

Where $m_1 = (m_{truck} + m_{cont.})$ as the mass of the truck and the container, and $m_2 = m_{truck}$ as the mass of the truck. $S_1(t) \cdot S_2(t)$ are the step-functions which describe the path from the ship to the stack ($S_1(t) = 1$, $S_1(t) = 0$) and the path from the stack to ship ($S_1(t) = 0$, $S_1(t) = 1$).

The total movement resistance force $F_T(t, v)$ of the body is calculated for each point in time t according to:

$$F_T(t, v) = F_{air}(t, v) + F_{roll}(t, v) + m_t a(t), \tag{3}$$

This force depends on the rolling resistance force $F_{roll}(t)$ and air drag force:

$$F_{air}(t, v) = \frac{1}{2} C_a A \rho (v - \vec{\tau}^T \vec{v}_w)^2 sign(v - \vec{\tau}^T v_w), \tag{4}$$

where $F_{air}(t, v)$ is the air drag force, C_a is the truck drag coefficient, $\vec{v}_w$ is the wind vector, ρ is the air density; A is the frontal cross-sectional area of the truck calculated according to:

$$A = A_1 S_1(t) + A_2 S_2(t), \tag{5}$$

where $S_1(t) = 0$, A_1 is the frontal area of a loaded truck and A_2 is the frontal area of the unloaded truck such that $A_1 > A_2$.

The rolling resistance force $F_{roll}(t)$ which acts on the moving truck at the specified time is calculated expressed by:

$$F_{roll}(t, v) = m_1 g f_{r1}(v) S_1(t) + m_2 g f_{r2}(v) S_2(t), \tag{6}$$

where $f_{r1}(v)$ is the rolling resistance coefficient with body mass body m_1, $f_{r2}(v)$ is the rolling resistance coefficient with body mass body m_2, and g is the acceleration due to gravity (9.81 m/s^2).

The power which is lost when the truck brakes is calculated according to:

$$P_{BR}(t) = v(t) F_T(t, v) H(\vec{\tau}^T \vec{a}(t)) H(-\vec{\tau}^T \frac{d\vec{a}(t)}{dt}) + v(t) m_t |a_{av}| H\left(-\vec{\tau}^T \frac{d\vec{a}(t)}{dt}\right), \tag{7}$$

The first member of equation (7) represents the power in the second mode, and the second member represents the power in the third mode (Figure 3), where:

$$a_{av} = 1/(t_2 - t_1) \int_{t_1}^{t_2} a(t) dt, \tag{8}$$

where the interval $t_j - t_i$ acceleration is negative, $a(t) < 0$ (braking in progress).

Energy consumption was calculated by numerical integration using the trapezoidal method. The integration step was determined by the data recording time-step, which was 10 ms.

Fuel consumption evaluation method

In the fuel consumption calculation, we assumed that the fuel consumption of a truck involved two components: fixed, to maintain the efficiency of the truck, and variable, to overcome the forces which resist movement during acceleration or maintaining a constant velocity. Variable fuel consumption has a linear relationship between the power supplied to the truck wheels and the fuel consumption of the engine at that time.
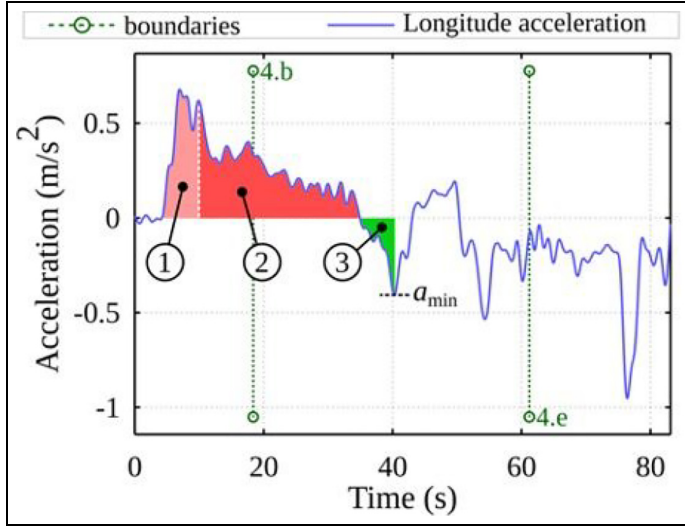
Figure 3. Container truck movement mode: 1—acceleration; 2—movement with inertia; 3—deceleration (braking process).

Constant fuel consumption at a specific point in time is expressed as:

$$C_0(t) = p_0 b(t), \tag{9}$$

where p_0 is the constant coefficient. The factor $b(t)$ is determined by:

$$b(t) = \begin{cases} 1, when & da(t)dt > 0 \\ 0, when & da(t)dt \leq 0 \end{cases}. \tag{10}$$

Variable fuel consumption at a particular point in time is expressed as:

$$C_d(t) = p_d P_{mov}(t), \tag{11}$$

where p_d is the coefficient and fuel consumption at a specific point in time. The total fuel consumption at any given time is obtained from:

$$C_t(t) = C_0(t) + C_d(t). \tag{12}$$

Each component's factors are calculated from the truck's measurement data: mass, acceleration, velocity, and total fuel consumption $C_t(t)$ during the measurement period.

By integrating (12) during the measurement period (from time t_s to time t_e) for each cycle, we obtain total fuel consumption (13). The fuel consumption after the Nth cycle is equal to:

$$\sum_{k=1}^{Ncycle} \int_{t_{sk}}^{t_{ek}} C_{0k}(t)dt + \sum_{k=1}^{Ncycle} \int_{t_{sk}}^{t_{ek}} C_{dk}(t)dt = \sum_{k=1}^{Ncycle} \int_{t_{sk}}^{t_{ek}} C_{tk}(t)dt, \qquad (13)$$

Equation (13) can be rewritten as:

$$ap_0 + bp_d = c, \qquad (14)$$

where a, b, c are the coefficients:

$$a = \sum_{k=1}^{Ncycle} \int_{t_{sk}}^{t_{ek}} C_{0k}(t)dt$$

$$b = \sum_{k=1}^{Ncycle} \int_{t_{sk}}^{t_{ek}} C_{dk}(t)dt, \qquad (15)$$

$$c = \sum_{k=1}^{Ncycle} \int_{t_{sk}}^{t_{ek}} C_{tk}(t)dt$$

The fuel consumption coefficients are determined after the Nth cycle by minimizing the objective function:

$$min\Phi = (ap_o + bp_d - c)^2, \qquad (16)$$

We introduce the variables vector $\vec{x}^T = [p_0, p_d]$. Minimization of the objective function is performed using the method of iterations, when each iteration k solves the following equation:

$$[I_k]^T[I_k]\Delta\vec{x}_k = -[I_k]^T\Phi_k, \qquad (17)$$

where the Jacobi matrix:

$$[I_k] = \left[\frac{d\Phi(x_k)}{d\vec{x}}\right]. \qquad (18)$$

After solving (17), we obtain the improved variable vector:

$$\vec{x}_{k+1} = \vec{x}_k + \Delta\vec{x}_k, \qquad (19)$$

where k is the iteration number.

To calculate fuel and energy consumption, it is necessary to know the components which resist movement of the truck. The calculation method of these components is presented in sub-section III. To find these components, experimental measurements were performed in the field to determine the necessary data for the calculations.

Method of estimation of the air and rolling resistance coefficients

To calculate the energy expended in transporting the container, it is necessary to assess the aerodynamic coefficients and total resistance to the movement of the truck. The method for determining these coefficients experimentally is given below.

The coefficient of the total rolling resistance is estimated for each period such that $t = t_{i+1} - t_i$. This allows evaluation of the fuel consumption of a truck with a cargo load during movement, where $S1(t) = 1$, and without a load, where $S2(t) = 1$. This improvement in the rolling resistance coefficient is necessary because it allows us to estimate the vertical strain on each truck wheel. This method can be applied up to velocities of $v_{al} = 30\,\text{km/h}$, which is suitable for the studied case since truck speed in the terminal is restricted up to $30\,\text{km/h}$.

The total rolling resistance coefficient during the period $t = t_{i+1} - t_i$ is calculated from the equation:

$$f_{rk,i,i+1} = \frac{28.2 \cdot \left(a_{i+1} \cdot v_i^2 - a_i \cdot v_{i+1}^2\right)}{1000 \cdot \left(v_i^2 - v_{i+1}^2\right)}, \tag{20}$$

where $k = 1$ when $S_i(t) = 1$, and $k = 2$ when $S_i(t) = 2$; $a_i = a(t_i)$ and $a_{i+1} = a(t_i + t)$; $v_i = v(t_i)$ and $v_{i+1} = v(t_i + t)$ for the movement velocities of periods t_i and t_{i+1}.

The movement velocity v_{i+1} is determined by using the acceleration values a_i and a_{i+1} according to:

$$v_{i+1} = v_i + \frac{t}{2}(a_i + a_{i+1}), \tag{21}$$

Determining the aerodynamic drag coefficient C_a applies the same procedures as determining the rolling resistance. The drag coefficient C_a in the period $t = t_{i+1} - t_i$ is calculated according to the expression:

$$c_{k,i,i+1} = \frac{6 \cdot m_t \cdot (a_i - a_{i+1})}{A \cdot \left(v_i^2 - v_{i+1}^2\right)}, \tag{22}$$

such that $v_i^2 - v_{i+1}^2 \neq 0$; where A is the frontal area of the truck determined from (5), m_t is the total mass of the truck calculated from (2) for $k = 1$ when $S_1(t) = 1, S_2(t) = 0$, and $k = 2$ when $S_1(t) = 0, S_2(t) = 1$.

Using these methods, we conducted a field experiment to determine the rolling resistance and air drag coefficients, which were then applied in the momentary energy (fuel) consumption model and energy (fuel) consumption calculation.

Setup of experimental equipment

This section describes the experimental conditions, measured parameters, and evaluated factors. Based on the presented methods, the equations can be applied to calculate the energy consumption required to transport a container at the container
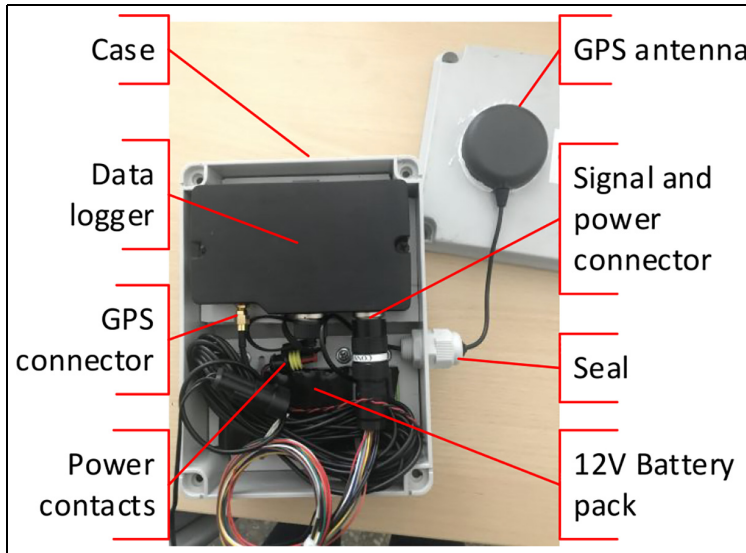
Figure 4. The measurement equipment is used to acquire the position of the truck and sensory data.

terminal using a diesel truck. We performed experimental studies to determine the coefficients of the resistances required for the calculations.

We used the measurement equipment shown in Figure 4 to acquire statistical data on the movement of diesel trucks at the Klaipėda port.

Using magnets, we mounted the equipment on the roof of a truck. The mounting position is shown in Figure 5.

At the start of the experiment, the fuel level was observed and recorded. The fuel level was then checked every half hour for the duration of the experiment. After an undefined period of operations, the vehicle was re-filled with fuel.

The operators checked the fuel levels before and after refueling, observing the amount of fuel displayed on the fuel pumps for more accurate results.

Results

Statistical analysis of the experimental data

Using modern instruments, we conducted experimental measurements of non-autonomous container handling in the port area. The movements of trucks and their container loads between the ship and container stacks were recorded. We analyzed 160 full cycles of the truck. The comparative results of the diesel truck route distance and travel time are presented in Figure 6.

Figure 5. Example of the trucks used in the experiment and the selected mounting point on the vehicle.
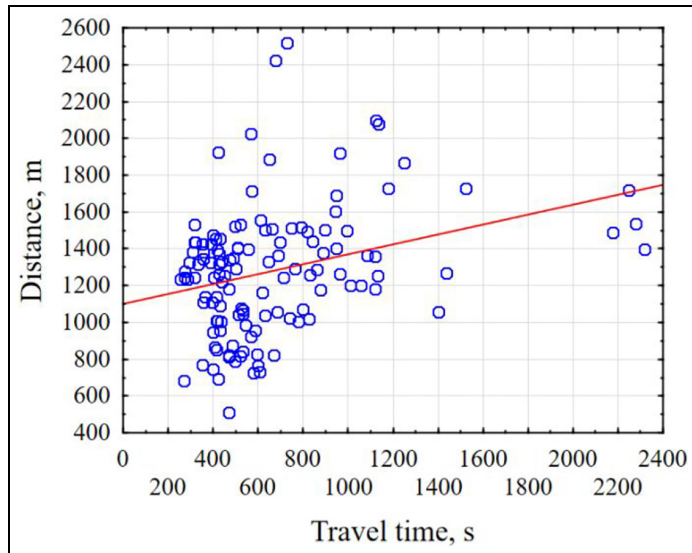

Figure 6. Relationship between the duration of a truck cycle in the port area and the distance traveled.

Linear equations can be written as $y = 1198 + 0.14x$, where y is the travel distance in meters and x is the time required to travel in seconds. The value of correlation coefficient r is 0.32. Figure 6 shows that the truck traveled a distance of 1200–1400 m in 200–1200 s. The time required can vary 10-fold.

The distribution of travel time is presented in Figure 8. In the case of non-autonomous loading, the data shows that the duration of transportation at the quay can vary from 253 to 2600 s. We can also see that the travel route is often
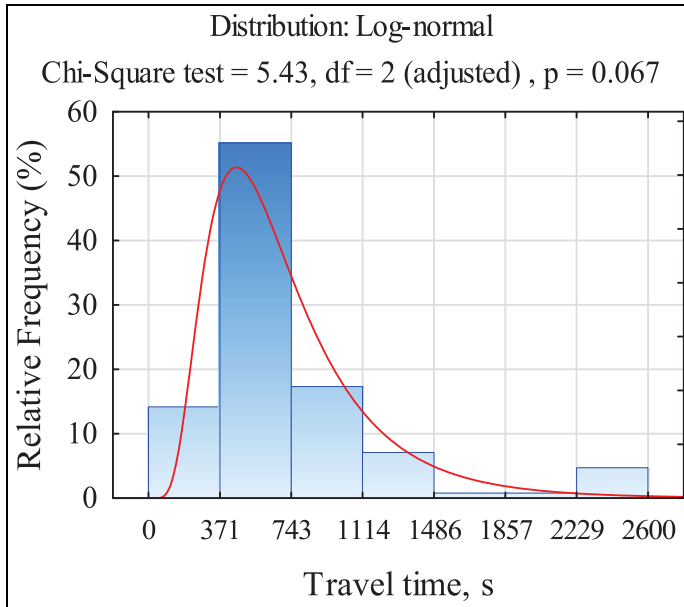
Figure 7. Distribution of the duration of truck movement in the port area.

longer than necessary, therefore, in general, managing the data and overall data flow between the loading process and transport equipment could optimize the travel time required for transportation, thereby reducing the required energy. We performed a statistical analysis of the measurement data using the Chi-Square method and found that the total driving time for "crane-stack-crane" movement is described by a lognormal distribution.

Statistical analysis of the measured travel times (Figure 7) showed that over 67% of the travel times did not last more than 743 s. However, approximately 35% of the travel times continued for more than 763 s as a result of interruptions, causing inefficient use of energy.

The travel distances measured in the port area are presented in Figure 8. The data for travel distance and duration indicated a very high scatter. The average travel distance was 1289 m, with a standard deviation of approximately 347 m. The largest distance traveled values was 2889 m, indicating that the vehicle traveled an inefficient trajectory (Figure 8).

The time taken for transportation in the port area could be reduced by synchronizing the work of vehicles and automating the port's entire loading and transportation process, thereby using energy resources more efficiently and producing less pollution. This would be especially significant for ports located in urban areas.

The next section of the article provides detailed measurements of truck movements in the port to identify transport interruptions and truck or crane downtime
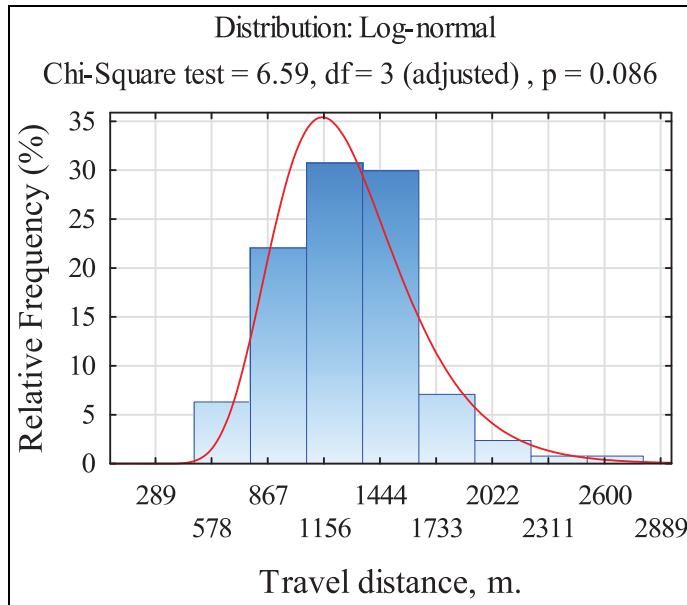
Figure 8. Distribution of the distance traveled in the port territory.

due to lack of coordination between the operational modes in the loading equipment.

Study of a single "ship-truck-stack-ship" cycle

The most common length of trajectory traveled by a truck is shown in Figure 9.

After receiving a container from the ship, the truck moved from the ship toward a designated stack to unload the container, then returned to the container loading area near the ship. Figure 9 shows the sections of the trajectory curve are marked with start "b" and end "e."

As mentioned above, the truck's position was measured using GPS equipment. Since the GPS information was transmitted by radio signal and the working environment at the port contained many metal structures, the experiment was exposed to a large amount of interference and the trajectory measurements were distorted.

Figure 10 shows the change of mass during a single route cycle of a truck loaded with a container.

Figure 11 graphs the measured velocities during the truck route cycle. The truck velocity was non-uniform and changed radically at each new turn.

Figure 12 shows the sudden and uneven changes in acceleration along the truck route (longitudinal acceleration). This unevenness may be a possible reason for the
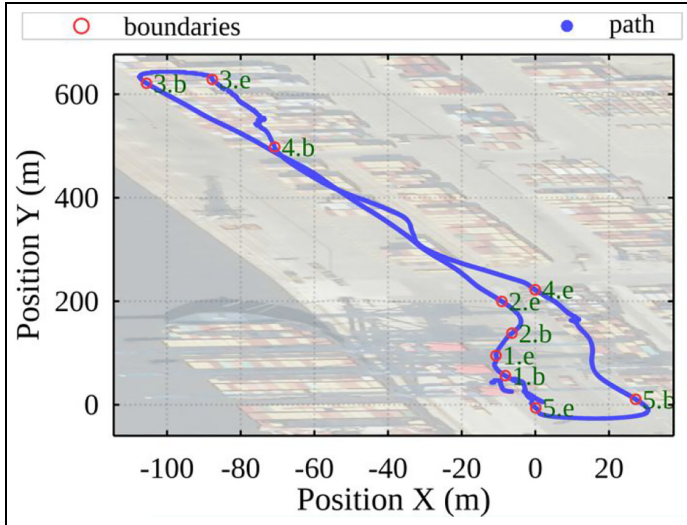
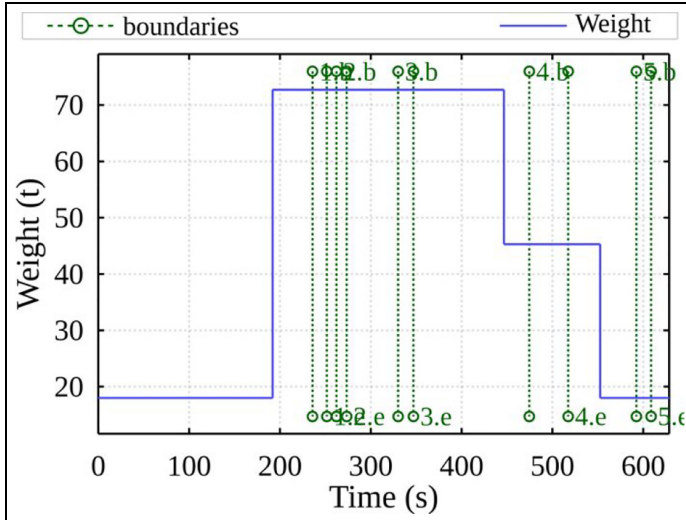**Figure 9.** Trajectory of a truck at the terminal.
e: end; s: start.

Figure 10. Variation of mass during the container transportation cycle.
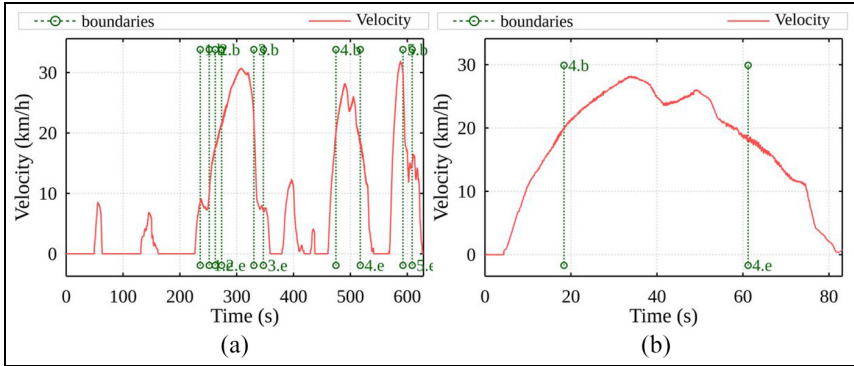
Figure 11. Truck velocity during a single transportation cycle: (a) full cycle and (b) period from 450 to 535 s.
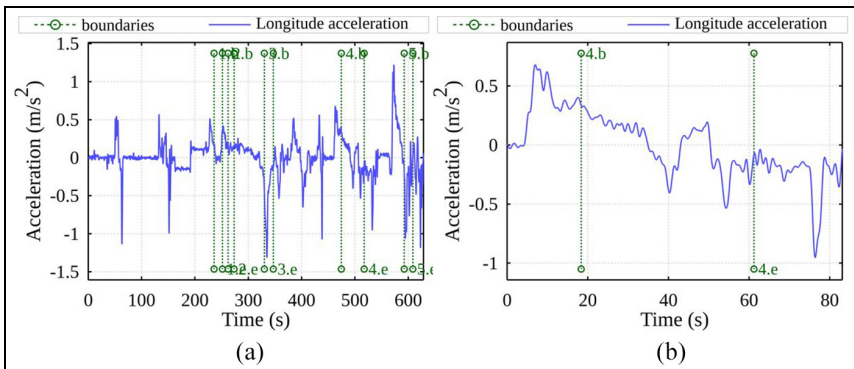

Figure 12. Changes in acceleration along the truck route (longitudinal acceleration: (a) full cycle and (b) period from 450 to 535 s.

high fuel consumption. The maximum variation in acceleration occurred during truck acceleration and deceleration.

Figure 13 shows the sudden and uneven changes in accelerations perpendicular to the truck route (lateral acceleration). The maximum accelerations occurred during a change in the truck movement direction. The vibrations (high spikes of lateral acceleration) also occurred because of insufficient fixation of the container. This acted on the driving performance and stability of the truck during the execution of a turn.

The instantaneous power calculated using the energy consumption model described in the above sections are shown in Figure 14. The presented results show
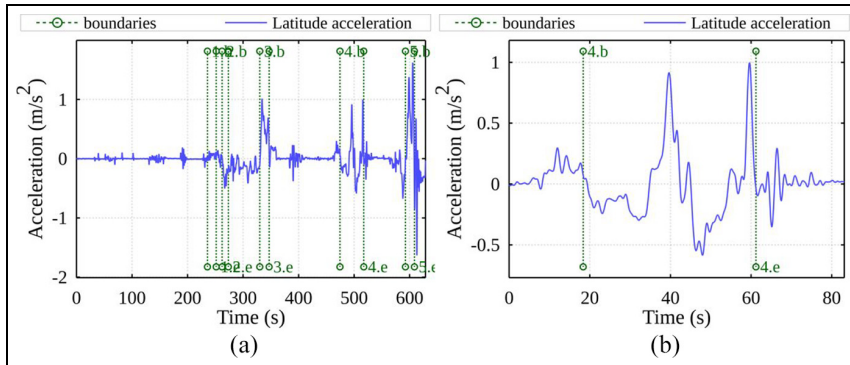
Figure 13. Changes in accelerations perpendicular to the truck route (lateral acceleration):
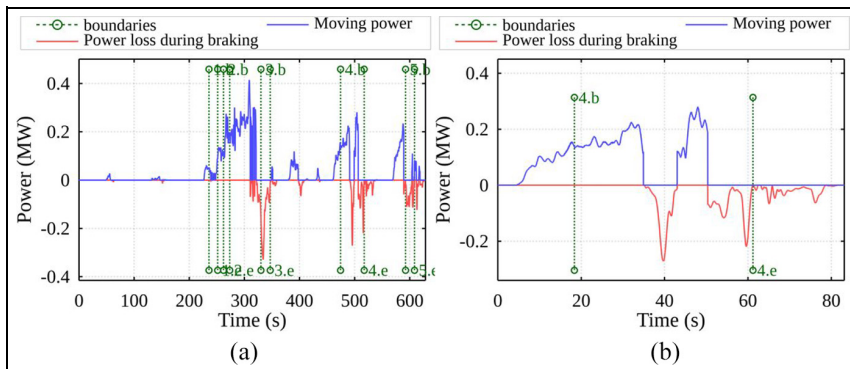(a) full cycle and (b) period from 450 to 535 s.

Figure 14. Instantaneous truck movement power (acceleration and continuous power for
driving) and braking power: (a) full cycle and (b) period from 450 to 535 s.

an exaggerated velocity increase at several moments: a source of increased fuel
consumption.

If the electric autonomous guided vehicle (AGV) ran on the same profile, its
electric motor-generator would be rather powerful ($>100\,$kW) and have a battery
power capacity capable of absorbing the energy which is recoverable during the
braking. The red line shows the power during active braking of the truck. In the
case of an internal combustion engine, the braking energy is converted into heat,
but with the installation of an electric motor-generator, it can be recovered as elec-
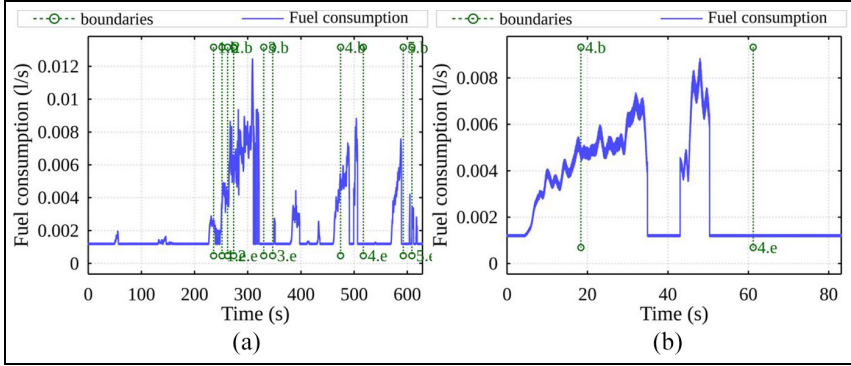trical energy.

Figure 15. Fuel consumption during a single drive cycle of a loaded truck: (a) full cycle and (b) period from 450 to 535 s.

Figure 15 shows the fuel consumption required to accelerate or maintain a constant truck velocity. Fuel consumption was calculated according to the method presented in Section IV Part B.

Figure 15 indicates that during acceleration, fuel consumption momentarily exceeded 0.004 l/s. Also, during downtime (periods of 0–90 s, 130–200 s, etc.), fuel consumption in the truck reached significant values of >0.001 l/s. We can assume that sudden increases in truck velocity such as these increase overall fuel consumption. We can also observe from this investigated cycle that the downtimes when the truck was not moving could be partially eliminated by synchronizing the operations with other machinery on-site. During this cycle, energy resources can be conserved through the application of adjustments to the driving and acceleration characteristics.

Energy calculations

By using the presented methods for the estimation of fuel consumption, we can estimate the losses of energy for each mode for each period t. If we know the exact amount of energy lost, we can analyze the non-obvious reasons for this loss.

The energy consumption for one cycle is described according to:

$$E_{mov} = \int_{t_s}^{t_e} (P_{mov}(t) + P_{BR}(t))dt, \qquad (23)$$

where t_s is the starting time point t of the truck work cycle (ship-stack-ship), t_e is the ending time point t of the truck work cycle (ship-stack-ship).

Measurements were taken for $N = 160$ truck work cycles at the terminal. After the measurement data were processed for all cycles, we discovered that the truck usually covered about 1.3 km of the road during its operating cycle. The
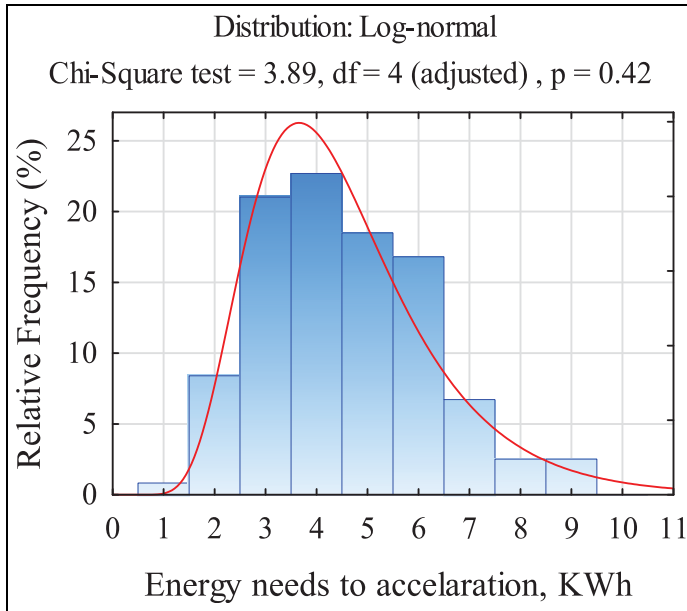
Figure 16. Histogram of the energy consumption of the truck.

distribution of the calculated energy consumption required to increase or maintain the velocity of the truck for each cycle is given in Figure 16.

We calculated that average amount of energy needed to accelerate the truck is at least 4.54 kWh for a 1.3 km cycle, that is, 3.49 kWh/km on average when the acceleration derivative is positive $da(t)/dt > 0$.

Figure 17 presents the loss of energy during the truck's braking cycle. The data best fits a lognormal distribution probability density (Chi-square test: $p = 0.48$). The observed mean is 1.99 kWh for 1.3 km, that is, 1.53 kWh/km on average. The energy loss during braking is about 43.8% of the total energy consumption of the truck. In this case, the truck executes braking by using the internal combustion engine in combination with brakes.

The diesel truck often queues or waits for the operation to start at the ship's crane or container crane during loading operations. Figure 18 shows the exact amounts of fuel consumed.

Lognormal distribution probability density can be applied to the data (Chi-square test: $p = 0.55$). These losses could be avoided by synchronizing cargo handling processes and integrating an electric drivetrain for the trucks. Calculations and experimental results show that during downtime, the trucks waste 0.13 l of fuel on 22% of the loading cycles.

The coefficient of correlation r between the energy required for acceleration and the energy lost during braking is equal to 0.83 and shows a strong relationship.
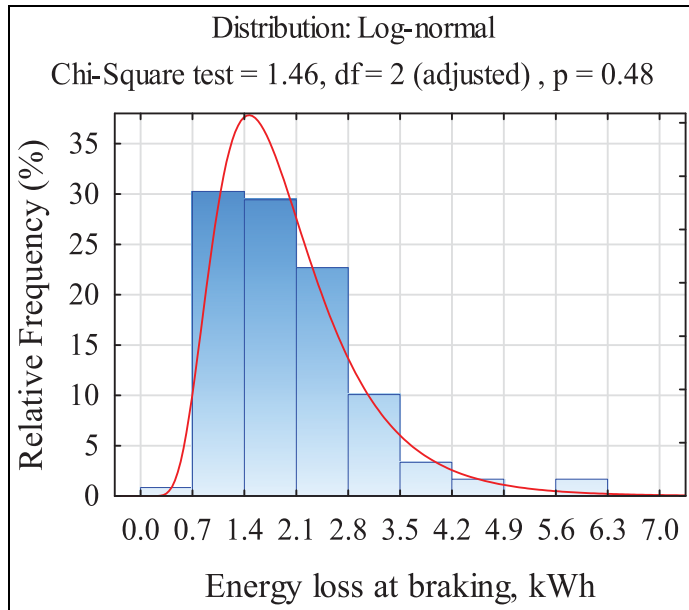
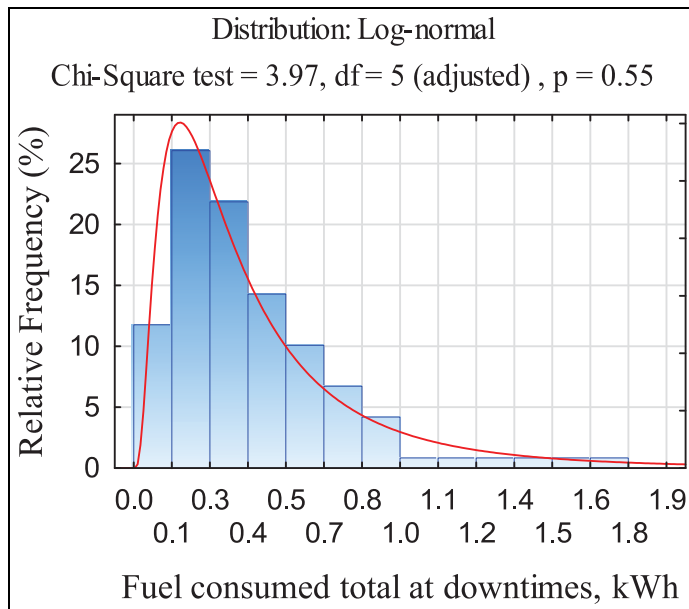**Figure 17.** Histogram of truck energy loss during active braking.

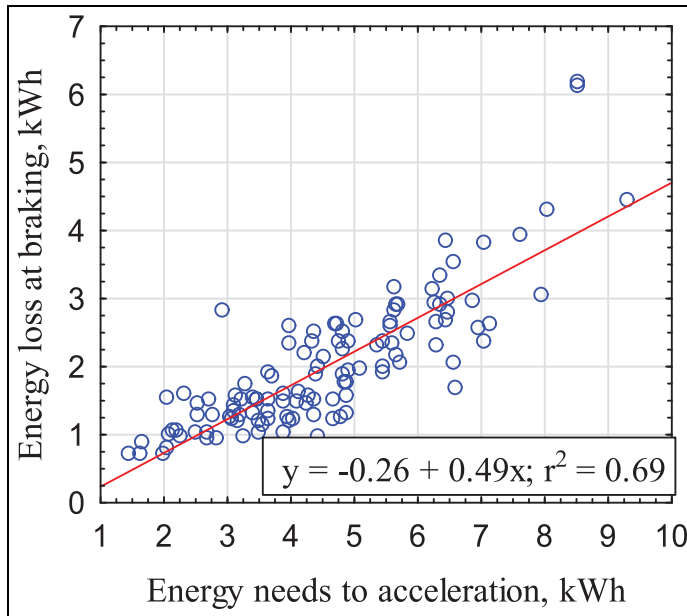**Figure 18.** Histogram of truck fuel consumption during downtime.

Figure 19. Relationship between energy required for acceleration and energy lost during braking.

Figure 19 presents a linear regression relationship $y = 0.497x - 0.26$ between the energy required for acceleration (x) and the energy lost (y) during braking.

The analysis shows that this energy could be recovered during the truck's operations via recuperation using an electric motor-generator and a smart battery storage system. Current transportation management is applied through non-optimal scheduling methods; cranes and trucks both experience frequent downtimes while they wait for container loading and unloading. Excess fuel is consumed as a result of these downtimes and raises the CO_2 emissions and other air pollution at the port. The pollution problem is serious, especially when a port, such as Klaipėda, is located in an urban area.

Notes and discussion

All the statistical data were acquired from the observation of 160 full work cycles of container trucks at the terminal. The effects of weather (wind speed, humidity, etc.) on the accuracy of the measurements was not considered in the model, nor was this information used to estimate the accuracy of the statistical data acquired. According to the on-site operators, the weather conditions do not significantly affect traction on the diesel truck tyres during summer and autumn. These conditions were therefore ignored, but they should be considered in future research.

According to the operators, visibility decreases during harsh weather conditions (heavy rain and wind) and they must be more cautious at these times. Crane operators are also more cautious under these conditions since they affect the speed of container placement on diesel trucks or AGVs. During winter, ice-covered roads may affect overall tyre traction by increasing the distance required to brake while transporting heavy cargo.

Downtime occurs frequently, and sometimes, either because of error or other scheduling reasons, the destination of the container changes several times per cycle. When the deck of the ship is fully unloaded, the lids which cover the ship's hull must be removed. This creates long waiting times (downtimes), the removal procedure taking up to 30 min to complete.

Fuel consumption is currently measured by acquiring the readings from sensors installed in the diesel truck's fuel tank. The observed measurements varied greatly in each work cycle. In future experiments, a different fuel consumption measurement method should be used. All these observations are critical and should be considered in future research and for the development of new synchronization tools and methods for port operations.

Conclusion

Each new solution and method must include concrete factors, that is, the travel speed of the trucks (with all acceleration points for each driver), and the quay crane and stack crane operational capabilities (for each operator). Consideration of these factors will certainly not only aid in increasing the efficiency of overall operations in the transport chain globally but will also help decrease harmful emissions.

The experimental measurements and the described methods show that the total energy losses reached 3.49 kWh/km during the transportation of a container, and the energy loss for braking reached 1.53 kWh/km on average. For each new cycle, the energy loss during braking reached 43.8% on average of the truck's total energy consumption.

The proposed fuel consumption model proved to be 91% accurate (it is very sensitive to real fuel consumption measurements and the statistical data of previous measurements with slight approximations). The coefficients of the proposed model were calculated from the two measurements taken during the on-site experimental study. The model was applied to calculate the theoretical fuel consumption for the third measurement. The results were compared to real fuel consumption, and only a 9% deviation was observed.

To ensure the model's long-term accuracy and possible adaptation in port operations, it is vital to measure the fuel consumption as accurately as possible. A slight change or deviation from the real value (up to 0.1 l) can have a critical effect on the final results (the accuracy of the proposed model). The methods, which we verified with an experimental study, can determine the fuel consumption of any port container truck (with or without a load), calculate the energy due to momentum, and determine the most rational control parameters for optimal fuel consumption

at any given moment based on real-time acceleration data. The truck, if operated effectively, would move with an even velocity to maximize fuel economy and solve the problem of fuel wasted as a result of downtime.

Declaration of conflicting interests

The author(s) declared no potential conflicts of interest with respect to the research, authorship, and/or publication of this article.

ORCID iD

Tomas Eglynas https://orcid.org/0000-0002-9973-5896

References

1. European Commission. The European Green Deal: Communication from the Commission to the European Parliament, the European Council, the Council, the European Economic and Social Committee and the Committee of the Regions, 2019, p. 24.
2. Serra P and Fancello G. Towards the IMO's GHG goals: a critical overview of the perspectives and challenges of the main options for decarbonizing international shipping. *Sustain* 2020; 12: 3220.
3. Nabavi-Pelesaraei A, Bayat R, Hosseinzadeh-Bandbafha H, et al. Modeling of energy consumption and environmental life cycle assessment for incineration and landfill systems of municipal solid waste management – a case study in Tehran Metropolis of Iran. *J Clean Prod* 2017; 148: 427–440.
4. Karakas S, Acar AZ and Kirmizi M. Development of a multidimensional performance evaluation model for container terminals at Marmara Sea. *Res Transp Bus Manag* 2020; 100498.
5. Harper P. Decomposition for decarbonisation: evaluation of decarbonisation programmes. *Sci Prog* 2016; 99: 235–261.

6. Geerlings H and Van Duin R. A new method for assessing CO2-emissions from container terminals: a promising approach applied in Rotterdam. *J Clean Prod* 2011; 19: 657–666.

7. Yun P, Xiangda L, Wenyuan W, et al. A simulation-based research on carbon emission mitigation strategies for green container terminals. *Ocean Eng* 2018; 163: 288–298.

8. Sim J. A carbon emission evaluation model for a container terminal. *J Clean Prod* 2018; 186: 526–533.

9. Martínez-Moya J, Vazquez-Paja B and Gimenez Maldonado JA. Energy efficiency and CO2 emissions of port container terminal equipment: evidence from the Port of Valencia. *Energy Policy* 2019; 131: 312–319.

10. Yu H, Ge YE, Chen J, et al. CO2 emission evaluation of yard tractors during loading at container terminals. *Transp Res Part D Transp Environ* 2017; 53: 17–36.

11. Khanali M, Akram A, Behzadi J, et al. Multi-objective optimization of energy use and environmental emissions for walnut production using imperialist competitive algorithm. *Appl Energy* 2021; 284: 116342.

12. Ghasemi-Mobtaker H, Mostashari-Rad F, Saber Z, et al. Application of photovoltaic system to modify energy use, environmental damages and cumulative exergy demand of two irrigation systems-a case study: barley production of Iran. *Renew Energy* 2020; 160: 1316–1334.

13. Sha M, Zhang T, Lan Y, et al. Scheduling optimization of yard cranes with minimal energy consumption at container terminals. *Comput Ind Eng* 2017; 113: 704–173.

14. Yang Y, Zhong M, Dessouky Y, et al. An integrated scheduling method for AGV routing in automated container terminals. *Comput Ind Eng* 2018; 126: 482–493.

15. Zhong M, Yang Y, Dessouky Y, et al. Multi-AGV scheduling for conflict-free path planning in automated container terminals. *Comput Ind Eng* 2020; 142: 106371.

16. Hu X, Guo J and Zhang Y. Optimal strategies for the yard truck scheduling in container terminal with the consideration of container clusters. *Comput Ind Eng* 2019; 137: 106083.

17. Zhen L, Hu H, Wang W, et al. Cranes scheduling in frame bridges based automated container terminals. *Transp Res Part C Emerg Technol* 2018; 97: 369–384.

18. Malekahmadi A, Alinaghian M, Hejazi SR, et al. Integrated continuous berth allocation and quay crane assignment and scheduling problem with time-dependent physical constraints in container terminals. *Comput Ind Eng* 2020; 147: 106672.

19. Zeng Q, Feng Y and Yang Z. Integrated optimization of pickup sequence and container rehandling based on partial truck arrival information. *Comput Ind Eng* 2019; 127: 366–382.

20. Zhou C, Lee BK and Li H. Integrated optimization on yard crane scheduling and vehicle positioning at container yards. *Transp Res Part E Logist Transp Rev* 2020; 138: 101966.

21. Dinu O, Rosca E, Dragu V, et al. Optimization of the transfer function through handling productivity control in port container terminals. *Procedia Manuf* 2018; 22: 856–863.

22. Zhou C, Wang W and Li H. Container reshuffling considered space allocation problem in container terminals. *Transp Res Part E Logist Transp Rev* 2020; 136: 1–23.

23. Genikomsakis KN and Mitrentsis G. A computationally efficient simulation model for estimating energy consumption of electric vehicles in the context of route planning applications. *Transp Res Part D Transp Environ* 2017; 50: 98–118.

24. Xu X, Aziz HMA and Guensler R. A modal-based approach for estimating electric vehicle energy consumption in transportation networks. *Transp Res Part D Transp Environ* 2019; 75: 249–264.

25. Xu X, Aziz HMA, Liu H, et al. A scalable energy modeling framework for electric vehicles in regional transportation networks. *Appl Energy* 2020; 269: 115095.

26. Ma N, Zhou C and Stephen A. Simulation model and performance evaluation of battery-powered AGV systems in automated container terminals. *Simul Model Pract Theory* 2021; 106: 102146.

Author biographies

Tomas Eglynas received his PhD degree in Transport Engineering in 2017. He now works as a researcher at the Marine Research Institute of Klaipeda University and as the CEO of "Inotecha" (Research company) Ltd. Topics of his research interests are intelligent systems, electronics, software development, and Industry 4.0.

Sergej Jakovlev received his PhD degree in Transport Engineering in 2016. He now works as a researcher at the Marine Research Institute of Klaipeda University and as a senior researcher at the Telecommunications Department of VSB-Technical University of Ostrava. Topics of his research interests are intelligent systems, operations research and big data analytics.

Valdas Jankunas received his PhD degree in Electrical and Electronics Engineering from Kaunas Technology University in 2013. His employment experience included Klaipeda University. His special fields of interest included Power Electronics and Embedded Systems.

Rimantas Didziokas obtained the qualification of a Mechanical engineer in 1976. Candidate of Technical Sciences (now Ph.D.). Highest professional achievements: 1995-1996 Member of Klaipeda City Municipal Council; 1996-2000 Member of Seimas of Lithuania; 1999-2000 Minister of Transport and Communications (Lithuania). His research interests are Mechanical engineering, control systems, and industrial applications.

Jolanta Januteniene received her Ph.D. in Mathematics in 2001. She is a member of editorial boards of journal Transport (CA) and reviewers of highly ranked CA and SCOPUS journals. Topics of her research interests are Mechanical engineering, mathematical modeling, composite materials, and statistical data analytics.

Darius Drungilas received his Ph.D. Degree in 2014 in Informatics engineering. Now works as a Researcher and Associate professor at Klaipeda University Marine Research Institute and Informatics and Statistics Department of Klaipeda University. Topics of his research interests are machine learning algorithms, industry 4.0, and affective computing.

Mindaugas Jusis acquired Master's Degree in Informatics engineering in 2014. Now work at Klaipeda University as a lecturer and junior researcher. Has experience working with international projects and with industry. He has excellent skills in programming: JAVA, PHP, Swift etc. His special fields of interest include data acquisition systems, Industry 4.0, Internet of Things.

Edvinas Pocevicius received his Bachelors degree in Electrical and Electronics Engineering in 2021. Now works in Klaipeda University at the Department of Informatics engineering as a junior researcher. Topics of his research interests are Electronics, Automation and Control Systems, Sensor systems.

Marijonas Bogdevicius is a habilitated Doctor of Technology, full member of the Lithuanian Academy of Sciences. Field of interest: dynamics of mechanical, hydraulic and pneumatic systems, computational mechanics, dynamics of vehicles, dynamics of traffic flows. Works at Vilnius Gediminas Technical University at the Departments of Mobile Machinery and Railway Transport.

Arunas Andziulis now works in Klaipeda University at the Department of Informatics engineering as a senior researcher, having more than 50 years' experience of working in Industry, developing electronics devices, semiconductors and smart systems. Topics of his research interests are Electronics, Automation and Control Systems, Big Data analytics.

2nd publication / 2 publikacija

2nd publication / 2 publikacija

Modeling and experimental research of quay crane cargo lowering processes

T. Eglynas, A. Andziulis, M. Bogdevičius, J. Janutėnienė, S. Jakovlev, V. Jankūnas, A. Senulis, **M. Jusis**, M. Bogdevičius, S. Gudas.

Modeling and experimental research of quay crane cargo lowering processes

Tomas Eglynas[1] , Arunas Andziulis[1], Marijonas Bogdevičius[2], Jolanta Janutėnienė[3], Sergej Jakovlev[1,3], Valdas Jankūnas[1], Audrius Senulis[1], Mindaugas Jusis[1,4], Paulius Bogdevičius[2] and Saulius Gudas[4]

Abstract

This article studies an operational problem arising at a container terminal. Klaipeda city port operations were surveilled up close and relevant remarks were made. The time efficiency of the existing container-lowering procedures using the simulation studies with a test-bed and with a real life crane operation was examined. Statistical analysis of the experimental results has showed that non-automated processes have higher time variance for the lowering process. The operations of quay crane for container handling "ship-to-shore" were analyzed, and lowering procedures time variations were determined. Each container is transported at operators own risk and with pre-defined time efficiency; therefore, it is hard to predict the optimal time for each container handling operation, thus, eventually, additional costs arise. Mathematical model was developed, which described dynamical characteristics of the container movement during lowering procedures. The lowering crane operation was modeled using known dynamic values for each separate case, and the complexity of the problem was proven. The results of modeling and experimental results show that it is possible to achieve optimal values with the existing processes.

Keywords

Dynamics modeling, quay crane, simulation, experimental research, container-lowering process, statistical analysis

Introduction

Intermodal shipping containers are widely adopted in the global transport chain to deliver various goods to end-users. Despite the obvious advantages, there is still plenty of room for improvements when it comes to time efficiency and quality increase. Global transport market is a network of companies and end-users, who rely on well-managed standards and systems. Recent trends and numbers suggest that about 90% of non-bulk global trade is being managed by shipping containers worldwide.[1,2] Europe alone in 2016 managed 0.8 billion tons of cargo.[3] Statistics shows that during the 10-year period between 2007 and 2017, shipping quantities increased by 66% (up to 148 million TEUs), taking into account the global merchandise trade by marine traffic.[4] Many engineers and managers worldwide foresaw such rapid increase. Yet, they could not manage it in an optimal manner. Thus, efficiency is a criterion which needs to be increased in order to adopt new challenges of the future. Cargo loading operations rely on loading and unloading speeds, safety of

[1]Klaipeda University, Klaipeda, Lithuania
[2]Vilnius Gediminas Technical University, Vilnius, Lithuania
[3]VSB-Technical University of Ostrava, Ostrava-Poruba, Czech Republic
[4]Cyber-Social Systems Engineering Group, Vilnius University, Vilnius, Lithuania

Corresponding author:
Tomas Eglynas, Klaipeda University, Herkaus Manto g. 84, LT-92294 Klaipeda, Lithuania.
Email: tmse@inbox.lt

operation,[5] and energy consumption in the vicinity of the port.[2] These factors tend to make final decisions when adopting new and untested technologies in practice.

The modernization of container terminals through modern ICT (information and communication technology) solutions partly solves the problems concerning the "Green" terminal initiative.[2] Autonomy of operations is adopted in many areas to control stability of container handling, transportation using terminal trucks, autonomous guided vehicle (AGV),[6] and so on. Even now, newly built cranes are using operator on site to manage the loading procedures.[7] Each new operator sees the loading standards as guidelines, but not strict rules. Therefore, crane autonomy[8] is necessary, in order to increase the efficiency of adopted standards and regulations, mechanical systems, and associated port investments. An autonomous quay crane is not an innovation on its own.[9] These complex systems already exist.[10] They are applied in many areas of industry including port operations.[11] However, modernization of existing infrastructure is a priority for most companies, working with container handling. More practical and real solution is to modernize existing systems, rather than purchase all new expensive infrastructure. Overall, there are crane stabilization systems that are already in use,[12] but they mostly lack of quality feedback and operator experience that makes huge impact on the efficiency of these expensive systems.[13]

In practice, the realization of complex control solutions is limited by the fluctuations of the spreader with load. Its movements are random in nature, due to external impacts, such as wind or physical contact with other objects.[14] It is difficult to predict such random deviations in practice. The most advanced European ports, such as Rotterdam or Hanover, the handling procedures and IT operations are mostly automated. However, the inclusion of the modern automated quay cranes is still an innovation for smaller ports throughout the world. In the light of the research and progress made in this area,[15–19] many ports in the world lack the application of these innovations.

Increasing the time efficiency of the cargo process is a topical issue addressed in the scientific work, for which various solutions are proposed, from management algorithms to cargo planning solutions.[2,6,20] The quay cranes are analyzed in the way of increasing loading time,[2,21] damping the load swinging during the loading–unloading process[21] using additional feedbacks in control system with the proportional–integral–derivative (PID) or proportional–integral (PI) controllers or using artificial intelligence analysis.[22,23]

The problem addressed in the port is the crane and the terminal truck synchronization means. The crane operator has to wait for the terminal truck or the terminal truck has to wait for the operator to finish his
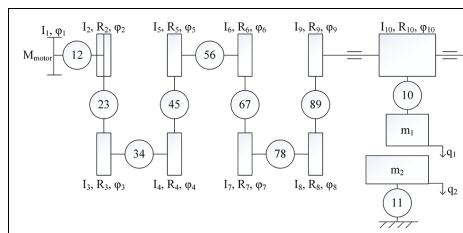

Figure 1. The overall dynamic model of the drive.

unloading routine. Due to constant operator faults, there is a delay in the end-of-shipment procedures. Especially, the container loading on terminal truck is managed difficultly. Authors propose to test analyze the lowering end procedure for the future control solution. The solution would use real terminal truck and spreader sensory data. Depending on the actual position of the terminal truck or the crane,[20] decisions are made systematically to slow down the speed of movement so that the target point reached at the same time by all involved bodies. This saves both energy resources and technical resources,[6] and increases crane and, consequently, the entire port efficiency.

Mathematical modeling of container-lowering procedure by quay crane

The mathematical model of the quay crane was developed. The quay crane consists of asynchronous electrical motor, gears, shafts, drum, cables, container, and vehicle. Because the most important part was the end of container loading, the sway of container was not taken into account. The sway of container will be included in the future improved model. The structure of this model is shown in Figure 1.

In Figure 1, $I_1, \ldots, I_9$ are the mass moments of inertia; $R_2, \ldots, R_9$ are the radii; $\varphi_1, \ldots, \varphi_{10}$ are the angles (rotation angles); M_{motor} is the quay crane spreader lowering motor; q_1 and q_2 are the displacements; 12, 34, 56, 78 are the shafts; 10 is the cable; and 11 is the vehicle suspension.

In Figure 2(a), H is the cargo height, H_1 is the distance between road surface and drum axis, H_2 is the distance between road surface and vehicle platform, L is the cable length, and F_{12} is the contact force. In Figure 2(b), q_i and q_j are the generalized displacements, e is the number of element; k_e, c_e, and Δ_e are the stiffness, damping coefficients, and gap, respectively.

The mechanical system in question (Figure 2) consists of an electric motor (1), gears (2–9), cable, container, and terminal truck. Main parameters of the analyzed system in Figures 1 and 2 are 500 kW power
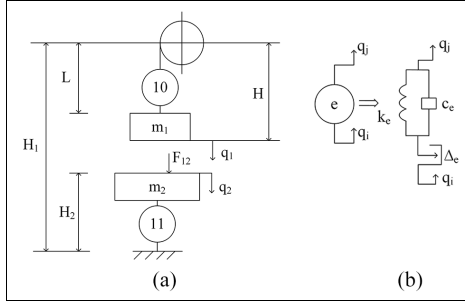
Figure 2. Container loading system design diagram: (a) dynamic model of spreader and transport, and cable (b) scheme of nonlinear element.

Table 1. The main parameters of transmission.

Parameter	Units	Value
Distance, H_1	m	11.0
Distance, H_2	m	1.50
Initial length of cable, L_0	m	2.0
Mass moment of inertia of rotor motor, I_1	$kg\,m^2$	2.0
Mass moment of inertia, I_2	$kg\,m^2$	0.0308
Mass moment of inertia, I_3	$kg\,m^2$	0.368
Mass moment of inertia, I_4	$kg\,m^2$	0.368
Mass moment of inertia, I_5	$kg\,m^2$	0.445
Mass moment of inertia, I_6	$kg\,m^2$	0.445
Mass moment of inertia, I_7	$kg\,m^2$	0.710
Mass moment of inertia, I_8	$kg\,m^2$	0.920
Mass moment of inertia, I_9	$kg\,m^2$	0.920
Mass moment of inertia, I_{10}	$kg\,m^2$	2.30
Mass of cargo and spreader, m_1	kg	22,572.0
Mass of vehicle, m_2	kg	10,000.0
Mass of 1 m cable, m_{L0}	kg	1.0
Modulus of elasticity of cable, E_L	GN/m^2	200.0
Cross section area of cable, A_L	m^2	3.1415E−4
Stiffness coefficient of contact, $k_{contact}$	MN/m	0.10E6
Damping coefficient of contact, $c_{contact}$	MN s/m	0.010E6
Integration time step	s	1.0E−6

in the main motor used for lowering container, $n = 995$ r/min, and frequency of $f = 50$ Hz. The main transmission parameters are given in Table 1.

The dynamics of the loading process are described in the equations below. Cargo distance from the axis of rotation of the drum $H(t)$, cable length $L(t)$, distance between the cargo and the terminal truck is $H_{12}(t)$ at any given time t is given in equation (1)

$$H(t) = L(t) + H_0, L(t) = L_0 + q_1(t),$$
$$H_{12}(t) = H_1 - H(t) - H_2 + q_2(t) \tag{1}$$

Here, h_0 is the height of the cargo. The rigidity coefficient of the cable is given in equation (2)

$$k_L(q_1) = \frac{E_L A_L}{L_0 + q_1(t)} \tag{2}$$

Here, E_L and A_L are the cable elastic modulus and cross-sectional area, respectively. The moment of inertia of the drum masses is given in equation (3)

$$I_{10} = I_{10,0} - r_{10}^2 m_{L0} L(t) \tag{3}$$

Here, m_{L0} is the mass per unit length of cable. The equations of motion of the load drive are derived using the second-order Lagrange equation (4)

$$\frac{d}{dt}\left(\frac{\partial E_K}{\partial q_j}\right) - \left(\frac{\partial E_K}{\partial q_j}\right) + \left(\frac{\partial E_P}{\partial q_j}\right) + \left(\frac{\partial D}{\partial q_j}\right) = Q_j \tag{4}$$

Here, E_k, E_P, and D are the kinetic energy of the drive, potential energy, and dissipative function, respectively; q_j and Q_j are the jth generalized coordinate and force, respectively. The torque of asynchronous motor M_{Motor} (the equation of variation) is given in equation (5)

$$\dot{M}_{Motor} = c_v\left(w_{M_0} - \dot{\phi}_1\right) - d_v M_{Motor} \tag{5}$$

Here, c_v and d_v are the asynchronous motor parameters, and w_{M0} is the motor rotor synchronic angular velocity. Asynchronous motor rotation (equation (6)) is given as

$$I_1\ddot{\phi}_1 = M_{Motor}(t) - M_b(t) - k_{12}(\phi_1 - \phi_2)$$
$$- c_{12}(\dot{\phi}_1 - \dot{\phi}_2) - c_1\dot{\phi}_1 \tag{6}$$

Here, $M_b(t)$ is the engine braking torque; k_{12} and c_{12} are the shaft stiffness and resistance coefficients, respectively; and $\phi_1, \phi_2, \dot{\phi}_1, \dot{\phi}_2$ are the first and second body rotation angles and angular velocities. Second- and third-gear rotations (equations (7) and (8)) are

$$I_2\ddot{\phi}_2 = -k_{12}(\phi_2 - \phi_1) - c_{12}(\dot{\phi}_2 - \dot{\phi}_1) - k_{23}R_2 u_{23} - c_2\dot{\phi}_2 \tag{7}$$

$$I_3\ddot{\phi}_3 = -k_{34}(\phi_3 - \phi_4) - c_{34}(\dot{\phi}_3 - \dot{\phi}_4) - k_{23}R_3 u_{23} - c_3\dot{\phi}_3 \tag{8}$$

where

$$u_{23} = \delta_{23p}sign\left(\delta_{23p}\right) + \delta_{23m}sign(-\delta_{23m}) \tag{9}$$

$$\delta_{23p} = R_2\phi_2 + R_3\phi_3 - \Delta_{23} \ldots \Delta_{23} \tag{10}$$

Here, Δ_{23} is the gap between gears 2 and 3

$$\delta_{23m} = R_2\phi_2 + R_3\phi_3 + \Delta_{23} \tag{11}$$

Here, R_2 and R_3 are the radii of the main circles of the gears 2 and 3; $sign(x) = 1$, when $x>1$ and otherwise 0. The fourth- to ninth-gear rotations are calculated

similarly as the second and third. Tenth gear rotation equation is as equation (12)

$$I_{10}\ddot{\phi}_{10} = \dot{I}_{10}\dot{\phi}_{10} + \frac{1}{2}\frac{\partial I_{10}}{\partial \phi_{10}}\left(\dot{\phi}_{10}\right)^2$$
$$- k_{910}(\phi_{10} - \phi_9) - c_{910}\left(\dot{\phi}_{10} - \dot{\phi}_9\right)$$
$$- c_{10}\dot{\phi}_{10} - R_{10}k_L(q_1)(R_{10}\phi_{10} - q_1) \qquad (12)$$
$$- R_{10}c_{10}\left(R_{10}\dot{\phi}_{10} - \dot{q}_1\right)$$

Cargo and vehicle movement equations (13) and (14) are

$$m_1\ddot{q}_1 = -\dot{m}_1\dot{q}_1 - k_L(q_1 - R_{10}\phi_{10})$$
$$- c_L\left(\dot{q}_1 - R_{10}\dot{\phi}_{10}\right) + m_1 g - F_{12}sign(\delta_{12})$$
$$+ \frac{1}{2}(R_6\phi_6 - q_1)^2\left(\frac{E_L A_L}{L^2}\right) - c_{aer0}(\dot{q}_1)^2 sign(\dot{q}_1)$$
$$(13)$$

$$m_2\ddot{q}_2 = F_{12}sign(\delta_{12}) + m_2 g - k_2 q_2 - c_2\dot{q}_2 \qquad (14)$$

Here, q_1, q_2 is the displacement of masses m_1 and m_2; m_1 and $\dot{m}_1$ are the cargo, spreader, and cable total mass and its derivative of time, respectively; c_L is the cable coefficient of resistance; and c_{aer0} is the aerodynamic force coefficient of resistance (equation (15))

$$\delta_{12} = (H_2 - q_2) - (H_1 - H(q_1)) \qquad (15)$$

Here, m_2 is the vehicle mass, and k_2 and c_2 is the coefficients of vehicle suspension stiffness and resistance, respectively.

Thus, the mathematical model of quay crane was constructed and the results of container-lowering were examined for the comparison with the experimental data and giving implication of the possible lowering time reduction.

Experimental investigation

The aim of research was to test the real working conditions of the quay crane, operators work, the spreader efficiency, and unnecessary forces accumulated during container loading.[24] A simulation model was developed and tested. In recent years, researchers work closely with electrically powered terminal trucks and cranes.[25] In order to assess the need for synchronization, authors conducted experimental research in Klaipeda port. During the experimental research, the quay crane carried out loading operations, during which the data were collected. The practical experiment collected data from 204 real cycles of the loading process from ship to the quay and back again. MK2 data logger hardware was used for these experimental measurements (see Figure 3).
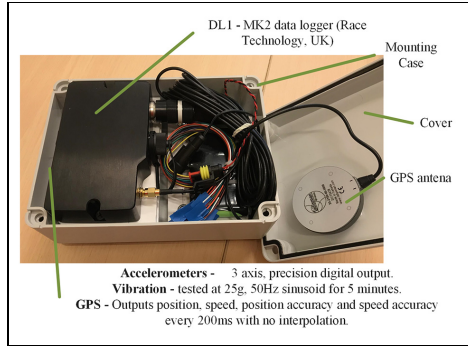

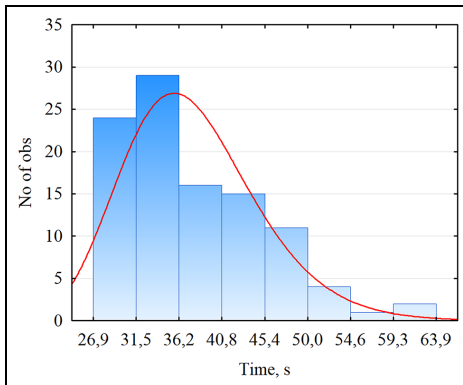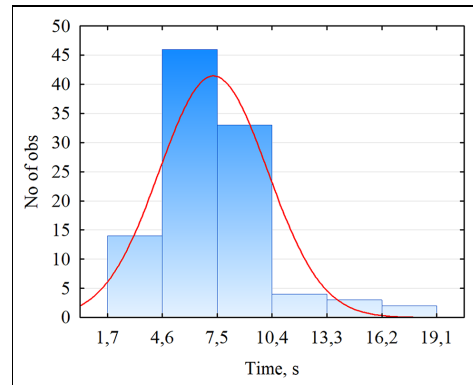**Figure 3.** DL1-MK2 data logger (Race Technology, UK).

When determining the dynamic parameters of the object under investigation (in this case, the container), data about its acceleration, speed, and position in space were measured and recorded. For this purpose, a DL1-MK2 data logger (Race Technology, UK), a three-way accelerometer (guaranteed 2 g minimum full scale on both axes; resolution of 0.005 g; optional 6 g sensor available as a factory option) vibration measurements (vibration factory tested at 25 g, 50 Hz sinusoid for 5 min), was used to record and store vehicle motion dynamics parameters. For positioning, the meter is connected to a GPS antenna (GPS—outputs position, speed, position accuracy, and speed accuracy every 200 ms with no interpolation; GPS tracking loops optimized for applications up to about 4 g; tracking of all satellites in view). Based on the time course of the vehicle and the acceleration readings, the device measures the speed of the test object with an accuracy of 0.16 km/h, with a measurement error of up to 1%. Longitudinal and transverse accelerometers record accelerations up to 20 m/s^2 and measurement error up to 0.05 m/s^2.

After processing the data collected during the experimental measurements, the entire loading process was divided into stages to identify which technological loading process takes the longest. The purpose of this experiment was to identify problematic operations in the loading process when scheduling a synchronization task, thereby justifying the need for synchronization. By synchronizing individual port facilities (such as terminal trucks and quay cranes) and by planning cargo operations accordingly, it is possible to minimize the impact of these problem areas on the loading time. These stages and summarized experimental results are given in Table 2.

Experimental measurements were implemented when the cargo was shipped from the ship to the shore. Depending on the loading process, the operations are

Table 2. Statistical data of container loading time.

Stage of loading	Mean	Min	Max	Standard deviation	Variation coefficient (%)
1. Start of lifting (hooking)	2.43	0.62	11.47	1.84	76.01
2. Vertical lifting	4.68	1.04	13.47	3.32	70.89
3. Diagonal lifting	5.14	0.79	9.84	1.97	38.28
4. Horizontal transportation	6.34	2.05	19.03	3.46	54.68
5. Diagonal lowering	6.36	2.72	23.97	3.05	47.90
6. Vertical lowering	7.25	1.66	19.13	2.86	39.42
7. Placing on vehicle	5.43	2.36	20.43	2.99	55.16
Total (Ship-to-shore)	37.63	26.91	63.87	7.68	20.42

Figure 4. Histogram of experimental load from ship-to-ship on the quay.

Figure 5. Histogram of experimental measurements of vertical lowering of container toward vehicle height.

divided into seven stages: (1) start of lifting (hooking), (2) vertical lifting, (3) diagonal lifting, (4) horizontal transportation, (5) diagonal lowering, (6) vertical lowering, and (7) placing on terminal truck. The overall loading cycle in the ship-to-shore process was also evaluated. The summarized results of experimental studies show that the entire duration of the ship-to-shore cycle of the loading process during the transfer of cargo from the ship to the shore is in accordance with statistical log-normal law.

The number of data $n = 102$ was measured (from ship to shore). The log-normal law hypothesis was tested by Pearson's χ^2 criterion. The histogram of the experimental loading times determined during experimental measurements is shown in Figure 4.

After analyzing the loading process measurements in stages, steps 6 and 7 were chosen for further analysis, that is, vertical lowering and positioning on the vehicle. These stages determine the crane-to-vehicle alignment to optimize the loading process and make it continuous. In Figure 5, the distribution of the vertical lowering time is presented.

We can see that the vertical lowering mean time of the container t is equal to 7.3 s, and the vertical lowering height mean value is 8.8 m, considering the standard deviation as 4.5 m. Hypothesis of lowering time distribution by Normal law was tested by Pearson's χ^2 criterion. Experimental results show that the average weight of the container load during the experimental measurements is 22.2 ton and the standard deviation is 10.2 ton, and coefficient of variation is 46%. In Figure 6, the distribution of the loading phase duration is presented, when the load is placed on the terminal truck and detached.

As we can see shorter intervals predominate, they represent about 50% of the total ($n = 102$) measurement result. Average is about 5.43 s; however, container placement can take up to 20 s. Duration of this step could be optimized by automation of loading process, and this process could be about 2 s, as show experimental results. The purpose of the synchronization task is to make the vehicle arrive when the load lowered during the loading process. Therefore, experimental measurements carried out when the equipment mounted on a container transport. Experimental research measured
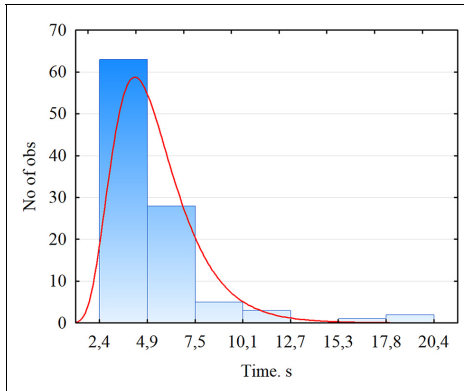
Figure 6. Histogram of experimental measurement container placement on terminal vehicle.
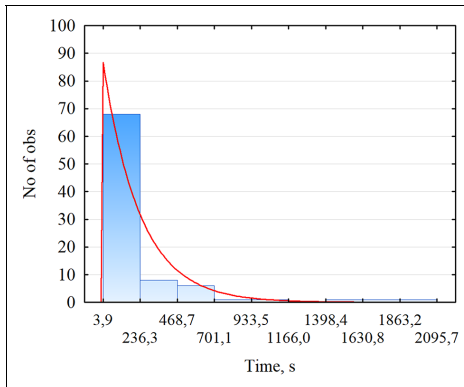

Figure 7. Histogram of experimental measurements of vehicle waiting time.

the trajectory of the terminal truck in the port area and its waiting time at the crane (see Figure 7).

The results show that the waiting time of the vehicle at the container crane varies from 4 s to 34 min (2096 s). The average waiting time is 229 s and standard deviation 346 s. The process is extremely unstable with a coefficient of variation of more than 150%. During the experimental measurements, the cargo was also evaluated (when mounting the equipment on the gripper—the closest point to the container). During these experimental measurements, the velocities and accelerations of the moving load were measured. After processing the results, we selected the best result—the experimental result of the fastest lowering of the load (see Figure 8).

The results show that investigated case of load lowering vertically was done in 1.9 s. The lowering speed of this situation is given in Figure 8(a). As a result, speed values are negative because the load is lowered. We also watched the fluctuations of the load that influence the full automation of the process. The load fluctuations in the horizontal plane during lowering are shown in Figure 8(b). As one can notice, container sways in a 10 cm boundary. This value suggests that the cargo lowered in a stable manner and no outer forces affect the sway (wind gusts or operator mistakes).

The experimental results show the need of more sophisticated control of the crane–container terminal truck system, but to work in real situation and to improve the performance are difficult due to the intervention into the port operation. Therefore, the mathematical model for lowering the container was developed to make adequate modeling and producing the tool for control system development.

Results and discussion

During the numerical simulation, the cargo lowering process was analyzed, which corresponds to the loading stage 6 of the experimental investigations. Simulation of the lowering process was completed by evaluating the force during contact placing the load on the vehicle. The results of numerical simulation are presented in Figure 9.

During numerical simulation, the load was lowered vertically down (see in Figure 9(a)). Due to the high weight of the load and the elasticity of the cable, the damping occurs. Figure 10 shows the situation when the load is placed on a vehicle with a dynamic force F12 of ~180 kN (see Figure 9(b)).

Changes of torque moment of the gear wheels during lowering presented in Figure 10.

During the modeling phase, the gap between the gear teeth was estimated. As we see during the lowering of the load, it has a negative effect; it excites the vibrations of the gears. This affects the lowering process; the vibrations pass to the cable and consequently worsen the loading conditions. Figure 11 shows the acceleration during horizontal lowering, and in Figure 11(a), the numerical simulations show that the acceleration values increase significantly when cargo has a contact with terminal truck. This is consistent with experimental measurements (Figure 11(b) (point 7)), with a significant increase in acceleration values and excitation of the terminal truck when the load is applied. On comparison, the results with the best experimental data that was achieved during the lowering (b) – was 2.4 s, but modeling results show that it is – in ideal conditions – possible to make the operation in 0.5 s (a). And, the results are comparable in time and amplitude, thus

Figure 8. Experimentally measured data: (a) the speed of the vehicle in the z-direction when the load lowered vertically and (b) container sway in horizontal plane during lowering.

Figure 9. The result of numerical simulation: (a) variation of the vertical distance *H* of the load to the vehicle and (b) variation of impact force during loading.

Figure 10. Numerical simulation result: torques during load lowering.

approving the model adequacy. So, the mean time of last stage of lowering of container could be moved toward the range of 0.5–2.5 s.

Figures above demonstrate that when the container is placed on the terminal truck, additional dynamic force is added, which at sometimes can be twice as large

Figure 11. Numerical modeling (a) and experiment (b) results comparison.

as the levering container weight. This is a known effect in classical mechanics. Such regularity is confirmed by the results of numerical simulation and experimental acceleration measurements (see Figure 11). Experimental measurements show a very similar tendency during container loading procedures.

Conclusion

In this article, as a result, we demonstrate the generalization of the measurements with real quay crane and terminal vehicle and propose a mathematical model describing the dynamic properties of both. Experimental measurements "in situ" of container-lowering to terminal t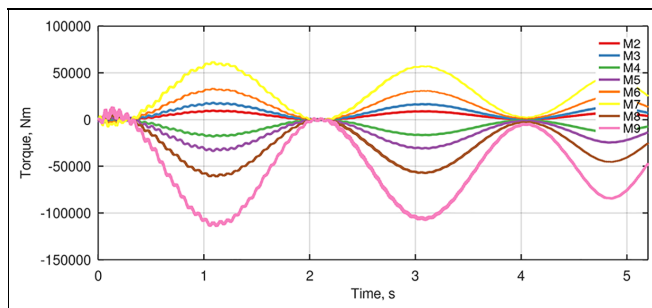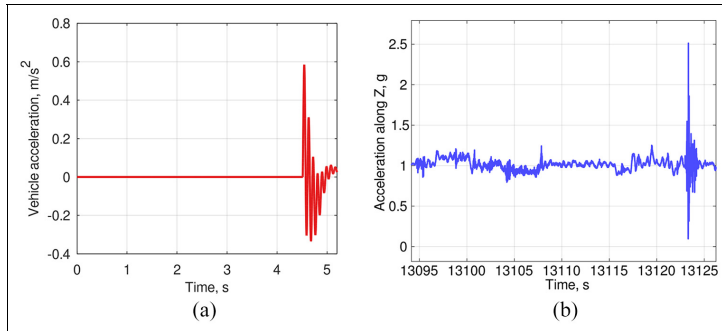ruck have been investigated in detail and statistical analysis of the new experimental results carried out. Experimental measurements showed that variance coefficient reached up to 150% on final handling operation. These operation durations varied between 2.36 and 20.43 s, with a mean value of 5.43 s. The entire lowering cycle variation coefficient reached 55.16%. Shorter time boundary shows that the handling process is optimizable up to two times by scheduling the operations between quay crane and terminal truck operators and using specialized algorithms for lowering process control for each individual case. This in fact could provide stability to port operations and make processes and procedures more agile for long-term planning. According to these new experimental data and research findings, further plans will be prepared to develop a methodology for crane and terminal truck, AGV synchronization in real time and will be used to bridge the scheduling mechanisms into a single real-time synchronization system.

ORCID iD

Tomas Eglynas (ID) https://orcid.org/0000-0002-9973-5896

References

1. Clausen U, Kaffka J and Meier F. CONTSIM—container terminal management with simulation. *Procedia: Soc Behav Sci* 2012; 54: 332–340.
2. Kavakeb S, Nguyen TT, McGinley K, et al. Green vehicle technology to enhance the performance of a European port: a simulation model with a cost-benefit approach. *Transp Res Part C Emerg Technol* 2015; 60: 169–188.
3. European Commission. *Annex to motorways of the sea detailed implementation plan*, 2018, https://vayla.fi/documents/20473/465955/Final-II-MoS-study-2018-2 + Annex. pdf/9cbe31a9-afde-4c79-9370-394bc864ffa5
4. Benamara H. Role of international shipping. In: *UNCTAD multiyear expert meeting on transport, trade logistics and trade facilitation*, Geneva, 21–23 November 2018, p.13. Geneva: United Nations Conference on Trade and Development.

5. Speier C, Whipple JM, Closs DJ, et al. Global supply chain design considerations: mitigating product safety and security risks. *J Oper Manag* 2011; 29: 721–736.

6. Xin J, Negenborn RR and Lodewijks G. Trajectory planning for AGVs in automated container terminals using avoidance constraints: a case study. *IFAC Proc Vol* 2014; 47: 9828–9833.

7. Hong KS and Ngo QH. Dynamics of the container crane on a mobile harbor. *Ocean Eng* 2012; 53: 16–24.

8. Zheng K, Lu Z and Sun X. An effective heuristic for the integrated scheduling problem of automated container handling system using twin 40' cranes. In: *Proceedings of the 2010 second international conference on computer modeling and simulation*, Sanya, China, 22–24 January 2010, pp.406–410. New York: IEEE.

9. Zhen L, Hu H, Wang W, et al. Cranes scheduling in frame bridges based automated container terminals. *Transp Res Part C Emerg Technol* 2018; 97: 369–384.

10. Alasali F, Haben S and Holderbaum W. Stochastic optimal energy management system for RTG cranes network using genetic algorithm and ensemble forecasts. *J Energy Storage* 2019; 24: 100759.

11. Papaioannou V, Pietrosanti S, Holderbaum W, et al. Analysis of energy usage for RTG cranes. *Energy* 2017; 125: 337–344.

12. Liu D and Ge YE. Modeling assignment of quay cranes using queueing theory for minimizing CO_2 emission at a container terminal. *Transp Res Part D Transp Environ* 2018; 61: 140–151.

13. Bichou K. An empirical study of the impacts of operating and market conditions on container-port efficiency and benchmarking. *Res Transp Econ* 2013; 42: 28–37.

14. Arena A, Lacarbonara W and Casalotti A. Payload oscillations control in harbor cranes via semi-active vibration absorbers: modeling, simulations and experimental results. *Procedia Engineer* 2017; 199: 501–509.

15. Tuan LA, Cuong HM, Trieu P, et al. Adaptive neural network sliding mode control of shipboard container cranes considering actuator backlash. *Mech Syst Signal Process* 2018; 112: 233–250.

16. Sha M, Zhang T, Lan Y, et al. Scheduling optimization of yard cranes with minimal energy consumption at container terminals. *Comput Ind Eng* 2017; 113: 704–713.

17. Ileš Š, Matuško J and Kolonić F. Sequential distributed predictive control of a 3D tower crane. *Control Eng Pract* 2018; 79: 22–35.

18. Verdés Kairuz RI, Aguilar LT, de Loza AF, et al. Robust positioning control law for a 3D underactuated crane system. *IFAC-PapersOnline* 2018; 51: 450–455.

19. Zhang M, Zhang Y, Chen H, et al. Model-independent PD-SMC method with payload swing suppression for 3D overhead crane systems. *Mech Syst Signal Process* 2019; 129: 381–393.

20. Li B, Liu H, Xiao D, et al. Centralized and optimal motion planning for large-scale AGV systems: a generic approach. *Adv Eng Softw* 2017; 106: 33–46.

21. Güven C and Eliiyi DT. Trip allocation and stacking policies at a container terminal. *Transp Res Proc* 2014; 3: 565–573.

22. Sun Z, Wang N, Bi Y, et al. A DE based PID controller for two dimensional overhead crane. In: *Proceedings of the 34th Chinese control conference*, Hangzhou, China, 28–30 July 2015, pp.2546–2550. New York: IEEE.

23. Jaafar HI, Mohamed Z, Abidin AFZ, et al. PSO-tuned PID controller for a nonlinear gantry crane system. In: *Proceedings of the 2012 IEEE international conference on control system, computing and engineering (ICCSCE 2012)*, Batu Ferringhi, Malaysia, 23–25 November 2012, pp.515–519. New York: IEEE.

24. Park KP, Cha JH and Lee KY. Dynamic factor analysis considering elastic boom effects in heavy lifting operations. *Ocean Eng* 2011; 38: 1100–1113.

25. Bahnes N, Kechar B and Haffaf H. Cooperation between intelligent autonomous vehicles to enhance container terminal operations. *J Innov Digit Ecosyst* 2016; 3: 22–29.

3rd publication / 3 publikacija

Analysis of the efficiency of shipping containers handling/loading control methods and procedures

T. Eglynas, **M. Jusis**, S. Jakovlev, A. Senulis, A. Andziulis, S. Gudas.

Research Article

Analysis of the efficiency of shipping containers handling/loading control methods and procedures

Tomas Eglynas[1,2] ID**, Mindaugas Jusis[2,3], Sergej Jakovlev[1,4], Audrius Senulis[1,5], Arunas Andziulis[2] and Saulius Gudas[3]**

Abstract

Most modern quay cranes operate under the operator's control. Lifting, lowering, and transporting a container from one platform to another are just some of the actions that a person is responsible for, but the negative consequences of handling can be caused not only by his actions. An error, loading transient instability, or an undervalued environmental factor in the control algorithm can cause a risk to human safety, container, and cargo security. In order to control cargo-handling risk, it is necessary to improve the cargo control systems not only by changing their software, but also by creating additional control algorithms and systems. These systems with programmed control algorithms should be integrated into existing systems to control cargo security and its transfer time. In this article, transient processes and dynamic property of the cargo-handling operation are described and multibody dynamics simulation performed using laboratory prototype of a quay crane. The experimental research performed and integrated autonomous quay crane control algorithm developed with the proposed embedded container swinging control subroutine operated in optimal mode when the control system used PID controller with a feedback including additional PI controller and S-shaped input signal for the analyzed case with the defined parameter set.

General introduction

Risk of cargo transportation process and impact of handling/loading procedures

Each year, millions of different types of containers are transshipped in intermodal terminals. Large quay cranes are used as the main transport means for loading cargo from ship to shore and back. Thus loading process is very important stage of intermodal transportation, where necessary measures have to be ensured to achieve high level of physical and technological safety. Incorrect operation of the operator or inappropriate crane control algorithms can not only damage the

[1]Marine Research Institute, Klaipėda University, Klaipėda, Lithuania
[2]Department of Informatics and Statistics, Klaipėda University, Klaipėda, Lithuania
[3]Institute of Data Science and Digital Technologies, Vilnius University, Vilnius, Lithuania
[4]VSB—Technical University of Ostrava, Ostrava, Czech Republic
[5]Department of Engineering, Klaipėda University, Klaipėda, Lithuania

Corresponding author:
Tomas Eglynas, Marine Research Institute, Klaipėda University, Universiteto ave. 17, LT-92294 Klaipeda, Lithuania.
Email: tmse@inbox.lt

containers or cargo, but also damage terminal property near the quay crane. Failure to comply with the safety requirements may result in an accident or technical disaster, such as a crane crash or container crash. Each quay crane is unique in its capabilities, so applying common restrictions to all cranes is not appropriate. Each container terminal, based on the needs and possibilities, builds quay cranes whose specifications meet loading needs. The main limitations of the crane in many cases are reflected in their technical characteristics, such as spreader lifting capacity, speed of the trolley, crane travel speed, carriage movement distance, stroke of the boom length and others. In order to ensure cargo safety, it is necessary to monitor and evaluate all parameters limiting the operation of the crane. Therefore, security is achieved through restrictions.[1] It is also necessary to assess critical situations. For example, what happens if one of the carrier ropes is broken, voltage variation hops in the high power supply network, and the impact of the opposite wind will affect the maximal allowable weight lifting process. This is just a small part of the situations that should be evaluated to ensure both the safety of the cargo and the smooth operation of the quay crane. One of the main causes of disasters has been identified as the swinging of the containers. The reasons for the aforementioned swinging are different. Starting from strong wind gusts, operator error, and ending with failure to stabilize the loaded cargo.[2–5] This kind of swinging is easy excited because the steel rods connecting load and the spreader of the trolley. Such swinging results increase the time of container transport from point "A" to "B" and decrease cargo safety factor.

In recent years, scientists are increasingly examining how to optimize existing quay cranes due to increased transport flows. One of the most commonly encountered problems in ports is the optimization of container lifting cranes and by means of specific control algorithms.[6–10] To date, many different control algorithms have been developed by many authors all around the world, which, under laboratory conditions, solve individual problems of crane control with limited applicability in real life scenarios. However, the need for complex algorithms representing real life scenarios remains the same, focusing not only on individual loading procedures, but also on the entire cargo ship–shore–ship process. Generally, the development of new quay crane control algorithms[11] is associated with the task of solving the problem of container sway during loading procedures. Causes of these sways may vary in each separate case.[2–4,12,13] Sometimes swinging is caused by the crane mechanisms (vibrations, motor transients, or uneven surface of the track of the moving devices), but there are cases, where the cause of swinging is unknown. They can be triggered by complex set of forces acting on the container and impact the cargo

inside the container. Other scientists[2,3,14] are trying to solve the problem of crane load swinging. The investigation is related to the crane-lifting mechanism where the container and crane connected by metal rods. Due to different container weights, wind gusts, and lifting control algorithms, containers often start swinging at the very beginning of its lifting processes. This requires more time for the container to be transported from point "A" to point "B" in the port. Due to changing accelerations, it is likely that the container gets damaged by collision with quay crane structures. As it is known, in the case of strong winds, quay cranes do not usually handle loading operations, which eventually increase loading costs. So, all of this should be avoided by developing more agile technical and software solutions for modernized cranes.[14,15]

Analysis of crane control algorithms and technologies

In the maritime intermodal terminal, the main controllable unit of the quay crane is a trolley, driven by electric motors moving to the intended position as quickly as possible, while maintaining the minimum load swinging.[16,17] Uncontrolled swinging leads to cargo stability and safety problems, especially in container take-off and lowering procedures. The most experienced crane operators are responsible for container handling operations. The latter, relying precisely on the positioning of the container by the quay crane, rely on their visual feedback (carrying out control operations, determined by visual field of view). Such handling procedures can prove to be very complex and time-consuming, especially in extreme situations, where precise positioning depends entirely on operator experience.[18] In any loading procedure, the load can easily swing. If such swinging exceeds the safety limits, swinging must be inhibited or the operator must suspend loading operations until the swinging fall to a safe limit. Complete elimination of such resulting swinging is practically impossible even with the use of modern control technologies, but in specific situations, such swinging can be easily suppressed. This swinging can be influenced by various external factors such as wind, weather changes, or operator actions.[16] This inevitable swinging of cargo often leads to reduced cargo-handling efficiency, container damage, or accidents in the terminal.[19] Moreover, the loading process requires a fast container transport to the required position, but the transport speed is as high as possible, thus the load varies more, thereby aggravating the operation of the operator and the entire transportation process.[20,21] Freight fluctuations also affect the operation of an experienced operator and reduce the positioning accuracy of the spreader. In order to achieve a higher positioning accuracy of the crane spreader, it is necessary to install a control system that evaluates the trolley acceleration and the amplitude of

swinging. One of the most effective, practically the cheapest and the most effective methods for managing the efficiency and speed of loading is the application of motion profiling methods. However, rapid movement greatly affects the uniformity of movement and causes persistent swinging. Motion control profiling techniques and the search for compromise parameters between the occurrence of motion speed and continuous swinging and their size are one of the main and most complex tasks of the motion profiling, which are solved by means of automatic control systems.[22] In order to increase the transport efficiency, it is necessary to increase the speed of the transportation. Therefore, it is necessary to control sudden changes in acceleration, which results high amplitude vibrations. In literature sudden changes in acceleration are called jerks.

These jerks can be controlled using their limitation rules. Jerks-limited motion profile is the main motion design tool in modern motion control systems. And this is also the optimal solution for body movement control. Loss limitation is used to reduce swinging that arise from the nature of the proclaimed motion process, which can also be optimized.[23] Slip-constrained integration of the motion profile into a trapezoidal speed profile enables control of the speed profile projections to produce a symmetric or asymmetric S-speed profile. The uniformity of motion using the S-shape profile depends on the duration of the tensile force. A longer period of time until the snap reaches the forged value increases the uniformity of the movement of the controlled object, but reduces the efficiency over time. Therefore, in the individual control stages, in order to ensure good S-shaped profile parameters, it is necessary to carry out appropriate experimental studies in order to determine the optimal parameters for the control system. The trapezoidal speed profile is based on the three-phase acceleration trajectory.[24] This type of method is one of the most commonly used motion control technologies applied to quay cranes.[24–26] However, the problem of infinite shuffle greatly limits the use of this profile in automated control systems. Three-phase acceleration control reduces overall system control capabilities compared to a more modern S-trajectory speed profile. The S-shaped speed profile is most commonly used to improve movement uniformity. This is done by reducing the amount of peak in the acceleration and deceleration phases.[22,26–28] This type of motion profile is based on a seven-phase acceleration trajectory, which is controlled by changing the value of the jerk. The motion limitation controlled by the motion profile effectively reduces the vibrations triggered during the acceleration procedure. First, this type of motion rate profile[23] is used to reduce uncontrolled swinging. Only if motion is not improved efficiently, the latter is combined with modern control technologies such as a PID (Proportional-Integral-Derivative) controller or ambiguous logic. Such use of

the speed profile with other control technologies, when the profile is used to form the input signal, also known as input profiling.[17] A great deal of research was devoted to the research of this control technique, in particular, where the input profiling plays a central role[16,17,23,29–31] in control techniques. Input profiling reduces vibrations by slightly adjusting the control command through the number of pulses. It generates a two-pulse sequence instead of one, thus obtaining the so-called zero-vibration profiling. When the pulse is properly formed, the subject moves without continuous swinging. One of the main advantages of input profiling in comparison to the feedback control systems is the need for additional sensors to form a control signal.[29]

In order to increase the safety of the transported cargo, new methods for modeling the dynamics of the container handling process are being developed. They aim to better simulate system behavior under different loading conditions and factors.[32–36] One such research is 3D Dynamic Modeling of the Marine Crane Movement System, presented by scientists Ismail and others.[33] The Lagrangian method was used for calculations. The data collected during the simulation of the dynamical system were collected and analyzed, and the position of the trolley and the angles of the spreader's tilt were recorded. The results obtained by a researcher are of great significance for the future development of control algorithms for the control system of double spreader quay crane. Jaafar and other scientists[32] developed a nonlinear model of the control system of the quay crane, which explored the factors that influence the capabilities of the system. During the study, the input voltage, cable length, load, and trolley mass were changed. The simulation results of this system indicate that the system response is very sensitive to these combinations of parameters. They have also found that inappropriate parameter selection may be one of the main reasons influencing the swinging of containers and posing problems of cargo security during transportation. Most of the models associated with dynamic control and cargo security issues are presented to address one type of problem. For example, a crane control system with state simulator,[35] in which the dynamic model is created, is intended to solve problems related only to handling operations and positioning in the presence of different wind interruptions. Also, the dynamic model created by another scientist[36] is intended only to simulate the process of lifting heavy loads using floating cranes. In order to increase the automation of quay crane processes, it is necessary to solve problems related to container swinging.[19] Each research carried out in this area brings to the creation of an intelligent control approach and application in real quay cranes as an industrial control tool. Fuzzy logic based control systems do not require very precise mathematical models or details of a controlled object,

and the applicability of such systems is relatively simple.[37] However, these control systems do not solve the complex control tasks that are relevant to the control of the quay crane. The application of this modern control tool alone results in insufficiently clear and efficient results in all situations, so that it can be applied in practice. Combined control of fuzzy logic using PID controller could be used as one of the possible solutions for the development of a modern intelligent crane control system.[19,38,39] However, the results of recent years show that input profiling together with the PID controller yields promising results.[16,17,30] Thus, the quay crane's control system has been offered in order to realize the concept of an autonomous port. The PID controller is most widely used in the industrial perspective due to its simple structure and stable operation under various conditions.[40] Scientists Liu et al.[19] developed a control system that used fuzzy logic and a PID controller to manage the transport of bridge crane loads. They presented a complete system, and the results of the research that shows that the combination of these modern control technologies yields effective results could possibly be realized in real systems. However, most scientists are confronted with the correct setting of the PID controller in the crane operation. Traditional parameter-matching techniques, such as the test and error method, are one of the easiest ways to reconcile the PID controller, but the results obtained by this method do not guarantee significant and effective results.[18,21,41] Another method for controlling the controller is Ziegler–Nichols,[20] which is most widely used because of its simplicity. Depending on the results obtained due to the aggressiveness and excessive fluctuations in the variations, researchers have used other methods to reconcile the parameters of the PID controller.

The most commonly used PID controller coupled with changeable optimization techniques based on parameter selection methods.[42] Some of these are genetic PID parameter selection algorithms for automated crane operations[20,42]; artificial bee colony algorithms used to reduce sharp spikes or time parameters.[43] Ant colony algorithms also used to optimize nonlinear PID controller parameters.[20] Scientist Jaafar not only analyzed PID controller technologies in crane control, but also applied a wide variety of controller combinations. This scientist proposes a control structure combining PID and PD controls. The PID controller used to position the quay crane trolley, while the PD controller is used to reduce cargo swinging. The control model structure that combines PID and PD controls to monitor different parameters applied across multiple systems. In many cases, the PID controller used to control the position, while the PD controller is used to reduce the swinging that occurs. However, for such a model, it is already necessary to combine the

five-parameter values. In the literature, it is often reported that the output of such control model controller uses the x-position and the swinging angle θ.

Problem formulation

In recent years, scientists are increasingly examining quay cranes in order to use the existing resources to manage the constantly growing cargo flow in containers in the world. Industry is lacking the necessary tools to increase crane work efficiency. One of the most commonly encountered problems in the engineering community is the development and application of container lifting crane control algorithms for improving existing crane control systems.[1–4,11] In this article, we are discussing the possibilities of improving crane control operations and utilizing the crane potential to manage even the hardest tasks, caused by weather conditions and operators inexperience. Most analyzed control algorithms developed to solve individual problems on-site. Used methods are oriented to single problem solving without the need for complex problem analysis. In this article, we have formulated a complex problem for controlling the loading procedures (ship–shore–ship) by developing integrated autonomous quay crane control algorithm with embedded container swinging control subroutine, operated in optimal mode for the analyzed case with the defined parameter set. We have used PID controller with additional PI with feedback and S-shaped input signal.

The laboratory quay crane Matlab Simulink model was developed where the main parameters for experimental research was used: maximum traveling distance—2.2 m, spreader with container mass m_g—7.45 kg, the trolley mass m_{vz}—3 kg, and the maximum spreader with container lifting height—1.9 m.

The important part of container swinging reduction control system is PID controller, which mathematical equation (1) is well known

$$\begin{cases} e_1(t) = g(t) - k_{fb1} \cdot v_{vz} \\ e_2(t) = g_{ref}(t) - k_{fb2} \cdot v_g \\ u_1(t) = Kp_1 \cdot e_1(t) + Ki_1 \cdot \int e_1(t)dt + Kd_1 \cdot \frac{de_1(t)}{dt} \\ u_2(t) = Kp_2 \cdot e_2(t) + Ki_2 \cdot \int e_2(t)dt \\ u(t) = u_1(t) - u_2(t) \end{cases} \quad (1)$$

here: $u_1(t)$—control signal output of PID controller, $u_2(t)$—control signal output of PI controller, $u(t)$—combined control signal, $e_1(t)$—error signal of main control loop, $e_2(t)$—error signal of auxiliary control loop, Kp_1—proportional coefficient of PID controller, Ki_1—integral coefficient of PID controller, Kd_1—differential coefficient of PID controller, Kp_2—proportional coefficient of PI controller, Ki_2—integral coefficient of PI controller, k_{fb1}—trolley velocity sensor transfer coefficient, k_{fb2}—spreader velocity sensor transfer coefficient,
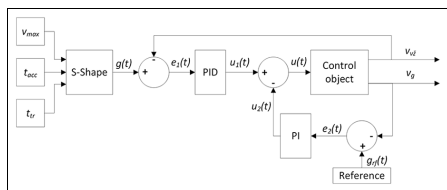
Figure 1. General block diagram of control system. t_{tr} is the trolley traveling time, and the reference block output $g_{ref}(t)$ is equal to zero because the spreader oscillation velocity must be reduced to zero.

and $g(t)$—input signal proportional to the reference trolley v_{max} velocity.

The S-shaped velocity profile (see Figure 2) was used as input signal for experimental and modeling and could be described (equations (2)–(7)).

The trolley acceleration was calculated

$$a_{TR} = \frac{v_{max}}{t_{acc}} \qquad (2)$$

The maximum possible acceleration of the S-shape speed profile was calculated as

$$a_{max} = \frac{a_{TR}}{1 - (j_\% \cdot 0.005)} \qquad (3)$$

here $j_\%$—the initial tangency value was selected which is equal to 50% of the original value. The breaking constant was calculated as

$$j = \frac{2 \cdot a_{max} \cdot 100}{t_{acc} \cdot j_\%} \qquad (4)$$

Jerk's value depends on the phase of the S-profile and it can be 0, j, and $–j$. The quay crane control

system recalculated the acceleration a, speed v, and position x within each time interval

$$a = a_0 + j \cdot \Delta t \qquad (5)$$

$$v = v_0 + a_0 \cdot \Delta t + \frac{j \cdot \Delta t^2}{2} \qquad (6)$$

$$x = x_0 + v_0 \cdot \Delta t + \frac{a_0 \cdot \Delta t^2}{2} + \frac{j \cdot \Delta t^3}{6} \qquad (7)$$

here: Δt is the time interval related to converter sample rate, a_0 is the acceleration value where initial value is 0 because the trolley starts moving from 0 acceleration and each calculation step after Δt the a_0 value is recalculated by equaling $a_0 = a$ by previous calculation step (from equation (5)), and v_0 is the value of the previous speed where initial value is 0 because the trolley starts moving from 0 velocity and each calculation step after Δt the v_0 value is recalculated by equaling $v_0 = v$ by previous calculation step (from equation (6)). x_0 is the value of the previous position, where initial value is 0 because the trolley starts moving from 0 position and each calculation step after Δt the x_0 value is recalculated by equaling $x_0 = x$ by previous calculation step (from equation (7)), and v_{max} was determined using real crane parameters and reduced up to laboratory crane prototype resulting 0.2 m/s.

The design variables of PID and PI controller that need to be determined are as follows: for PID controller in main control loop—Kp_1, Ki_1, and Kd_1, and for additional PI controller in auxiliary control loop—Kp_2 and Ki_2.

Development of crane's control system prototype

To date, many different control algorithms were developed that solve individual problems,[2,6–8] but there is still a need for the development of complex algorithms that are oriented not only to individual loading
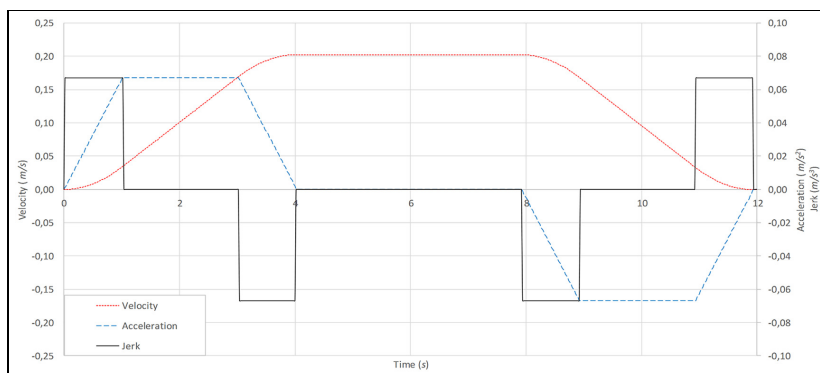

Figure 2. S-shape velocity profile: velocity (red dotted), acceleration (blue dashed), and jerk (black solid).
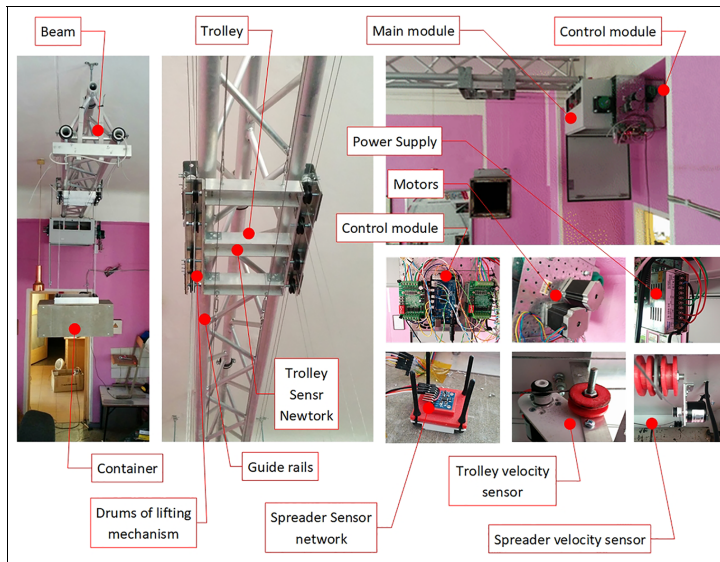
Figure 3. The main system components of quay crane prototype.

procedures but also to a full ship–shore–ship stevedoring cycle. Frequently, the creation of new quay crane control algorithms[9,44] is associated with solving problems, which attempt to solve the problem of container swinging,[45,46] the causes of which can occur in each case.[10,11] Sometimes swinging caused by the mechanisms of the crane itself, such as the engine, or uneven track surfaces on which the devices move. However, there are cases in which the causes of swinging are unknown—they can be caused by a complex set of effects on the container area or even within the container itself. The basic structure of the developed laboratory prototype is presented in Figure 3.

The laboratory crane fixed by a relatively flexible connection to the laboratory ceiling. The lower arms of the boom are facing the guideways for the horizontal trolley movement. The trolley top is equipped with a sensor net for trolley movements and position measurement. In the lower part, the pulleys used for lifting a spreader holder. A sensor network also installed at the top of the spreader, recording its swing angle, speed, and position. The spreader and the lifting mechanism controlled through the main unit, which is equipped with transmission gear and an electronic automatic control system installed. This system consists of a control module, motors, trolley, and clamp speed sensors and a power supply. After performing virtual checks of the quay crane–lifting mechanism and spreader system and

constructing a laboratory prototype for experimental research, it was necessary to simulate the quay crane's control system in a computer environment. The control task signal programmed using a speed change profile was selected through experimental and theoretical studies. Based on the analysis of the scientific literature and the evaluation of the effectiveness of the PID controller in this type of crane control systems, it was decided, first, to select the appropriate speed profile for the input, which was combined with the PID controller for the control of the quay crane transportation process. Experimental studies have been carried out to select the input forecourt method, which compared the efficiency of two speed profiles to evaluate the container's continuous swinging. In order to compare these profiles, mathematical calculations were carried out with respect to crane speed, lifting power, and other characteristics and setting similar acceleration and deceleration parameters. As the input signal shaping is one of the important actions for the reduction of the initial sway of the container, the S-shaping of the input signal is analyzed. The initial acceleration and deceleration settings in both above-mentioned cases of the Y-axis are $t_{acc} = 4\,s$, which corresponds to the synchronous speed profile.

The calculations using above-mentioned equations (equations (2)–(7)) are implemented in the Arduino Control Module and Simulink modeling. During the
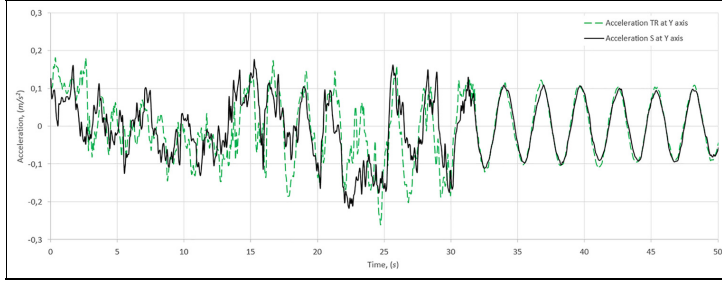
Figure 4. Cargo oscillation comparison using trapezoidal and S-shaped velocity profile.

experiment, the container was raised to a height of 1.52 m (Z-axis) relative to the horizontal reference plane (this plane is kept in the experimental stand's floor), and transported by Y-axis at 1.61 m and eventually lowered to 0.58 m (Z-axis). This transportation case has been applied to both speed profiles. When comparing the velocity of the container and the velocity profile in both cases on the Y-axis (see Figure 4), the residual oscillations at the end of the transportation process is the same. Although in individual cases, the use of S-profiles in different systems shows significantly smaller load swinging, due to the complexity of the crane system in which the load is suspended on the ropes, the results do not provide the result of the desired oscillation suppression. Scientists KH Rew et al.[22] adapted the S-shaped speed profile to the robot manipulator when a boom is mounted with a rigid connection. During case study, the S-shaped speed profile was adapted to the quay crane spreader for controlling cargo variations when the spreader is connected to the trolley with a flexible connection. As in the case of KH Rew et al.,[22] the steeper movement of the trolley has been realized, but the continued swinging in the unassembled spreader holder have remained and are similar in both cases.

Depending on the results of other researchers described in the first section, it can be concluded that such complex control system requires combined control technologies. Regarding the control signal $u(t)$, the plant consists of converter, motor, and crane with cargo models. The converter performs conversion of control signal to PWM (pulse-width modulation) signal that afterwards generates the motor phase voltages U_A and U_B (equation (8))

$$\begin{cases} U_A = f(u(t)) \\ U_B = f(u(t)) \end{cases} \tag{8}$$

The generation of voltages U_A and U_B are implemented in using PWM signal modulation (presented in Figure 5). These voltages were used as an input signals

for the stepper motor, used in laboratory prototype, which could be described using system of equations (9):

$$\begin{cases} \frac{di_A}{dt} = \frac{1}{L}(U_A - Ri_A - e_A) \\ \frac{di_B}{dt} = \frac{1}{L}(U_B - Ri_B - e_B) \\ M_v = -K_m\left(i_A - \frac{e_A}{R_m}\right)sin(N_r\theta) + K_m\left(i_B - \frac{e_B}{R_m}\right) \\ \quad cos(N_r\theta) - M_{bt}cos(4N_r\theta) \\ \frac{d\theta}{dt} = \omega_v \end{cases} \tag{9}$$

here: K_m—torque constant of stepper motor, i_A and i_B—stepper motor coil current, e_A and e_B—electromotive force of stepper motor, R_m—magnetization resistor, N_r—stepper motor tooth per pole, θ—single-step rotation angle, M_{bt}—internal braking torque, R—winding resistance, L—winding inductance, and U_A and U_B—A and B phase winding voltages.

Therefore, the use of the S-shaped profile, as part of a single control system, can be used as reference signal of control system. A comprehensive mathematical model (equation (10)) was also developed

$$\begin{cases} \frac{d\varphi_g}{dt} = \omega_g, \frac{ds_{v\tilde{z}}}{dt} = v_{v\tilde{z}}, \\ \left[\begin{array}{l} \left(m_g + m_{v\tilde{z}}\right)\frac{ds_{v\tilde{z}}}{dt} + \\ + m_g L\frac{d\omega_g}{dt} + \\ + \frac{1}{R^2}(J_b + J_v U^2)\frac{dv_{v\tilde{z}}}{dt} \end{array}\right] \cdot R_{dr} + M_{fr} = M_v U\eta \\ m_g L\frac{dv_{v\tilde{z}}}{dt} + m_g L^2\frac{d\omega_g}{dt} + m_g Lg\varphi_g = 0 \\ J_v\frac{d\omega_v}{dt} = -B\omega_v + M_v \end{cases} \tag{10}$$

Based on the crane-lifting mechanism and spreader holder control system, the model was transformed in the Matlab Simulink environment structure (see Figure 5).

Here, η—the efficiency of the mechanical transmission, φ_g—the angle of the spreader (gripper) swinging, ω_g—the angular velocity of the spreader (gripper)
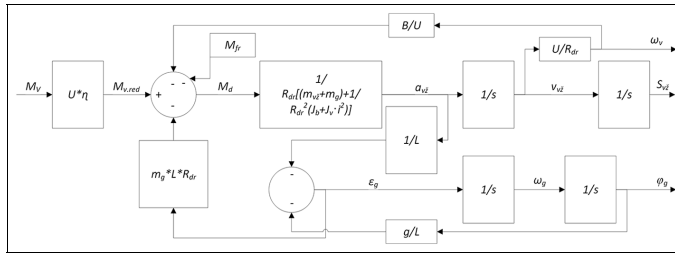
Figure 5. Block diagram of lifting mechanism mechanical subsystem. $M_{v.red}$—gear reduced motor torque, M_d—dynamic torque of plant, a_{vz}—trolley linear acceleration, ε_g—angular acceleration of spreader, and s—Laplace operator.
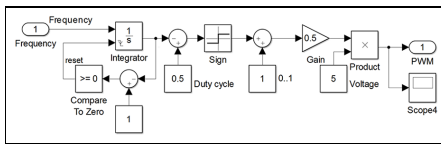

Figure 6. Pulse-width modulation generator block internal structure.

swing, s_{vz}—trolley displacement, v_{vz}—trolley speed, m_g—the mass of the spreader with the load, m_{vz}—the weight of the trolley, L—the length of the cable rods, R_{dr}—drum radius, J_b—moment of drum inertia, J_v—moment of inertia of electric motor, U—reduction gear ratio, M_{fr}—friction moment, M_v—engine moment, and indices: v_z—trolley, g—spreader (gripper), s—pulley, v—motor, and B—motor rotation damping.

In addition, in this model, a computational structure was developed for calculating linear kinematic parameters of cargo, linear load variation, speed, and displacement. The crane-lifting mechanism and the trolley's mechanical subsystem unit consists of two inputs and 12 exits for monitoring the system. Outputs describe the kinematic characteristics of the trolley and the load. Inputs are provided for the momentum of the frictional force and the torque input. The Matlab Simulink stepper motor unit (model) was simulated by compiling a mathematical model according to the technical characteristics of the laboratory physical model. Low-power asynchronous motors were used in the prototype. However, stepper motors were used to create a control system for the new gantry and lifting mechanisms for laboratory prototype. The available material resources influenced their use. The stepper motor model consists of three inputs and one output. A PWM signal from the PWM generator block is fed into the input of the controllable power converter subsystem unit, and the unit generates a signal for the stepper motor

to operate in half-step mode, thereby increasing positioning accuracy. An PWM generator block is depicted in Figure 6.

The purpose of this Simulink unit is to realize the internal function of the Arduino mathematical models, which is converted from the frequency that is proportional to the Y-axis of the crane trolley with the load movement of the linear velocity of the crane to the PWM signal for the input of the power converter unit. This frequency change is realized structurally. The Simulink in the mathematical model also has two additional blocks—one for changing the speed signal to the set frequency that feds PWM generator input and the other block is for the S-shaped velocity profile set-top square signal formation block.

Simulation results and discussion

The Simulink model has been tested by feeding the S-profile inlet profile when the crane trolley control system is open-ended (without feedback) and a crane trolley with a load of 1.9 m in length runs at a speed of 0.2 m/s. The resulting graph is shown in Figure 7—where the S-shaped profile signal is green, the speed of the crane trolley is a blue line, and the linear velocity of the cargo swinging relative to the cargo hanging point is red. As shown in Figure 7, in addition to the control trolley, the response lags the reference signal in the dynamic mode and has a dynamic error. Due to the absence of a PID controller and feedback, there is also a static error, which in this case is equal to 1.3% and does not have a significant effect on the system for operation. The load-swinging rate reaches almost 0.15 m/s, amplitude variation during the period is 7.7%, and the frequency is 0.374 Hz. These experiments are the starting point for setting the PID controller parameters. This mathematical Simulink model was designed to determine the parameters of the PID controller, which minimize load swinging in the trolley. Many literature reviews were made on this topic, and
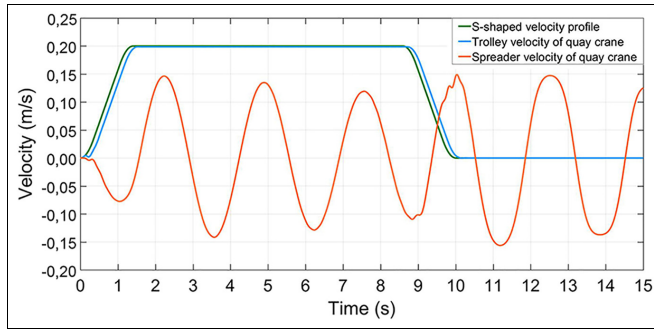
Figure 7. S-shape velocity profile (green), trolley velocity (blue), and spreader oscillation velocity (red) graphs.

Table 1. The table of proportional, integral, differential and proportional, integral controllers values calculations.

No.	Kp_1 PID	Ti_1	Td_1	Kp_2 PI	Ti_2	$\frac{1}{2} \int E_{v\bar{z}}^2 dt$	$\frac{1}{2} \int E_g^2 dt$
1	0.6	13	0.01	0	0	0.0002155	0.06237
2	0.6	13	0.01	0.1	0	0.0002468	0.06568
3	0.6	13	0.01	0.2	0	0.0003128	0.06883
4	0.6	13	0.01	0.1	1	0.0008445	0.03695
5	0.6	13	0.01	0.1	2	0.002096	0.01187
6	0.6	13	0.01	0.1	3	0.002881	0.01541
7	0.6	13	0.01	0.2	2	0.002071	0.01107
8	0.6	13	0.01	0.3	2	0.002079	0.01065
9	0.6	13	0.01	0.4	2	0.002143	0.01045
10	0.6	13	0.01	0.5	2	0.00223	0.01033
11	0.6	13	0.01	0.6	2	0.002359	0.01062

many methods were examined for adjusting the PID controller. In addition, some finding were also applied to our experimental test-bed, taking into account the complexity of the system and the hanging load, whose swinging is minimized. In our example, the research findings do not produce the desired results, and it was decided to combine the controller empirical and experimental results, by determining the controller coefficients resulting minimal swinging during the grabbing and the transportation procedures.

It is difficult to reconcile the parameters of this controller in a physical laboratory prototype due to technical limitations and the possible failure of prototype in case of inappropriate parameters. Therefore, the parameters of the PID and PI controllers were prepared using the mathematical model of Matlab Simulink by utilizing the method of minimization using the integral criterion of the square error of trolley velocity ($E_{v\bar{z}} = v_{v\bar{z}} - v$, where v are from equation (6)) and spreader oscillation velocity ($E_g = 0 - v_g$). The integral criterion of the square error mathematical formulation are presented in Table 1, accordingly seventh and eighth columns. The procedure of PID and PI controllers

parameters determination was divided in two steps. First, the PID controller parameters were determined without auxiliary feedback to find the minimum value of integral square error of trolley velocity and was obtained by modeling (first line of Table 1) for initial calculations. Then the auxiliary feedback was activated and using MatLab simulation, the PI controller parameters were determined, calculating the minimum integral criterion of the square error of spreader oscillation velocity. The first step of controller (PID) parameter estimation was carried out without feedback (crane trolley velocity and load variation linear velocity). The proportional part is Kp_1, the integral part is Ti_1, and the coefficient of the differential part is Td_1 (presented in Table 1). Initial approximation sets the parameters of the PID controller when there is only a crane trolley's speed feedback in the system. In the second simulation, the minimum square error tolerance has been set, but this is explained by the fact that the trolley does not reach the set speed (0.2 m/s) due to low amplification and therefore, by increasing the proportional part of Kp_1, this deviation decreases. Therefore, $Kp_1 = 0.2$ was selected for another search and the PID controller
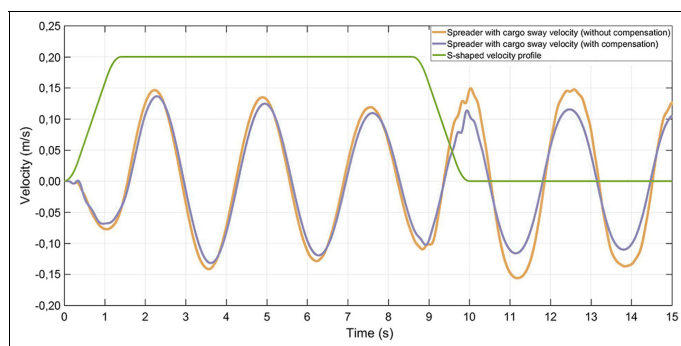
Figure 8. S-shape velocity profile (green), trolley velocity (blue), and spreader oscillation velocity (red) graphs with PID controller and one feedback.

integral component of the factor was determined. This step is used to minimize the steady state error of the trolley's speed, as increasing the coefficient of the integrative component increases the system response speed, and therefore the load swinging is much higher. According to the simulation results with only one feedback, the following parameters of the PID controller were obtained: $Kp_1 = 0.6$, $Ki_1 = 13$, and $Kd_1 = 0.01$. Using these parameters, the transition process of crane trolley and load variation rates is presented, which is shown in Figure 8.

The second step was performed for the auxiliary feedback control loop with PI controller designed to suppress container swinging (shown in Table 1). According to the results, it was determined that the additional PI system for reducing the intensity of cargo volatility has a higher error (Table 1, Results 8-11) only with the proportional controller (Table 1, Results 8-11). This is a result of the integral part of PI controller, and the square error is increasing by increasing the Kp_2 coefficient.

According to the data of Table 1 and modeling results, the following PID and PI coefficients were chosen: PID: $Kp_1 = 0.6$, $Ki_1 = 13$, $Kd_1 = 0.01$, and additional PI controller: $Kp_2 = 0.2$ and $Ki_2 = 2$. Selected seventh case is based on the trolley's integral square error minimal value in the PID and PI control system, and the square integral error of the load swinging varies from this value every 3%. These control parameters are the initial data of the PID and PI controller for experimental evaluation.

Conclusion

In this article, an integrated autonomous quay crane control algorithm was developed with the proposed embedded container swinging control subroutine, operated in optimal mode when the control system used PID (set parameters: $Kp_1 = 0.6$, $Ki_1 = 13$, and $Kd_1 = 0.01$) controller with additional PI (set parameters: $Kp_2 = 0.2$ and $Ki_2 = 2$) with feedback and S-shaped signal. These PID and PI controllers' parameters were determined by finding the minimum integral criterion of the square error (Table 1) of spreader traveling speed. These optimal parameters are suitable for case studied in the article; therefore, system parameter changes the PID and PI parameters should vary and be adaptable, and such investigation is planned for future research. The experimental laboratory physical model was designed to verify the theoretical and simulation findings. Results suggest that during loading process using the S-shaped velocity profile in dynamic mode as control system input provides a possibility to obtain a most suitable solution for the transport modes of a specific container. The results of comparative and experimental studies show that proposed autonomous quay crane's control algorithm, with a PI subsystem for decreasing container swinging during loading, can be used to accelerate the handling process.

ORCID iD

Tomas Eglynas (iD) https://orcid.org/0000-0002-9973-5896

References

 1. Barysienė J. A multi-criteria evaluation of container terminal technologies applying the COPRAS-G method. *Transport* 2012; 27: 364–372.
 2. Cao L and Liu L. Adaptive fuzzy sliding mode method-based position and anti-swing control for overhead cranes. In: *Proceedings of the 2011 third international conference on measuring technology and mechatronics automation*, Shangshai, 6–7 January 2011, vol. 2, pp.335–338. New York: IEEE.
 3. Yoshihara H, Fujioka N and Kasahara H. A new vision-sensorless anti-sway control system for container cranes. In: *Proceedings of the 38th IAS annual meeting on conference record of the industry applications conference*, Salt Lake City, UT, 12–16 October 2003, pp.262–269. New York: IEEE.
 4. Sano H, Ohishi K, Kaneko T, et al. Anti-sway crane control based on dual state observer with sensor-delay correction. In: *Proceedings of the 11th IEEE international workshop on advanced motion control (AMC)*, Nagaoka, Niigata, 21–24 March 2010, pp.679–684. New York: IEEE.
 5. Kawai H, Choi Y, Kim YB, et al. Position measurement of container crane spreader using an image sensor system for anti-sway controllers. In: *Proceedings of the international conference on control, automation and systems*, Seoul, South Korea, 14–17 October 2008, pp.683–686. New York: IEEE.
 6. Chao SL and Lin YJ. Evaluating advanced quay cranes in container terminals. *Transport Res E: Log* 2011; 47: 432–445.
 7. Schaub H. Rate-based ship-mounted crane payload pendulation control system. *Control Eng Pract* 2008; 16: 132–145.
 8. Chang C, Chiang K and Description AS. The nonlinear 3-D crane control with an intelligent operating method. In: *Proceedings of the 2008 SICE annual conference*, Tokyo, Japan, 20–22 August 2008, pp.2917–2921, 2008.
 9. Zhi-Jun LI, Zhen LI, Hui-Jie LI, et al. Research of coordinated control method of hybrid power crane system. In: *Proceedings of the international conference on modelling, identification and control*, Wuhan, China, 24–26 June 2012, pp.1093–1097. New York: IEEE.
10. Tanaka Y, Konishi Y, Araki N, et al. Development of high speed controller of container crane by binary input using mixed logical dynamical theory. In: *Proceedings of the 2009 fourth international conference on innovative computing, information and control (ICICIC)*, Kaohsiung, Taiwan, 7–9 December 2009, pp.181–184. New York: IEEE.
11. Chang D, Jiang Z, Yan W, et al. Integrating berth allocation and quay crane assignments. *Transport Res E: Log* 2010; 46: 975–990.
12. Fang Y, Wang P and Zhang X. A motion planning-based adaptive control method for an underactuated crane system. *IEEE T Control Syst Tech* 2012; 20: 241–248.
13. Tanaka Y, Konishi Y, Araki N, et al. Control of container crane by binary input using mixed logical dynamical system. In: *Proceedings of the international conference on control, automation and systems*, Seoul, South Korea, 14–17 October 2008, vol. 2, pp.13–17.
14. Nundrakwang S, Benjanarasuth T, Ngamwiwit J, et al. Multivariable control of overhead crane system by CRA method. In: *Proceedings of the SICE annual conference*, Tokyo, Japan, 20–22 August 2008, vol. 1, pp.3278–3282. New York: IEEE.
15. Roso V, Woxenius J and Lumsden K. The dry port concept: connecting container seaports with the hinterland. *J Transp Geogr* 2009; 17: 338–345.
16. Elbadawy AA and Shehata MMG. Anti-sway control of marine cranes under the disturbance of a parallel manipulator. *Nonlinear Dynam* 2015; 82: 415–434.
17. Majid MA, Ibrahim WSW, Mohamad S, et al. A comparison of PID and PD controller with input shaping technique for 3D gantry crane. In: *Proceedings of the IEEE conference on systems, process & control (ICSPC)*, Kuala Lumpur, Malaysia, 13–15 December 2013, pp.144–148. New York: IEEE.
18. Wong TT, Tang CHH and Mailah M. Winch driven active heave compensation for load transfer in overhead crane system. In: *Proceedings of the 4th international conference on intelligent and advanced systems (ICIAS2012)*, Kuala Lumpur, Malaysia, 12–14 June 2012, pp.34–39. New York: IEEE.
19. Liu C, Zhao H and Cui Y. Research on application of fuzzy adaptive PID controller in bridge crane control system. In: *Proceedings of the 2011 international conference on control, automation and systems engineering (CASE)*, Beijing, China, 27–29 June 2014, pp.1–4. New York: IEEE.
20. Jaafar HI, Mohamed Z, Abidin AFZ, et al. PSO-tuned PID controller for a nonlinear gantry crane system. In: *Proceedings of the IEEE international conference on control system, computing and engineering*, Penang, Malaysia, 23–25 November 2012, pp.515–519. New York: IEEE.
21. Jaafar HI, Sulaima MF, Mohamed Z, et al. Optimal PID controller parameters for nonlinear gantry crane system via MOPSO technique. In: *Proceedings of the IEEE conference on sustainable utilization and development in engineering and technology (CSUDET)*, Selangore, Malaysia, 30 May–1 June 2013, pp.86–91. New York: IEEE.
22. Rew KH, Ha CW and Kim YS. A practically efficient method for motion control based on asymmetric velocity profile. *Int J Mach Tools Manuf* 2009; 49: 678–682.
23. Béarée R. New damped-jerk trajectory for vibration reduction. *Control Eng Pract* 2014; 28: 112–120.
24. Sun N, Zhang X, Fang Y, et al. Transportation task-oriented trajectory planning for underactuated overhead cranes using geometric analysis. *IET Control Theory Appl* 2012; 6: 1410–1423.
25. Xuebo Z, Yongchun F, Ning SUN, et al. A pseudospectral time-optimal motion planner for underactuated overhead crane systems. In: *Proceedings of the 32nd Chinese control conference*, Xi'an, China, 26–28 July 2013, vol. 3, pp.4397–4402. New York: IEEE.
26. Sun N, Fang Y, Member S, et al. Phase plane analysis based motion planning for underactuated overhead

cranes. In: *Proceedings of the IEEE international conference on robotics and automation*, Shanghai, China, 9–13 May 2011, pp.3483–3488. New York: IEEE.

27. Stoychitch M. An algorithm of linear speed control of a stepper motor in real time. *Ann Fac Eng* 2013; 11: 51–56.

28. Wu Z and Xia X. Optimal motion planning for overhead cranes. *IET Control Theory Appl* 2014; 8: 1833–1842.

29. Vaughan J, Yoo J, Knight N, et al. Multi-input shaping control for multi-hoist cranes. In: *Proceedings of the American control conference*, Washington, DC, 17–19 June 2013, pp.3455–3460. New York: IEEE.

30. Prof A, Brock S, Member I, et al. Analysis of input shaping and PID-controller interaction structures for two-mass systems. In: *Proceedings of the 16th international conference on mechatronics–mechatronika*, Brno, 3–5 December 2014. New York: IEEE.

31. Ngo OH, Nan Y and Hong K. Command shaping for vibration reduction of container cranes. In: *Proceedings of the 12th international conference on control, automation and systems*, JeJu Island, South Korea, 17–21 October 2012, pp.651–655. New York: IEEE.

32. Jaafar HI, Mohamed ZZ, Jamian JJ, et al. Dynamic behaviour of a nonlinear gantry crane system. *Proc Technol* 2013; 11: 419–425.

33. Ismail RMTR, Ahmad MA, Ramli MS, et al. Nonlinear dynamic modelling and analysis of a 3-D overhead gantry crane system with payload variation. In: *Proceedings of Third UKSim European symposium on computer modeling and simulation*, Athens, 25–27 November 2009, pp.350–354. New York: IEEE.

34. Bogdevicius M and Vika A. Investigation of the dynamics of the overhead crane lifting process in the vertical plane. *Transport* 2005; 20: 176–180.

35. Tomczyk J, Cink J and Kosucki A. Dynamics of an overhead crane under a wind disturbance condition. *Autom Constr* 2014; 42: 100–111.

36. Cha JH, Roh MI and Lee KY. Dynamic response simulation of a heavy cargo suspended by a floating crane based on multibody system dynamics. *Ocean Eng* 2010; 37: 1273–1291.

37. Ranjbari L and Shirdel AH. Designing precision fuzzy controller for load swing of an overhead crane. *Neural Comput Appl* 2015; 26: 1555–1560.

38. Wang L, Zhang H and Kong Z. Anti-swing control of overhead crane based on double fuzzy controllers. In: *Proceedings of the 27th Chinese control and decision conference (2015 CCDC)*, Qingdao, 23–25 May 2015, pp.981–986. New York: IEEE.

39. Yang C, Zhang Z and Zhao Q. Study on intelligent control of two-dimensional precision positioning system. In: *Proceedings of the international conference on computer science and software engineering*, Hubei, China, 12–14 December 2008, vol. 4, pp.835–838. New York: IEEE.

40. Sun Z, Wang N, Bi Y, et al. A DE based PID controller for two dimensional overhead crane. In: *Proceedings of the 34th Chinese control conference*, Hangzhou, China, 28–30 July 2015, pp.2546–2550. New York: IEEE.

41. Wong TT, Tang CHH and Mailah M. Robust active heave compensated winch-driven overhead crane system for load transfer in marine operation. In: *Proceedings of the robust active heave compensated winch-driven overhead crane system for load transfer in marine operation*, Kuala Lumpur, Malaysia, 12–14 June 2012, vol. 1, pp.111–116. New York: IEEE.

42. Lv N, Li H, Li M, et al. Based on PID control optimization of synchronous motor control. In: *Proceedings of the conference on measurement, information and control (MIC)*, Harbin, China, 18–20 May 2012, pp.2111–2114.

43. Li P, Li Z and Yang Y. The application research of ant colony optimization algorithm for intelligent control on special crane. In: *Proceedings of the 2012 second international conference on instrumentation, measurement, computer, communication and control*, Harbin, China, 8–10 December 2012, pp.999–1004. New York: IEEE.

44. Maghsoudi MJ, Mohamed Z, Tokhi MO, et al. Control of a gantry crane using input-shaping schemes with distributed delay. *Trans Inst Meas Control* 2017; 39: 361–370.

45. Schmidt R, Barry N and Vaughan J. Tracking of a target payload via a combination of input shaping and feedback control. *IFAC—PapersOnLine* 2015; 48: 141–146.

46. Ahmad MA, Ismail RR, Ramli MS, et al. Investigations of NCTF with input shaping for sway control of a double-pendulum-type overhead crane. In: *Proceedings of the 2nd international conference on advanced computer control*, Shenyang, China, 27–29 March 2010, vol. 3, pp.456–461. New York: IEEE.

4th publication / 4 publikacija

Multibody dynamic simulation and transient analysis of quay crane spreader and lifting mechanism

A. Andziulis, T. Eglynas, M. Bogdevičius, **M. Jusis**, A. Senulis.

Research Article

Multibody dynamic simulation and transient analysis of quay crane spreader and lifting mechanism

Arunas Andziulis[1], Tomas Eglynas[1,2], Marijonas Bogdevicius[2], Mindaugas Jusis[1] and Audrius Senulis[1]

Abstract

Nowadays, container shipment in the intermodal terminals is overloaded. The quay crane and its control system have to be properly prepared for rapid cargo reloading. The advanced control system may increase container loading efficiency due to the reduced transportation time. However, faster transportation demands higher safety. In this article, the authors performed multibody dynamics simulation of the container spreader and lifting mechanism by analyzing more advanced mathematical model of the quay crane. Trolley motion and cargo swing angle transient responses of the dynamic system were acquired and analyzed during model simulation. The main target of this research is to determine the system behavior during transients. The simulation results showed that the transients induced by startup of the vertical spreader travel affect the whole crane system in all the investigated cases. In addition, the influence of flexible cable causes additional oscillations of cargo and reciprocating trolley displacement. The simulation of the container spreader and lifting mechanism will help detect motion deviations of the quay crane in real time.

Keywords

Multibody dynamics, transients, simulation, mathematical modeling, quay crane

General introduction

Risk of cargo transportation process and impact of crane restrictions

Every year, container shipment is increasing and the container terminals get loaded more. Because of this situation, the terminals must load more containers using the same transportation equipment. One of the most important aspects of cargo loading is operation safety which can decrease in overloaded terminals.[1–3] In order to ensure safety of the container during transportation, an optimal operational strategy[4,5] of a quay crane control has to be ensured. In addition, the restrictions and limitations of the intermodal quay crane have to be appropriately assessed performing numerical simulations of multibody dynamics and the transient processes.

One of the most researched cargo damage reasons in the past years is container swinging.[2,6,7] The main cause of the container and spreader swinging is the flexible steel cable connection between the spreader and trolley of the quay crane.[8] The container can produce swinging motion because of different container weights, wind gusts, and human actions. As a result, more time is required for the container shipment from point A to

[1]Marine Science and Technology Centre, Klaipeda University, Klaipeda, Lithuania
[2]Department of Transport Technological Equipment, Vilnius Gediminas Technical University, Vilnius, Lithuania

Corresponding author:
Tomas Eglynas, Marine Science and Technology Centre, Klaipeda University, Bijunu g. 17-206, LT-91225 Klaipeda, Lithuania.
Email: tmse@inbox.lt

Figure 1. Quay crane in port of Rotterdam.

point B due to the container swinging reduction process. Moreover, due to unstable crane motions, there is a probability that the container can be damaged if the collision with the quay crane structures occurs. Because of high safety risks, the container crane operation mostly is suspended during strong winds.

The numerical simulations of multibody system dynamics enable to apply limitations for better investigation of container sway reasons. Therefore, applying a common set of limitations to all cranes would not be efficient. Most of the container terminals use quay cranes with specifications depending on their loading demands. Some of the main technical limitations of the quay crane are hoisting capacity, hoisting speeds of the spreader, trolley traveling speed, gantry traveling speed, traveling distances, boom hoisting time, wind speed, and power supply.[9]

The most active recent research area is modeling of crane dynamics to increase cargo safety. The main target of such research is to determine the system behavior in different conditions.[9–11] A dynamic model of a three-dimensional (3D) overhead gantry crane system motion is proposed by Ismail et al.[10] The Lagrangian method is used for calculations. The trolley position and swing angle responses of the dynamic system have been acquired and analyzed during system simulation. These results are suitable for the development of effective control algorithms for a double-pendulum gantry crane system. Jaafar et al.[9] presented the development of nonlinear gantry crane system model, and the factors affecting the performance in terms of input voltage, cable length, payload mass, and trolley mass were investigated. The simulation results had shown that system response is very sensitive to the variation in the parameters. This is the main reason for container swinging and safety issues. The results of this research are very beneficial for the development of control algorithms.

Most of the models related to dynamic control and safety problems represent only one side of the problem, such as a crane control system with a state simulator. For example, in Tomczyk et al.,[12] a dynamic model for solving problems of load operation and positioning under different wind disturbances is developed. Cha et al.[13] investigated problems involving floating crane and the dynamics model was developed to simulate the motion of the heavy cargo.

The most recent research results by Wu et al.,[14] and Qian et al.,[15] which addresses container sway problem, provide solutions related to the design of control algorithms dedicated to compensate or minimize the sway movement of the container. The presented solutions give positive results, although not all the container sway reasons were estimated. Therefore, by additionally estimating more reasons of container sway, these control algorithms could be made more efficient.

In this article, the dynamic model of a quay crane container spreader and lifting mechanism is presented. The proposed multibody system could also be used as a tool for solving multiple problems, such as wind disturbances, transportation trajectory, and predictive control. The developed multibody numerical model of a quay crane spreader and lifting mechanism is based on real quay crane (Figure 1) mechanical structure.

According to the analysis of the other research, the more sophisticated and accurate model is presented, which evaluates additional factors such as motor-induced vibrations, eight flexible cable system, transmission, and pulleys. The model is used for estimating the dynamics of the crane container spreader. It was developed using the parameters of manufactured prototype size, motor performance, lifting power, and so on. In addition, the authors developed motion equations of the crane systems and defined the initial parameters for system simulation. So in the next section, a dynamic
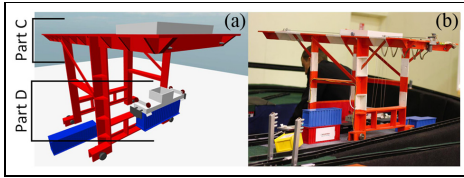
Figure 2. Scaled prototype of intermodal quay crane: (a) virtual prototype and (b) physical prototype.

model of container spreader dynamics and lifting mechanism is proposed.

Mathematical model and dynamics of container spreader transients

Before the development of better algorithm, a new mathematical model of the crane spreader and real quay crane prototype was created (Figure 2). The

model will provide theoretical data about spreader status. The vibrations and their sources in the crane spreader and lifting mechanism were evaluated and provided additional information for new mathematical model for the crane (Figure 3). The mathematical model (Figure 3) marked "Part C" (trolley with lifting mechanism) and "Part D" (container spreader) is the same like in prototype (Figure 2).

Most attention is paid to motor vibrations and cable tensions. Because of very long cables in cranes, additional container swinging can appear. Mostly, it is caused by the weather conditions and wrong algorithms for operating devices. The best solution for this problem is adding additional sensors, such as, in our case, an accelerometer. The sensor's data could be used for containers' position estimation, detection, and reduction in container swinging. This could increase transportation security. Combined algorithm generator and real-time sensor data will provide the best algorithm for a particular kind of cargo that is stored in the container. In addition, it will allow adjusting algorithm in
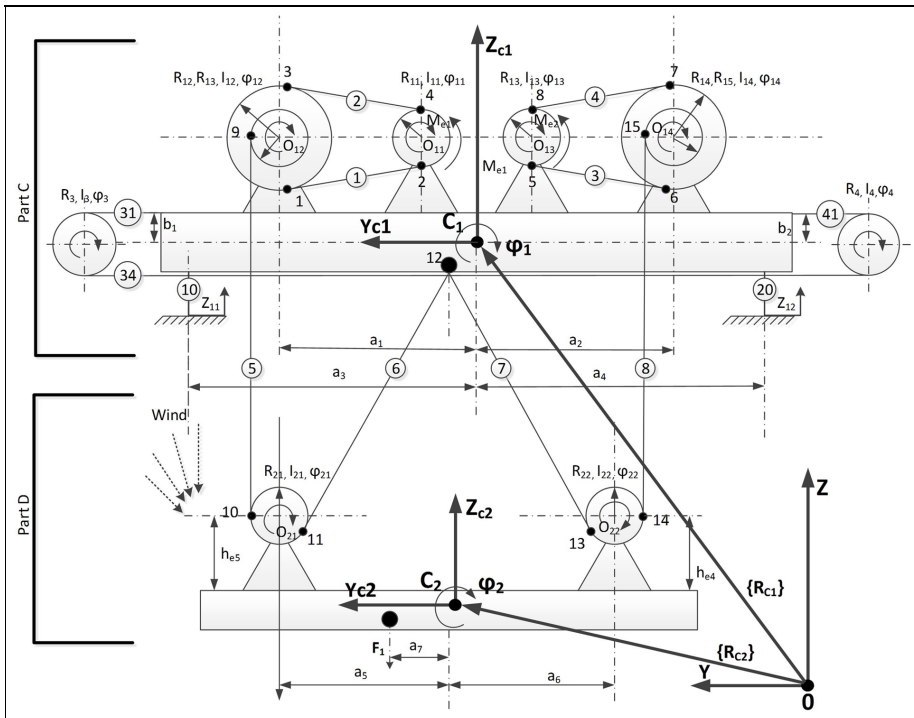

Figure 3. Dynamic model of quay crane spreader and lifting mechanism.

real time, if the weather conditions change or some unexpected situation appears (uneven control, shift of the cargo in the container, crane swinging due to the wind, etc.).

The developed model of the quay crane spreader and lifting mechanism is based on several assumptions. First, all bodies in the model are considered as solid bodies that cannot be deformed. The physical and mechanical properties of all the cables (such as stretching of cables while carrying heavy cargo) were assumed and estimated and their mathematical models are included in equations. Additionally, the electromechanical transient processes of electric motors and imperfections of trolley path were estimated.

For better container transportation problem solution, the new mathematical model was used for the container spreader and lifting mechanism, which will help to evaluate the situation. Torque mathematical equation of first electrical asynchronous motor with gear $\dot{M}_{ei}$ is shown below

$$\dot{M}_{ei} = U_{redei}C_{ei}(\omega_{ei0} - U_{redei}\dot{\varphi}_i) - d_{ei}M_{ei} \qquad (1)$$

Here, d_{ei} and C_{ei} are the motor parameters, ω_{ei0} is the angular velocity, and U_{redei} is the gear ratio of the motor reduction. The analyzed system consists of two bodies with mass centers in points C_i and C_j. They are connected to the cable at mounting points i and j. The cable stiffness and damping coefficients are k_{ij} and c_{ij}, respectively. The tension force in this cable is F_{ij}, and the variation in mechanical work of this force is equal to

$$\delta W_{ij} = F_{ij}\delta L_{ij} \qquad (2)$$

Here, L_{ij} is the distance between i and j; δL_{ij} is the variation in distance between i and j. The distance of L_{ij} is equal to

$$L_{ij}^2 = (\mathbf{r}_i - \mathbf{r}_j)^T(\mathbf{r}_i - \mathbf{r}_j) \qquad (3)$$

Here, $\mathbf{r}_i$ and $\mathbf{r}_j$ are the vectors of i and j, respectively, in common coordinate system OXYZ

$$\begin{aligned} \mathbf{r}_i &= \mathbf{r}_{ci} + \mathbf{A}(\varphi_i)\mathbf{r}_{ci,i} \\ \mathbf{r}_j &= \mathbf{r}_{cj} + \mathbf{A}(\varphi_j)\mathbf{r}_{cj,j} \end{aligned} \qquad (4)$$

Here, $\mathbf{r}_{Ci}$ and $\mathbf{r}_{Cj}$ are the vectors of mass centers of bodies, $\mathbf{A}(\varphi_i)$ and $\mathbf{A}(\varphi_j)$ are the matrixes of angular rotation (about X-axis), $\mathbf{r}_{ci,i}$ is the distance between body mass center C_i and body point i, and $\mathbf{r}_{cj,j}$ is the distance between body mass center C_j and body point j. The variation in distance L_{ij} is

$$\delta L_{ij} = \frac{\delta \mathbf{r}_{ij}^T}{L_{ij}}\mathbf{r}_{ij} \qquad (5)$$

Here

$$\delta \mathbf{r}_{ij} = \delta \mathbf{r}_{ci} + \delta\varphi_i\left[\frac{d\mathbf{A}(\varphi_i)}{d\varphi_i}\right]\mathbf{r}_{ci,i} - \delta \mathbf{r}_{cj} - \delta\varphi_j\left[\frac{d\mathbf{A}(\varphi_j)}{d\varphi_j}\right]\mathbf{r}_{cj,j} \qquad (6)$$

Using equations (5) and (6), the variations in mechanical work can be calculated as

$$\delta W_{cj} = \delta \mathbf{r}_{ci}^T \cdot \mathbf{q}_{r_{ci}} + \delta\varphi_i q_{r_i} + \delta \mathbf{r}_{cj}^T \mathbf{q}_{r_{cj}} + \delta\varphi_j q_{r_j} \qquad (7)$$

Here, $\mathbf{q}_{r_{ci}}$ and $\mathbf{q}_{r_{cj}}$ are the vectors of the generalized forces that apply to bodies i and j; q_{r_i} and q_{r_j} are the generalized forces that apply to bodies i and j

$$\mathbf{q}_{r_{ci}} = \frac{F_{ij}}{L_{ij}}\mathbf{r}_{ij}, q_{\varphi i} = \frac{F_{ij}}{L_{ij}}r_{ci,i}^T\left[\frac{d\mathbf{A}(\varphi_i)}{d\varphi_i}\right]^T\mathbf{r}_{ij} \qquad (8)$$

$$\mathbf{q}_{R_{cj}} = \frac{F_{ij}}{L_{ij}}\mathbf{r}_{ij}, q_{\varphi j} = \frac{F_{ij}}{L_{ij}}\mathbf{r}_{cj,j}^T\left[\frac{d\mathbf{A}(\varphi_j)}{d\varphi_j}\right]^T\mathbf{r}_{ij} \qquad (9)$$

The cable tension force is

$$F_{ij} = \left(-k_{ij}(L_{ij} - L_{ij,0}) - C_{ij}\dot{L}_{ij}\right)H(L_{ij} - L_{ij,0}) \qquad (10)$$

Here, $H(L_{ij} - L_{ij,0})$ is the Heaviside function and $L_{ij,0}$ is the initial cable length between i and j. $\dot{L}_{ij}$ is the cable linear speed

$$\dot{L}_{ij} = \frac{1}{L_{ij}}\dot{\mathbf{r}}_{ij}^T \cdot \mathbf{r}_{ij} \qquad (11)$$

Here, $\dot{\mathbf{r}}_{ij}$ is the time derivative of vector $\mathbf{r}_{ij}$

$$\dot{\mathbf{r}}_{ij} = \dot{\mathbf{r}}_{ci} + \dot{\varphi}_i\left[\frac{d\mathbf{A}(\varphi_i)}{d\varphi_i}\right]\mathbf{r}_{ci,i} - \dot{\mathbf{r}}_{cj} - \dot{\varphi}_j\left[\frac{d\mathbf{A}(\varphi_j)}{d\varphi_j}\right]\mathbf{r}_{cj,j} \quad (12)$$

Equations of motions
System of motion equations for the first body (crane without load)

$$\begin{aligned} m_1\ddot{q}_{12} = &-k_{31}(q_{12} - R_3\varphi_3) - c_{31}(\dot{q}_{12} - R_3\dot{\varphi}_3) \\ &- k_{41}(q_{12} - R_3\varphi_4) - c_{41}(\dot{q}_{12} - R_4\dot{\varphi}_4) \\ &+ \mathbf{e}_2^T(F_5\mathbf{q}_{51} + F_6\mathbf{q}_{61} + F_7\mathbf{q}_{71} + F_8\mathbf{q}_{81}) \\ &- \dot{m}_1\dot{q}_{12} + F_{1R2} \end{aligned} \qquad (13)$$

$$\begin{aligned} m_1\ddot{q}_{13} = &-k_{10}(q_{13} + a_3\varphi_1 - \mathbf{Z}_{11}) \\ &- k_{20}(q_{13} - a_4\varphi_1 - \mathbf{Z}_{12}) - c_{20}(\dot{q}_{13} - a_4\dot{\varphi}_1 - \mathbf{Z}_{12}) \\ &- c_{10}(\dot{q}_{13} + a_3\dot{\varphi}_1 - \mathbf{Z}_{11}) - m_1g - \dot{m}_1\dot{q}_{13} \\ &+ \mathbf{e}_3^T(F_5\mathbf{q}_{51} + F_6\mathbf{q}_{61} + F_7\mathbf{q}_{71} + F_8\mathbf{q}_{81}) + F_{1R3} \end{aligned} \qquad (14)$$

$$I_1 \ddot{\varphi}_1 = - k_{10} a_3 (q_{13} + a_3 \varphi_1 - \mathbf{Z}_{11})$$
$$- c_{10} a_3 (\dot{q}_{13} + a_3 \dot{\varphi}_1 - \mathbf{Z}_{11})$$
$$- k_{20} a_4 (q_{13} - a_4 \varphi_1 - \mathbf{Z}_{12})$$
$$+ c_{20} a_4 (\dot{q}_{13} - a_4 \dot{\varphi}_1 - \mathbf{Z}_{12}) - \dot{I}_1 \dot{\varphi}_1 + M_{51}$$
$$+ M_{61} + M_{71} + M_{81} + M_{1R} \qquad (15)$$

Here, m_1 is the mass of the first body, I_1 is the inertial moment of the first body about the *X*-axis, $\dot{m}_1$ and $\dot{I}_1$ are the first time derivatives of mass and mass inertial moment of the first body (assumption of cable winding on the pulley), respectively. a_3 and a_4 are the geometrical parameters. $\mathbf{Z}_{11}$ and $\mathbf{Z}_{12}$ are the kinematic excitations of the first body pulleys; $\mathbf{Z}_{11}$ and $\mathbf{Z}_{12}$ are the derivatives of kinematic excitations by time. $\mathbf{e}_2$ and $\mathbf{e}_3$ are the unit vectors on *Y*- and *Z*-axis in common coordinate system OXYZ. k_{31}, k_{41}, c_{31}, and c_{41} are stiffness and damping coefficients of trolley positioning system belts. k_{10}, k_{20}, c_{10}, and c_{20} are the stiffness and damping coefficients of the pulleys of trolley positioning system. F_5, F_6, F_7, and F_8 are the cable tension forces. M_{51}, M_{61}, M_{71}, M_{81}, and M_{1R} are the torques of the first body, transferred by cables 5, 6, 7, and 8. F_{1R2} and F_{1R3} are the air resistance forces (projection on *Y*- and *Z*-axis) and torques $\mathbf{q}_{51}$, $\mathbf{q}_{61}$, $\mathbf{q}_{71}$, and $\mathbf{q}_{81}$ are the vectors of the generalized forces of cables 5, 6, 7, and 8, respectively, determined using equation (8).

System of motion equations for the second body (spreader with the container)

$$\mathbf{M}_2 \ddot{\mathbf{r}}_{C_2} = \mathbf{q}_{52} + \mathbf{q}_{62} + \mathbf{q}_{72} + \mathbf{q}_{82} + \mathbf{f}_{2W} + \mathbf{f}_{2R} \qquad (16)$$

$$I_2 \ddot{\varphi}_2 = M_{52} + M_{62} + M_{72} + M_{82} + M_{R2} \qquad (17)$$

$$I_{21} \ddot{\varphi}_{21} = R_{21}(F_5 - F_6) - M_{fr_{21}} sign(\dot{\varphi}_{21}) \qquad (18)$$

$$I_{22} \ddot{\varphi}_{22} = R_{22}(F_7 - F_8) - M_{fr_{22}} sign(\dot{\varphi}_{22}) \qquad (19)$$

Here, F_{2W} is the vector of weight force (20); $\mathbf{f}_{2R}$ and M_{R2} are the vector of air resistance force and torque of the second body, respectively. $\mathbf{q}_{52}$, $\mathbf{q}_{62}$, $\mathbf{q}_{72}$, and $\mathbf{q}_{82}$ are the vectors of the generalized forces of cables 5, 6, 7, and 8, respectively, calculated using equation (8). M_{52}, M_{62}, M_{72}, and M_{82} are the torques of the first body, transferred by cables 5, 6, 7, and 8, respectively. $\mathbf{M}_2$ is the matrix of masses of the second body calculated using equation (19). $M_{fr_{21}}$ and $M_{fr_{22}}$ are the torques of friction of polyspast

$$\{\boldsymbol{F}_{2W}\}^T = [0, 0, -m_2 g] \qquad (20)$$

$$[\boldsymbol{M}_2] = diag(m_2, m_2, I_2) \qquad (21)$$

System of motion equations for the third and fourth bodies and the third asynchronous motor torque (trolley motion equations)

$$\dot{M}_{e3} = U_{rede3} C_{e3}(\omega_{e30} - U_{rede3} \dot{\varphi}_3) - d_{e3} M_{e3} \qquad (22)$$

$$I_3 \ddot{\varphi}_3 = - k_{31} R_3 (R_3 \varphi_3 - q_{12}) - c_{31} R_3 (R_3 \dot{\varphi}_3 - \dot{q}_{12})$$
$$- k_{34} R_3 (R_3 \varphi_3 - R_4 \varphi_4) - c_{34} R_3 (R_3 \dot{\varphi}_3 - R_4 \dot{\varphi}_4)$$
$$+ M_{e3} - M_{e3R} \qquad (23)$$

$$I_4 \ddot{\varphi}_4 = - R_4 k_{41}(R_4 \varphi_4 - q_{12}) - R_4 c_{41}(R_4 \dot{\varphi}_4 - \dot{q}_{12})$$
$$- R_4 k_{34}(R_4 \varphi_4 - R_3 \varphi_3)$$
$$- R_4 c_{34}(R_4 \dot{\varphi}_4 - R_3 \dot{\varphi}_3) - M_{e4R} \qquad (24)$$

Here, k_{31}, k_{34}, c_{31}, and c_{34} are the stiffness and damping coefficients of belts. φ_3, φ_4, $\dot{\varphi}_3$, and $\dot{\varphi}_4$ are the angular position and speed of the third and fourth bodies. R_3 and R_4 are the radii of the pulleys, I_3 is the mass moment of inertia of the third motor and pulley, and I_4 is the moment of inertia of the fourth pulley. M_{e3} is the torque of the motor. C_{e3} and d_{e3} are the motor parameters. M_{e3R} is the torque of resistance of the third body. ω_{e30} is the motor angular velocity.

System of motion equations for lifting mechanism

$$\dot{M}_{e1} = U_{rede1} C_{e1}(\omega_{e110} - U_{rede1} \dot{\varphi}_{11}) - d_{e1} M_{e1} \qquad (25)$$

$$I_{11} \ddot{\varphi}_{11} = - R_{11}(k_1(R_{11} \varphi_{11} - R_{12} \varphi_{12})$$
$$+ c_1(R_{11} \dot{\varphi}_{11} - R_{12} \dot{\varphi}_{12}))(1 - e^{-f_{belt}\beta_{24}}) \qquad (26)$$
$$+ M_{e1} - M_{fr_{11}} sign(\dot{\varphi}_{11})$$

$$I_{12} \ddot{\varphi}_{12} = - R_{12}(k_1(R_{12} \varphi_{12} - R_{11} \varphi_{11})$$
$$+ c_1(R_{12} \dot{\varphi}_{12} - R_{11} \dot{\varphi}_{11}))(1 - e^{-f_{belt}\beta_{13}}) \qquad (27)$$
$$- M_{9,5} - M_{fr_{12}} sign(\dot{\varphi}_{12})$$

$$\dot{M}_{e2} = U_{rede2} C_{e2}(\omega_{e130} - U_{rede2} \dot{\varphi}_{13}) - d_{e2} M_{e2} \qquad (28)$$

$$I_{13} \ddot{\varphi}_{13} = - R_{13}(k_3(R_{13} \varphi_{13} - R_{14} \varphi_{14})$$
$$+ c_3(R_{13} \dot{\varphi}_{13} - R_{14} \dot{\varphi}_{14}))(1 - e^{-f_{belt}\beta_{58}}) \qquad (29)$$
$$+ M_{e2} - M_{fr_{13}} sign(\dot{\varphi}_{13})$$

$$I_{14} \ddot{\varphi}_{14} = - R_{14}(k_3(R_{14} \varphi_{14} - R_{13} \varphi_{13})$$
$$+ c_3(R_{14} \dot{\varphi}_{14} - R_{13} \dot{\varphi}_{13}))(1 - e^{-f_{belt}\beta_{67}})$$
$$- M_{fr_{14}} sign(\dot{\varphi}_{14}) - M_{15,8} - M_{fr_{14}} sign(\dot{\varphi}_{14})$$
$$\qquad (30)$$

$$M_{9,5} = F_5 R_{13}, M_{15,8} = F_8 R_{14} \qquad (31)$$

where M_{e1} and M_{e2} are the torques of the first and second asynchronous motors, respectively; φ_{11}, φ_{12}, φ_{13}, and φ_{14} are the angular positions of the first, second, third, and fourth pulleys, respectively. C_{e1}, d_{e1}, C_{e2}, and d_{e2} are the first and second motor parameters. ω_{e110} and ω_{e130} are the first and second motor angular velocities, respectively. I_{11}, I_{12}, I_{13}, and I_{14} are the moments of inertia of the first, second, third, and fourth pulleys,

respectively. R_{11}, R_{12}, R_{13}, and R_{14} are the radii of the first, second, third, and fourth pulleys, respectively. k_1, k_2, k_3, k_4, c_1, c_2, c_3, and c_4 are the stiffness and damping coefficients of the belts. $M_{9,5}$ and $M_{15,8}$ are the moments of inertia of the second and fourth pulleys, caused by the tension forces in cables 5 and 8, on points 9 and 15 of the pulleys, respectively. $M_{fr_{11}}$, $M_{fr_{12}}$, $M_{fr_{13}}$, and $M_{fr_{14}}$ are the torques of the friction force of the first, second, third, and fourth pulleys, respectively. f_{belt} is the friction coefficient; β_{24}, β_{13}, β_{58}, and β_{67} are the angles of belt warp.

System of equations for generalized forces of the fifth cable

$$\mathbf{q}_5 = \frac{F_5}{L_{9,10}}(\mathbf{r}_9 - \mathbf{r}_{10}) \tag{32}$$

$$F_5 = -k_5(L_{9,10} - L_{9,10,0}) - c_5\dot{L}_{9,10} \tag{32a}$$

$$\mathbf{r}_9 = \mathbf{r}_{C1} + \mathbf{A}_1(\varphi_1)\mathbf{r}_{C1,9} \tag{32b}$$

$$\mathbf{r}_{C1,9} = \mathbf{r}_{C1,O12} + \mathbf{r}_{O12,9} \tag{32c}$$

$$\mathbf{r}_{10} = \mathbf{r}_{C2} + \mathbf{A}_2(\varphi_2)(\mathbf{r}_{C2,O21} + \mathbf{r}_{O21,10}) \tag{32d}$$

$$\mathbf{r}_{9,10} = \mathbf{r}_9 - \mathbf{r}_{10} \tag{32e}$$

$$L_{9,10}^2 = \mathbf{r}_{9,10}{}^T\mathbf{r}_{9,10} \tag{32f}$$

$$\dot{L}_{9,10} = \frac{1}{L_{9,10}} - \dot{\mathbf{r}}_{9,10}{}^T\mathbf{r}_{9,10} \tag{32g}$$

$$\dot{\mathbf{r}}_{9,10} = \dot{\mathbf{r}}_9 - \dot{\mathbf{r}}_{10} \tag{32h}$$

$$\dot{\mathbf{r}}_9 = \dot{\mathbf{r}}_{C1} + \dot{\varphi}_1\left[\frac{d\mathbf{A}_1}{d\varphi_1}\right]\mathbf{r}_{C1,9} + \mathbf{A}_1(\varphi_1)\dot{\mathbf{r}}_{C1,9} \tag{32i}$$

$$\dot{\mathbf{r}}_{10} = \dot{\mathbf{r}}_{C2} + \dot{\varphi}_2\left[\frac{d\mathbf{A}_2}{d\varphi_2}\right]\mathbf{r}_{C2,10} + \mathbf{A}_2(\varphi_2)\dot{\mathbf{r}}_{C2,10} \tag{32j}$$

$$\dot{\mathbf{r}}_{10} = \dot{\mathbf{r}}_{C2} + \dot{\varphi}_2\left[\frac{d\mathbf{A}_2}{d\varphi_2}\right]\mathbf{r}_{C2,10} + \mathbf{A}_2(\varphi_2)\dot{\mathbf{r}}_{C2,10} \tag{32k}$$

$$\mathbf{r}_{O12,9} = \left\{ \begin{matrix} R_{13}\cos\beta_{9,10} \\ R_{13}\sin\beta_{9,10} \end{matrix} \right\} \tag{32l}$$

$$\beta_{9,10} = \alpha_{O12,O21} - \gamma_{9,10} \tag{32m}$$

$$\sin\alpha_{O12,O21} = \frac{Y_{O21} - Y_{O12}}{L_{O12,O21}} \tag{32n}$$

$$\sin\gamma_{9,10} = \frac{R_{13} - R_{21}}{L_{O12,O21}} \tag{32o}$$

$$L_{O12,O21}^2 = (\mathbf{r}_{O12} - \mathbf{r}_{O21})^T(\mathbf{r}_{O12} - \mathbf{r}_{O21}) \tag{32p}$$

$$\mathbf{r}_{O21,10} = \left\{ \begin{matrix} R_{21}\cos\beta_{O11,O21} \\ R_{21}\sin\beta_{O11,O21} \end{matrix} \right\} \tag{32q}$$

$$\mathbf{r}_{C2,10} = \mathbf{r}_{C2,O21} + \mathbf{r}_{O21,10} \tag{32r}$$

$$\mathbf{r}_{O21,10} = \left\{ \begin{matrix} R_{21}\cos\beta_{9,10} \\ R_{21}\cos\beta_{9,10} \end{matrix} \right\} \tag{32s}$$

Here, k_5 and c_5 are the stiffness and damping coefficients of the fifth cable, respectively (k_5 depends on line length $L_{9,10}$). R_{21} is the radius of the left pulley on the trolley.

System of equations for generalized forces of the sixth, seventh, and eighth cables using system of equations (32)

$$\mathbf{q}_6 = \frac{F_6}{L_{11,12}}(\mathbf{r}_{12} - \mathbf{r}_{11}) \tag{33}$$

$$\mathbf{q}_7 = \frac{F_7}{L_{12,13}}(\mathbf{r}_{12} - \mathbf{r}_{13}) \tag{34}$$

$$\mathbf{q}_8 = \frac{F_8}{L_{14,15}}(\mathbf{r}_{14} - \mathbf{r}_{15}) \tag{35}$$

Moments applied on the first and second bodies

$$
\begin{aligned}
M_{51} &= \mathbf{e}_x{}^T\left(\tilde{\mathbf{r}}_{C1,9} \cdot \mathbf{A}_1(\varphi_1)^T \cdot \mathbf{q}_5\right) \\
M_{61} &= \mathbf{e}_x{}^T\left(\tilde{\mathbf{r}}_{C1,12} \cdot \mathbf{A}_1(\varphi_1)^T \cdot \mathbf{q}_6\right) \\
M_{71} &= \mathbf{e}_x{}^T\left(\tilde{\mathbf{r}}_{C1,12} \cdot \mathbf{A}_1(\varphi_1)^T \cdot \mathbf{q}_7\right) \\
M_{81} &= \mathbf{e}_x{}^T\left(\tilde{\mathbf{r}}_{C1,15} \cdot \mathbf{A}_1(\varphi_1)^T \cdot \mathbf{q}_8\right) \\
M_{52} &= \mathbf{e}_x{}^T\left(\tilde{\mathbf{r}}_{C2,10} \cdot \mathbf{A}_2(\varphi_2)^T \cdot \mathbf{q}_5\right) \\
M_{62} &= \mathbf{e}_x{}^T\left(\tilde{\mathbf{r}}_{C2,11} \cdot \mathbf{A}_2(\varphi_2)^T \cdot \mathbf{q}_6\right) \\
M_{72} &= \mathbf{e}_x{}^T\left(\tilde{\mathbf{r}}_{C2,13} \cdot \mathbf{A}_2(\varphi_2)^T \cdot \mathbf{q}_7\right) \\
M_{82} &= \mathbf{e}_x{}^T\left(\tilde{\mathbf{r}}_{C2,14} \cdot \mathbf{A}_2(\varphi_2)^T \cdot \mathbf{q}_8\right) \\
M_{1R} &= \mathbf{e}_x{}^T\left(\tilde{\mathbf{r}}_{C1p} \cdot \mathbf{A}_1(\varphi_1)^T \cdot \mathbf{f}_{1R}\right) \\
M_{2R} &= \mathbf{e}_x{}^T\left(\tilde{\mathbf{r}}_{C2p} \cdot \mathbf{A}_2(\varphi_2)^T \cdot \mathbf{f}_{2R}\right)
\end{aligned}
\tag{36}
$$

Here, $\{e_x\}$ and $\{e_z\}$ are the unit vectors; $\{e_x\}^T = [1, 0, 0]$ and $\{e_z\}^T = [0, 0, 1]$. $[\tilde{r}_{Cl,k}]$ is the asymmetric matrix

$$\tilde{\mathbf{r}}_{Cl,k} = \begin{bmatrix} o & -r_{Cl,kZ} & r_{Cl,kY} \\ r_{Cl,kZ} & o & -r_{Cl,kX} \\ -r_{Cl,kY} & r_{Cl,kX} & o \end{bmatrix} \tag{37}$$

Here, $k = 9, 10, 11, 12, 13, 14, 15$ and $l = 1, 2$.

Equations of air resistances of the first and second bodies

$$
\begin{aligned}
\mathbf{f}_{1R} = &-\left(\frac{1}{2}\rho_{air}A_{1R}C_{1R}\dot{\mathbf{r}}_{C1}{}^T\dot{\mathbf{r}}_{C1}\right)\frac{\dot{\mathbf{r}}_{C2}}{|\dot{\mathbf{r}}_{C2}|} \\
&+ \left(\frac{1}{2}\rho_{air}A_{1R}C_{1R}\mathbf{v}_{wind}{}^T\mathbf{v}_{wind}\right)
\end{aligned}
\tag{38}
$$

Table 1. Initial values and model parameters used for the mathematical experiment.

System parameters	Units of measurement	Values	System parameters	Units of measurement	Values
a_1	m	0.062	R_{11}	m	0.02
a_2	M	0.1	R_{12}	m	0.04
a_3	m	0.2	R_{13}	m	0.02
a_4	m	0.2	R_{14}	m	0.02
a_5	m	0.1	R_{15}	m	0.04
a_6	M	0.1	R_{16}	m	0.02
l_1	kg m^2	10^{-3}	R_{21}	m	0.02
l_2	kg m^2	10^{-3}	R_{22}	m	0.02
l_{11}	kg m^2	10^{-4}	b_1	m	0.02
l_{12}	kg m^2	10^{-4}	b_2	m	0.02
l_{13}	kg m^2	10^{-4}	b_3	m	0.1
l_{14}	kg m^2	10^{-4}	b_4	m	0.1
l_3	kg m^2	10^{-3}	b_5	m	0.1
l_4	kg m^2	10^{-3}	b_6	m	0.1
l_{21}	kg m^2	10^{-4}	b_7	m	0.2
l_{22}	kg m^2	10^{-4}	m_{C1}	kg	1.872
C_{ei}	N m	379.12	m_{C2}	kg	0.765
d_{e1}	1/s	46.728	U_{red1}	–	20
k_x	N/m	106	U_{red2}	–	20
c_x	N s/m	0.01	Δt	s	10^{-5}

$$\mathbf{f}_{2R} = -\left(\frac{1}{2}\rho_{air}A_{2R}C_{2R}\dot{\mathbf{r}}_{C2}{}^T\dot{\mathbf{r}}_{C2}\right)\frac{\dot{\mathbf{r}}_{C1}}{|\dot{\mathbf{r}}_{C1}|}$$
$$+ \left(\frac{1}{2}\rho_{air}A_{2R}C_{2R}\mathbf{v}_{wind}{}^T\mathbf{v}_{wind}\right) \quad (39)$$

where A_{1R} and A_{2R} are the frontal areas of the first and second bodies, respectively, and C_{1R} and C_{2R} are the aerodynamic coefficients of bodies. ρ_{air} is the air density, and $\mathbf{v}_{wind}$ is the vector of wind speed. General system of equations of the container spreader and lifting mechanism can be written as

$$\dot{\mathbf{x}}(t) = \{f(\mathbf{x}(t), \mathbf{u}(t), \mathbf{d}(t))\} \quad (40)$$

Here, $\mathbf{d}(t)$ is the vector of the excitation and disturbance forces (wind and other factors), and $\mathbf{x}(t)$ is the vector of dynamic system state

$$\mathbf{x}(t) = \left\{ \begin{array}{l} M_{e1}, M_{e2}, M_{e3}, \varphi_{11}, \varphi_{12}, \varphi_{13}, \varphi_{14}, \varphi_3, \varphi_4, \mathbf{r}_{C1} \\ \varphi_1, \mathbf{r}_{C2}, \varphi_2, \varphi_{21}, \varphi_{22}, \dot{\varphi}_{11}, \dot{\varphi}_{12}, \dot{\varphi}_{13}, \dot{\varphi}_{14} \\ \dot{\varphi}_3, \dot{\varphi}_4, \dot{\mathbf{r}}_{C1}, \dot{\varphi}_1, \dot{\mathbf{r}}_{C2}, \dot{\varphi}_2, \dot{\varphi}_{21}, \dot{\varphi}_{22} \end{array} \right\}$$
$$(41)$$

$\mathbf{u}(t)$ is the action vector

$$\mathbf{u}(t) = \{U_{rede1}, U_{rede2}, U_{rede3}\}^T \quad (42)$$

In the next section, the results of multibody dynamic simulation are presented.

Simulation results and discussions

The simulation of the container spreader and lifting mechanism will help detect motion deviations of the quay crane in real time. The mathematical model was developed for scaled quay crane prototype as shown in the previous section. Any crane's control algorithm optimization was not included in the simulation. In the mathematical experiment, the vibrations were simulated during the transient processes. The main target of the simulation was to calculate the influence of the transient processes for quay crane model. The cargo lifting process was simulated for the first and second motors.

The initial values of the model parameters used for the mathematical experiment are presented in Table 1. The duration of simulation was 10 s, but the transient motions stabilize after about 2 s and most of the represented results are in this time period.

The graphs of the angular velocity of the first and second motors with the pulleys are presented in Figure 4. This is a standard transient process of the asynchronous motor. The transient processes of both the motors last for 0.2 s as shown in Figure 4. The motor's pulley's transient lasts longer—about 1.0 s. These simulation results show that both the motors in the crane system work similar.

The motors also have an impact on the cargo lifting speed due to the transient processes. As shown in Figure 5, high-amplitude vibrations affect the vertical velocities of cargo lifting. These vibrations last longer than motor transient process, because the container is suspended and the cables are tensioned by cargo weight. As shown in Figure 5, the transient process lasts about 1.4 s.

The cargo displacements are shown in Figure 6. There are two components (coordinates by *Y*- and *Z*-axis) of vector $\mathbf{r}_{C2}$. The cargo horizontal displacement
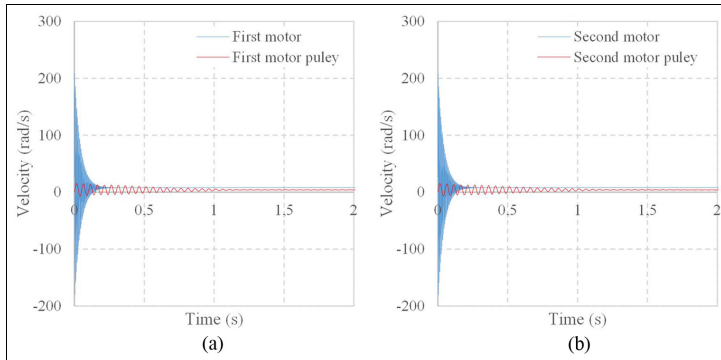
Figure 4. Angular velocities of motor and pulley: (a) first motor with pulley and (b) second motor with pulley.
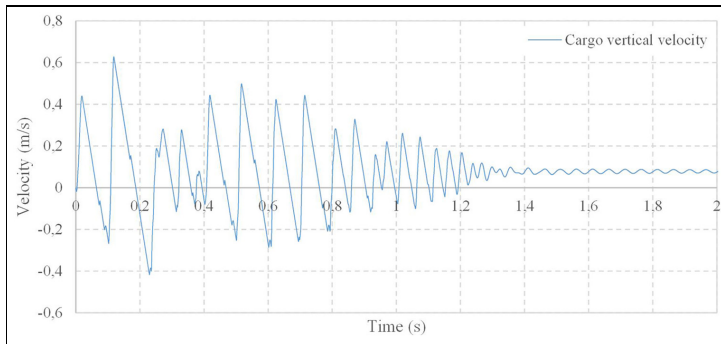

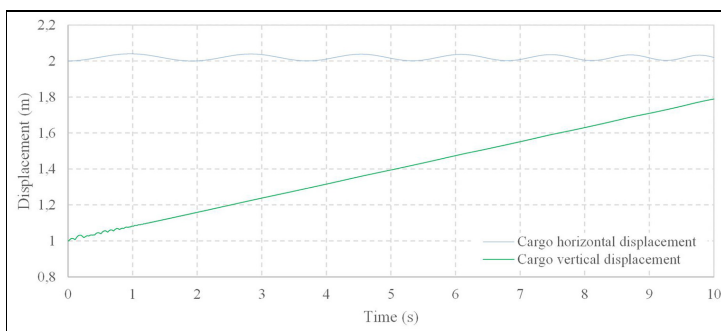**Figure 5.** Vertical velocities of cargo lifting.

Figure 6. Cargo horizontal (by *Y*-axis) and vertical (by *Z*-axis) displacements.
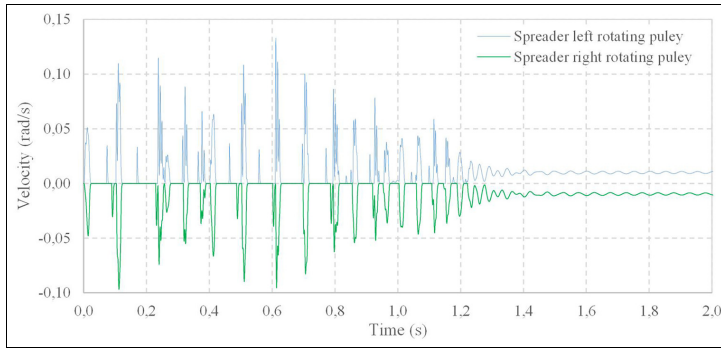
Figure 7. Velocities of left and right rotating pulleys on spreader.

(by *Y*-axis) shows the sway, where the amplitude is about 5 cm. The vertical displacement (by *Z*-axis) shows the coordinate of cargo lifting. The estimated cargo lifting speed is 0.08 m/s. During the simulation, the cargo is lifted up to 0.8 m (from 1 to 1.8 m) in 10 s.

In Figure 7, the angular velocities of the pulleys of the spreader are presented. Both the pulleys rotate at the same speed but in opposite direction. The right pulley rotates clockwise and left anticlockwise. During the lifting process, both the pulleys rotate at low angular velocities and the transient process lasts about 1.4 s. As it is shown in Figure 8, after the transient behavior of the rotating pulleys, the angular velocity is about 0.01 rad/s. The pulleys on the spreader are affected by friction. This leads to excessive vibrations during the transient. The simulation results presented in Figures 6 and 7 show even lift of the cargo.

During the simulation of container lifting, the motors' transient processes affect the whole crane system. This influence is presented in Figure 8. Although the trolley is stationary, the transient process spreads vibration to all axes. In Figure 8(a) and (c), the horizontal and vertical trolley velocities are shown. This transient process lasts about 1.5 s and after the transient behavior, the velocity becomes equal to 0 (stabilizes dynamic balance of the trolley). In Figure 8(b) and (d) the phase space diagrams of the reciprocating motion of the horizontal and vertical displacements are presented. These phase space diagrams show the maximum displacements of the trolley, minimal, and maximal velocities. Also, the dynamic balance of the trolley stabilizes and the displacement becomes equal to 0. It happens because a cargo is lifted at a constant speed.

The performed multibody dynamics simulation of the container spreader and lifting mechanism shows that vibrations affect the whole system. Typical transient of asynchronous motor caused vibrations during system startup.[16,17] These vibrations induced by motors

show that the developed dynamics model and its simulation results can be applied to future research to solve predictive control problems.

Conclusion

In this article, a multibody, more accurate mathematical model was designed to investigate the transients of the quay crane trolley and spreader on the quay crane system startup. The dynamics simulation was performed for the vertical crane spreader travel to imitate the container vertical motion and its influence for cargo sway and trolley displacements when the trolley motor is not running. The simulation results were obtained and investigated. According to the simulation results, in all the cases, the transients induced by startup of the vertical spreader travel affect the whole crane system. Due to the influence of flexible cable, lifting of the spreader causes oscillations which results in additional sway of cargo and reciprocating trolley displacement. These transient processes affect the whole system of the crane and last from 0.2 s at motors to 1.4 s at rotating pulleys on the spreader because the mathematical model includes flexible cables. The pulley–flexible cable system prolongs transients approximately seven times. The maximum vertical displacement ($68 \cdot 10^{-5}$) of the trolley is 42 times higher than the horizontal displacement ($1,6 \cdot 10^{-5}$). As a result, the spreader stabilizes after 2 s from crane system startup.

The developed mathematical model of the intermodal crane spreader can be used for real size crane transportation process imitation, but some parameters have to be adjusted. In addition, this mathematical model could be improved by adding additional functions and used as tool for crane control algorithm verification and detection of weak points in similar systems. This will help to improve safety in cargo transportation process by including transient-induced vibration
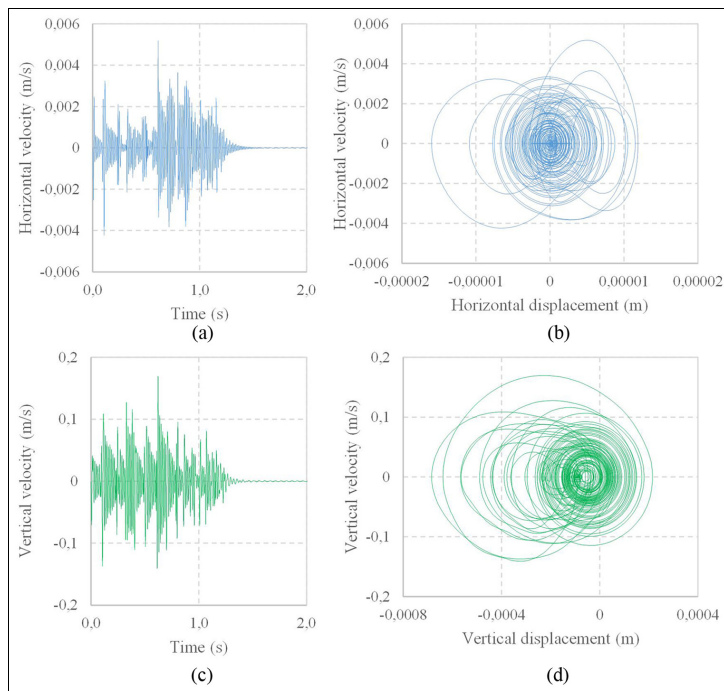
Figure 8. Trolley vibrations: (a) horizontal velocity of trolley, (b) phase space diagram of reciprocating motion horizontal displacement, and (c) vertical velocity of trolley, and (d) phase space diagram of reciprocating motion vertical displacement.

information to quay crane control algorithm as container additional sway compensator.

References

1. Roso V, Woxenius J and Lumsden K. The dry port concept: connecting container seaports with the hinterland. *J Transp Geogr* 2009; 17: 338–345.

2. Kawai H, Choi Y, Kim YB, et al. Position measurement of container crane spreader using an image sensor system for anti-sway controllers. In: *Proceedings of the international conference control, automation and systems*, Seoul, South Korea, 14–17 October 2008, pp.683–686. New York: IEEE.

3. Chang C-H, Xu J and Song D-P. An analysis of safety and security risks in container shipping operations: a case study of Taiwan. *Safety Sci* 2014; 63: 168–178.

4. Hellendoorn H, Mulder S and De Schutter B. Hybrid control of container cranes. In: *Proceedings of the IFAC proceedings volumes*, vol. 44, January 2011, pp.9697–9702. Elsevier, http://www.sciencedirect.com/science/article/pii/S1474667016451694

5. Ahmad MA, Saealal MS, Zawawi MA, et al. Classical angular tracking and intelligent anti-sway control for rotary crane system. In: *Proceedings of the international conference on electrical, control and computer engineering 2011 (InECCE)*, Kuantan, Malaysia, 21–22 June 2011, pp.82–87. New York: IEEE.

6. Cao L and Liu L. Adaptive fuzzy sliding mode method-based position and anti-swing control for overhead cranes. In: *Proceedings of the 2011 third international conference measuring technology and mechatronics automation*, Shanghai, China, 6–7 January 2011, pp.335–338. New York.

7. Yoshihara H, Fujioka N and Kasahara H. A new vision-sensorless anti-sway control system for container cranes. In: *Proceedings of the 38th IAS annual meeting conference record of the industry applications conference*, Salt Lake City, UT, 12–16 October 2003, vol. 1, pp.262–269. New York: IEEE.

8. Nundrakwang S, Benjanarasuth T, Ngamwiwit J, et al. Multivariable control of overhead crane system by CRA method. In: *Proceedings of the 2008 SICE annual conference*, Tokyo, Japan, 20–22 August 2008, vol. 1, pp.3278–3282. New York: IEEE.

9. Jaafar HI, Mohamed Z, Jamian JJ, et al. Dynamic behaviour of a nonlinear gantry crane system. *Proced Technol* 2013; 11: 419–425.

10. Ismail RMTR, Ahmad MA, Ramli MS, et al. Nonlinear dynamic modelling and analysis of a 3-D overhead gantry crane system with payload variation. In: *Proceedings of the 2009 third UKSim European symposium on computer modeling and simulation*, Athens, 25–27 November 2009, pp.350–354. New York: IEEE.

11. Bogdevicius M and Vika A. Investigation of the dynamics of the overhead crane lifting process in the vertical plane. *Transp* 2005; 20: 176–180.

12. Tomczyk J, Cink J and Kosucki A. Dynamics of an overhead crane under a wind disturbance condition. *Automat Constr* 2014; 42: 100–111.

13. Cha J-H, Roh M-I and Lee K-Y. Dynamic response simulation of a heavy cargo suspended by a floating crane based on multibody system dynamics. *Ocean Eng* 2010; 37: 1273–1291.

14. Wu T-S, Karkoub M, Yu W-S, et al. Anti-sway tracking control of tower cranes with delayed uncertainty using a robust adaptive fuzzy control. *Fuzzy Set Syst* 2016; 290: 118–137.

15. Qian D, Tong S and Lee S. Fuzzy-logic-based control of payloads subjected to double-pendulum motion in overhead cranes. *Automat Constr* 2016; 65: 133–143.

16. Sarac V and Cvetkovski G. Transient analysis of induction motor using different simulation models. *Acta Tech Jaurinensis* 2013; 6: 65–75.

17. Slater RD, Sc B, Wood WS, et al. Constant-speed solutions applied to the evaluation of induction-motor transient torque peaks. *Inst Electr Eng* 1967; 114: 1429–1435.

5th publication / 5 publikacija

Use Case of Quay Crane Container Handling Operations Monitoring Using ICT to Detect Abnormalities in Operator Actions

S. Jakovlev, T. Eglynas, **M. Jusis**, S. Gudas, V. Jankunas, M. Voznak.

6th publication / 6 publikacija

Analysis of the Efficiency of Quay Crane Control

S. Jakovlev, T. Eglynas, **M. Jusis**, S. Gudas, E. Pocevicius, V. Jankunas.

7th publication / 7 publikacija

Research of Quay Crane Control Algorithm with Embedded Sway Control Sub-routine

T. Eglynas, **M. Jusis**, S. Jakovlev, A. Senulis, P. Partila, S. Gudas.

8th publication / 8 publikacija

Pietryčių Baltijos konteinerių terminalų apžvalga ir krovos tendencijos

M. Jusis, T. Eglynas, A. Senulis, S. Gudas, S. Jakovlev, M. Bogdevičius.

NOTES

NOTES

NOTES